THE ASTROPHYSICAL JOURNAL SUPPLEMENT SERIES, 97:141–184, 1995 March

A MULTIPARAMETRIC ANALYSIS OF THE *EINSTEIN* SAMPLE OF EARLY-TYPE GALAXIES. I. LUMINOSITY AND ISM PARAMETERS

PAUL B. ESKRIDGE[1] AND GIUSEPPINA FABBIANO
Harvard-Smithsonian Center for Astrophysics, 60 Garden Street, Cambridge, MA 02138; paul@hera.astr.ua.edu, pepi@cfa.harvard.edu

AND

DONG-WOO KIM
Harvard-Smithsonian Center for Astrophysics, 60 Garden Street, Cambridge, MA 02138; and Department of Astronomy and Space Science, Chungnam National University, Taejon, 305-764, South Korea; kim@cfa.harvard.edu
Received 1994 May 16; accepted 1994 July 28

ABSTRACT

We have conducted bivariate and multivariate statistical analysis of data measuring the luminosity and interstellar medium of the *Einstein* sample of early-type galaxies (presented by Fabbiano, Kim, & Trinchieri 1992). We find a strong nonlinear correlation between L_B and L_X, with a power-law slope of 1.8 ± 0.1, steepening to 2.0 ± 0.2 if we do not consider the Local Group dwarf galaxies M32 and NGC 205. Considering only galaxies with $\log L_X \leq 40.5$, we instead find a slope of 1.0 ± 0.2 (with or without the Local Group dwarfs). Although E and S0 galaxies have consistent slopes for their L_B-L_X relationships, the mean values of the distribution functions of both L_X and L_X/L_B for the S0 galaxies are lower than those for the E galaxies at the 2.8 σ and 3.5 σ levels, respectively. We find clear evidence for a correlation between L_X and the X-ray color C_{21}, defined by Kim, Fabbiano, & Trinchieri (1992b), which indicates that X-ray luminosity is correlated with the spectral shape below 1 keV in the sense that low-L_X systems have relatively large contributions from a soft component compared with high-L_X systems. We find evidence from our analysis of the 12 μm *IRAS* data for our sample that our S0 sample has excess 12 μm emission compared with the E sample, scaled by their optical luminosities. This may be due to emission from dust heated in star-forming regions in S0 disks. This interpretation is reinforced by the existence of a strong L_{12}-L_{100} correlation for our S0 sample that is not found for the E galaxies, and by an analysis of optical-IR colors. We find steep slopes for power-law relationships between radio luminosity and optical, X-ray, and far-IR (FIR) properties. This last point argues that the presence of an FIR-emitting interstellar medium (ISM) in early-type galaxies is coupled to their ability to generate nonthermal radio continuum, as previously argued by, e.g., Walsh et al. (1989). We also find that, for a given L_{100}, galaxies with larger L_X/L_B tend to be stronger nonthermal radio sources, as originally suggested by Kim & Fabbiano (1990). We note that, while L_B is most strongly correlated with L_6, the *total* radio luminosity, both L_X and L_X/L_B are more strongly correlated with $L_{6\text{co}}$, the *core* radio luminosity. These points support the argument (proposed by Fabbiano, Gioia, & Trinchieri 1989) that radio cores in early-type galaxies are fueled by the hot ISM.

Subject headings: galaxies: elliptical and lenticular, cD — galaxies: general — galaxies: ISM — X-rays: galaxies

1. INTRODUCTION

The classic view of early-type (E and S0) galaxies, as put forth in the preface to the Hubble Atlas (Sandage 1961) is that of pure Population II stellar systems, with little or (ideally) no optical signatures of an interstellar medium (ISM). It was already clear by then that a significant fraction of luminous early-type galaxies do indeed possess some quantity of optical emission-line gas (Mayall 1939; Humason, Mayall, & Sandage 1956). Furthermore, as the angular resolution of radio telescopes improved throughout the 1950s and 1960s, it also became clear that many early-type galaxies are powerful radio continuum sources (e.g., Maltby & Moffet 1962). It was thus obvious that they contain relativistic electrons, moving under the influence of magnetic fields (e.g., Hoyle 1960). By the 1970s, a few early-type galaxies were also known to have some amount of H I gas, based on 21 cm line observations (e.g., Bottinelli & Gouguenheim 1977; Gallagher et al. 1977; Whiteoak & Gardner 1977; Knapp, Gallagher, & Faber 1978; Fosbury et al. 1978). However, all available evidence pointed toward very small mass fractions for the ISM in early-type galaxies.

That this was, in fact, a serious problem was pointed out in a landmark paper by Faber & Gallagher (1976). They noted that the stellar populations of early-type galaxies are dominated by old stars, and that stars lose a significant amount of mass in the course of stellar evolution. Thus a typical early-type galaxy ($L_B \approx 10^{10}\ L_\odot$) *should* contain $\approx 10^9\ M_\odot$ of ISM if this material were not either converted into new stars (not considered a major sink either then or now) or swept from the system by some internal or external process.

For a number of years, theoretical work focused on the latter possibility, the main mechanisms considered being ram-pressure stripping due to interactions of the early-type galaxies with the intracluster medium of their host clusters (Gunn & Gott 1972; Gisler 1976; Frank & Gisler 1976) and galactic winds generated by energy input from supernovae (Johnson & Ax-

[1] Current address: Department of Physics and Astronomy, University of Alabama, Tuscaloosa, AL 35487.

ford 1971; Mathews & Baker 1971). Indeed, cluster effects do appear to be a significant contributor to the overall state of the ISM in at least some early-type galaxies (e.g., Forman et al. 1979; Forman, Jones, & Tucker 1985; Trinchieri, Fabbiano, & Canizares 1986; Trinchieri & di Serego Alighieri 1991). But the crucial development required to address the problem of the ISM in early-type galaxies turned out to be technological: the invention of ~arcminute resolution X-ray imaging devices (Giacconi et al. 1979).

Among the most important results from the *Einstein Observatory,* the first satellite to contain such devices, was the observation that many early-type galaxies contain significant amounts (10^8–10^9 $M_\odot$) of gas at temperatures of 10^6–10^7 K (Forman et al. 1979). Once it became clear that this material was often the dominant phase of the ISM in early-type galaxies, the problem posed by Faber & Gallagher (1976) was largely resolved, and work became focused on exploring the nature of this newly discovered phase of the ISM (see Fabbiano 1989 and references therein).

In the meantime, improvements in detector technology in other wave bands led to detections of, or increasingly strict upper limits on, characteristic emission from all other phases of the ISM in early-type galaxies (e.g., Knapp, Turner, & Cunniffe 1985, and Wardle & Knapp 1986 for H I; Knapp et al. 1989 for FIR; Sage & Wrobel 1989 and Thronson et al. 1989 for CO). By the mid-1980s it became possible to begin truly multivariate studies of the ISM from statistically significant (for astronomers!) samples of early-type galaxies (Fabbiano et al. 1987; Fabbiano et al. 1989, hereafter FGT).

The final catalog and atlas of *Einstein* observations of galaxies (Fabbiano et al. 1992, hereafter P0) contains X-ray data on 148 normal early-type galaxies. Until a comparable study of results from *ROSAT* become available, this will be the largest-extent sample of X-ray observations of normal early-type galaxies. We have therefore undertaken a multiparametric analysis of the optical, ISM, and structural properties of this sample. In § 2 we describe our sample construction. In § 3 we address the L_X-L_B relationship. We move in § 4 to explore the relationships between X-ray emission and infrared and radio emission. We summarize our results, and discuss possible areas for future research in § 5. Analysis of the structural and stellar data for our sample will be presented in subsequent papers.

2. SAMPLE CONSTRUCTION

As noted above, the *Einstein* galaxy catalog (P0) provides X-ray fluxes or upper limits for 148 early-type (S0 and earlier) galaxies. This represents the largest body of data currently available on the X-ray properties of early-type galaxies. A number of earlier papers have examined the relationships between X-ray emission and other properties of early-type galaxies using smaller samples (e.g., Fabbiano et al. 1987; FGT; Bregman, Hogg, & Roberts 1992). We have undertaken the current study to reexamine the conclusions of these earlier works, and to address a more complete set of properties describing the current physical conditions in early-type systems. Our X-ray data are from P0. The sources of the (B-band) optical data and assumed distances to our sample are also given in P0. We have included all published information from the *IRAS* survey on our sample. The *IRAS* data are 91% complete (134 of 148 at 12 μm, and 135 of 148 at the remaining wavelengths). Five of the systems in our sample are in regions of the sky not well sampled by *IRAS*. We have also included all published 6 cm radio data for our sample. Fluxes or upper limits are available for 90% (133 of 148) of the galaxies. High-resolution data, providing information on the core radio flux, are available for 67% (99 of 148) of our sample. Measurements of the 21 cm H I line flux (or upper limit) are available for 79% (117 of 148) of our sample. Axial ratios are included and have been taken from de Vaucouleurs et al. (1991, hereafter RC3). All these data are summarized, with references, in Table 1.[2] The X-ray and optical data in Table 1 are taken from P0. Sources for the remaining data are given in the table.

We use luminosities (or luminosity ratios) including both detections and upper limits for our analysis of these data below. Arguments regarding the validity of this approach are presented in detail in a number of previous papers (Fabbiano et al. 1987; Fabbiano, Gioia, & Trinchieri 1988; FGT). We note that the lack of any a priori flux limits in our sample will minimize the possibility of any significant effect due to a Malmquist-like bias.

3. THE L_X-L_B RELATIONSHIP

There have been a number of previous attempts at determining the relationship between the X-ray and optical luminosities of early-type galaxies (e.g., FGT; Donnelly, Faber, & O'Connell 1990; Bregman et al. 1992). We have reinvestigated this relationship, examining correlations between L_X, L_B, L_X/L_B, and C_{21} (an X-ray color, defined in Kim et al. 1992b, that gives the ratio between the emission in the 0.8–1.36 keV band and that in the 0.16–0.8 keV band). We also investigate the use of subsamples based on high- and low-luminosity cutoffs and on morphology, breaking the sample into E and S0 subsets.

3.1. *The Full Sample*

3.1.1. *Correlations over the Full Range in Luminosity*

In Figure 1 we plot L_X against L_B for our sample. Because of the upper limits in L_X, standard statistical tests for correlation are invalid. We have instead applied the correlation tests available for censored data sets discussed by Isobe, Feigelson, & Nelson (1986) and LaValley, Isobe, & Feigelson (1992). For samples with censoring in one variable, such as the L_X-L_B data set, the three available tests are the Cox-Hazard model, the modified Kendall's τ-test, and the modified Spearman rank test. The result of each of these tests is that the probability that the X-ray and optical luminosities are uncorrelated is $P < 10^{-4}$. These results are presented in Table 2A. Various regression algorithms are available for data sets with censoring in only one variable. These are the expectation and maximization (E-M) algorithm, the Buckley-James (B-J) algorithm (see Isobe et al. 1986), and Schmitt's binning method (Schmitt 1985). We have used all of them. The results of this regression analysis are shown in Table 3A and, along with the data, in Figure 1. All methods give the result $L_X \propto L_B^{1.8\pm0.1}$.

When performing any regression, one is required to make decisions about the nature of one's data. The central question

[2] These data will be made available to the community via EINLINE.

TABLE 1A

FLUX DATA

Name	B_T^0	Type	log(a/b) RC3	f_X[a] 10^{-13} cgs	σ_X	D Mpc	f_{12} mJy	σ_{12}	f_{25} mJy	σ_{25}	f_{60} mJy	σ_{60}	f_{100} mJy	σ_{100}	f_6 mJy	σ_6	$f_{6,co}$ mJy	$\sigma_{6,co}$	f_{HI}[a] Jy km/sec	σ_{HI} mJy	References
NGC 127	14.68	-2	0.16	< 4.27		80.0															6
NGC 128	12.63	-2	0.52	< 4.17		82.6	0	42	220	61	750	41	1550	115	0	6.67			1.5		1,11,41
NGC 130	14.78	-3	0.31	< 4.36		88.9															6
NGC 205	8.60	-3	0.30	< 17.88		0.7	110	31	130	22	570	37	3130	102	0	0.33			3.3		1,4,10,41
NGC 221	8.79	-6	0.13	9.21		0.7	480	36	220	33	0	87	0	1260	0	0.33			0	18.0	11,41
NGC 315	12.20	-3	0.20	9.69	0.54	99.9	0	31	0	49	320	52	360	90	1045.2		554	33.5	< 1.33		1,10,24,42
NGC 499	12.64	-3	0.10	30.01	1.19	88.6	0	29	0	23	0	40	0	112	60	20			< 1.16		1,14,42
NGC 507	11.76	-2	0.00	93.95	2.32	99.3	0	23	0	37	0	39	0	141	0	20	0	10	< 5.1		1,14,33,42
NGC 533	12.75	-5	0.21	31.42	4.82	107.9	0	44	0	53	0	44	0	96	12						1,21
NGC 584	11.20	-2	0.26	< 2.89		37.6	0	44	0	62	0	41	520	90	0	0.33	0	0.33	0	4.0	1,10,31,41
NGC 596	11.88	-5	0.19	< 2.44		38.2	0	33	0	50	0	26	0	100	0	0.33	0	0.32			1,11,31
NGC 720	11.15	-5	0.29	17.02	1.60	32.6	90	28	0	33	0	42	0	56	0	0.34	0	0.29	0	3.0	1,10,31,41
NGC 984	14.70	-2	0.17	< 4.54		87.5	0	24	0	45	140	37	120	106	78.7	0.11			7.8		1,10,42
NGC 1044	14.00	-3	0.00	< 1.41		122.5									320	10	17				19,35
NGC 1052	11.53	-3	0.16	5.28	0.56	28.6	220	18	510	37	900	31	1400	60	1270.0	40.0	1230	40	5.6		1,11,25,41
NGC 1167	12.79	-3	0.07	< 3.03		99.9	0	30	0	37	120	28	930	133	911.8	0.98	0	243	13.32	0.66	1,10,36,42
NGC 1172	13.00	-2	0.11	< 1.59		29.4	0	26	0	31	0	41	0	72					0	6.9	1,41
NGC 1201	11.56	-2	0.23	< 5.70		32.5	0	38	0	28	0	35	0	72	0	4.00			0	17.0	1,11,41
NGC 1316	9.32	-2	0.15	19.86	0.99	27.2	310	39	270	20	3160	30	14200	3000	6600		90	10	< 1.27		1,10,26,42
NGC 1332	11.29	-2	0.51	6.72	0.66	28.4	90	17	100	23	520	27	1610	51	0	0.33			0	5.4	1,10,41
NGC 1387	11.83	-2	0.00	6.43	1.32	27.2	160	31	170	24	2370	28	6030	44	0	4.00					1,11
NGC 1389	12.39	-2	0.22	< 2.60		27.2	0	24	0	25	0	28	0	89	0	0.33	0	0.33			1,11,37
NGC 1395	11.18	-5	0.12	11.14	1.07	32.1	130	26	50	27	50	26	300	42	2.0	0.2	2.02	0.17			1,10,38
NGC 1399	10.79	-5	0.03	215.72	5.82	27.2	90	23	0	18	0	32	270	72	230.4		110		0	3.1	1,10,27,41
NGC 1404	11.06	-5	0.05	33.22	2.00	27.2	90	41	0	23	0	28	240	49	0	0.23	0	0.23			1,11,37
NGC 1400	12.08	-3	0.06	< 4.98		8.0	0	36	100	23	760	40	2920	129	2.0	0.12			0	13.0	1,10,41
NGC 1407	10.93	-5	0.03	14.18	1.50	34.7	110	29	0	27	140	30	430	65	44.0	4.00			0	3.3	1,11,41
NGC 1497	14.20	-2	0.17	< 2.06		122.6			0	167	0	167	0	500	39.7	0.14	8.17	0.11	0.37		7,10,44
NGC 1510	13.24	-6	0.26	< 4.20		16.6	0	93	0	97	3100	372	10820	1298	0	7			1.61	0.14	6,20,42
NGC 1553	10.36	-2	0.20	14.36	3.28	21.5	170	16	130	26	570	24	1010	51	0	4.00			0	21.2	1,11,41
NGC 1574	11.13	-2	0.04	< 7.01		21.5	100	14	70	17	370	22	590	64	0	3.95					1,10
NGC 1600	12.01	-5	0.17	9.19	1.97	90.3	0	14	0	25	100	27	170	65	22.0	3.00			0	9.0	1,11,41
NGC 1947	11.75	-2	0.07	< 4.45		19.4	140	32	90	20	1100	24	4270	50	18.0	3.00					1,11
NGC 2314	12.83	-5	0.09	< 3.01		84.6	0	24	0	27	70	22	300	55	700.0	233	8.0	0.13	0	4.0	1,10,14,41
NGC 2300	11.99	-5	0.14	10.85	1.68	49.8	90	18	0	28	0	25	0	81	0.7	0.12	0.7	0.12	0	6.0	1,10,11,41
NGC 2444	13.43	-2	0.16	< 5.17		86.4	0	83	530	64	3390	407	6320	758	0	11			0	6.0	6,17,42
NGC 2562	13.37	-1	0.18	< 3.07		102.4	0	31	0	47	170	51	360	161	0	4.3			< 0.53		1,21,42
NGC 2563	12.92	-2	0.14	12.00	1.05	96.1	0	18	0	54	0	27	0	187	0	0.11			< 0.55		1,10,42
NGC 2629	13.30	-2	0.07	< 2.20		80.8	0	21	0	19	100	31	410	109	50.8	0.15	45.2	0.18			8,10
NGC 2685	11.85	-2	0.28	< 3.53		26.0	100	31	0	37	370	42	1660	100	3.3	0.16			32.3		1,10,41
NGC 2694	14.96	-5	0.01	< 3.56		107.5									0	60					14
NGC 2693	12.70	-5	0.16	< 3.40		103.7	0	29	0	32	210	37	790	114	1.7	0.10	1.4	0.14	0	8.0	1,10,41
NGC 2716	12.90	-1	0.10	< 1.50		73.7	140	34	0	28	310	37	920	102	0	3.33					1,16
NGC 2832	12.39	-5	0.10	22.85	2.75	142.3	80	26	0	43	440	27	1330	137	0	11.0			0	2.2	2,11,41
NGC 2859	11.75	-2	0.05	< 1.20		40.8	0	28	0	36	320	31	830	72	0	0.33	0	0.17	0	1.0	1,11,34,41
NGC 2911	12.53	-2	0.11	< 3.76		69.2	0	28	0	36	290	28	560	79	120.0	5.00	163	7	4.4		1,11,25,41
NGC 2974	11.68	-5	0.23	3.32	0.79	45.8	0	21	0	27	430	33	1690	47	7.3	0.10	9.6	0.10	6.0		1,10,41
NGC 3078	11.92	-5	0.08	4.30	0.73	53.7									167.0	5.00	123.5	1.00	0	3.1	3,10,11,41
NGC 3065	12.81	-2	0.01	7.88	1.85	50.3	0	26	290	19	1550	25	1780	88:					7.8		1,41
NGC 3115	9.89	-2	0.47	< 6.41		10.8	290	40	150	33	140	36	0	159	0	0.11			0	1.8	8,10,41
NGC 3222	13.39	-2	0.08	< 2.58		117.2									0	4.3			< 4.72		21,42
NGC 3258	12.48	-5	0.07	7.02	1.36	60.3	0	22	0	34	160	38	640	149	52.0	5.00	3.7		0	1.2	1,11,37,41
NGC 3377	11.10	-5	0.24	< 1.36		13.0	100	33	0	67	140	46	310	57	0	0.20	0	0.20	0	0.3	1,10,31,41
NGC 3379	10.33	-5	0.05	< 6.62		13.0	250	39	0	47	0	42	0	96	2.0		0.8	0.08	0	0.2	1,10,41
NGC 3384	10.70	-2	0.34	< 3.76		13.0	180	28	0	56	0	39	400	75	0	3.9	0	0.17	0	0.5	1,21,34,41
NGC 3458	13.15	-2	0.20	< 3.92		47.4	0	21	0	38	0	33	0	80			0	0.17	0	4.0	1,34,41
NGC 3516	12.34	-2	0.11	30.80	1.30	62.5	390	18	940	14	1900	29	1890	197	15.5	1.70	15.5	1.70	0	4.1	1,11,34,41
NGC 3585	10.81	-3	0.26	1.63	0.35	34.7	110	33	200	28	160	42	0	78	0	0.40			0	16.0	1,10,41
NGC 3607	11.08	-2	0.30	6.19	0.53	32.0									3.9	0.09	2.9	0.12	0	0.5	3,10,41
NGC 3608	11.88	-5	0.09	1.87	0.32	37.6									0.9	0.09	0	0.22	0	0.3	3,10,31,41
NGC 3818	12.79	-5	0.22	< 4.86		40.3	0	45	0	28	0	49	0	85	0	0.33	0	0.22	0	10.0	1,15,31,41
NGC 3894	12.90	-5	0.21	4.93	1.05	74.7	0	22	120	26	140	60	430	140	522.2		577	0.90			1,10,45
NGC 3923	10.79	-3	0.18	10.96	1.19	41.5	120	36	0	27	0	35	0	120	4.5	1.00	0	0.29	0	12.0	1,11,31,41
NGC 3990	13.11	-3	0.24	< 2.98		27.3	0	23	0	26	0	44	410	90							1
NGC 3998	11.50	-2	0.08	59.88	3.92	34.7	130	23	120	21	570	27	1020	110	92.0	3.00	59.4	0.22	6.4		1,10,11,41
NGC 4105	11.76	-2	0.13	3.58	0.77	43.6	0	21	0	36	270	40	740	135	3.7	0.08			11.7		1,10,42
NGC 4168	12.21	-5	0.08	2.26	0.57	27.0	0	42	0	37	0	37	590	139:	4.0		4.5	0.2			1,11,34
NGC 4203	11.62	-2	0.03	31.42	2.55	15.6	0	39	170	26	610	30	1920	71	14.6	0.14	11.6	0.11	27.4		1,10,41
NGC 4215	13.04	-2	0.42	< 2.04		56.4	0	35	0	26	0	31	0	92	0	3.3	0	0.17	0	1.3	1,21,34,41
NGC 4251	11.62	-2	0.39	< 1.22		15.6	0	32	0	42	120	39	0	80	0	0.40	0	0.17	0	0.7	1,11,34,41
NGC 4261	11.38	-5	0.05	13.18	0.94	56.4	170	44	80	60	80	35	130	43	8300.0		315	5	0	7.2	1,11,31,42
NGC 4267	11.78	-2	0.03	< 2.23		27.0	0	26	0	40	190	35	1030	36	0	11	0	0.17	0	0.9	1,21,34,41
NGC 4291	12.26	-5	0.08	8.24	0.64	47.2	0	16	0	19	0	30	0	44	0	0.10	0	0.17			1,10,34
NGC 4340	11.93	-2	0.10	< 2.37		27.0	0	24	310	51	90	25	330	55			0	0.17	0	0.7	1,34,41
NGC 4350	11.88	-2	0.32	< 1.64		27.0	140	43	0	37	370	35	970	74	0	3.1	0	0.17	0	0.8	1,21,34,41

TABLE 1A—*Continued*

Name	B_T^o	Type	log(a/b) RC3	f_X[a] 10^{-13} cgs	σ_X	D Mpc	f_{12} mJy	σ_{12}	f_{25} mJy	σ_{25}	f_{60} mJy	σ_{60}	f_{100} mJy	σ_{100}	f_6 mJy	σ_6	$f_{6,co}$ mJy	$\sigma_{6,co}$	f_{HI}[a] Jy km/sec	σ_{HI} mJy	References
NGC 4365	10.60	-5	0.14	2.99	0.41	27.0	150	30	0	43	0	45	580	116	0	0.17	0	0.15	0	0.3	1,11,31,41
NGC 4386	12.53	-2	0.26	< 1.01		45.2	0	20	50	16	120	23	0	79			0	0.17	0	5.0	1,34,41
NGC 4374	10.23	-5	0.06	16.43	0.70	27.0	210	35	180	39	510	27	1030	109	2880.0	240	178.0	0.70	< 7.6		1,10,11,42
NGC 4382	10.10	-2	0.11	6.02	0.48	27.0	0	40	0	59	0	30	0	70	0	0.33	0	0.17	0	0.6	1,10,34,41
NGC 4387	12.75	-5	0.21	< 3.89		27.0	0	33	0	43	0	53	0	158	0	0.33	0	0.18	< 0.34		1,12,31,42
NGC 4406	10.02	-3	0.19	198.81	4.83	27.0	150	35	0	56	110	35	290	59	0	0.20	0	0.18	1.3		1,11,31,41
NGC 4417	12.07	-2	0.41	< 13.13		27.0	0	30	0	77	0	44	0	106	0	3.1	0	0.13	0	0.8	1,21,22,41
NGC 4425	12.79	-2	0.47	< 2.05		27.0	0	33	0	49	0	60	0	146	0	3.0	0	0.17	0	0.7	1,21,34,41
NGC 4435	11.72	-2	0.14	< 3.80		27.0	120	45	210	50	2050	44	4160	106:			1.2	0.1	0	0.7	1,34,41
NGC 4458	12.70	-5	0.04	1.91	0.54	27.0	90	25	0	58	0	34	0	126	0	0.33	0	0.17	< 0.35		1,12,31,42
NGC 4459	11.49	-2	0.12	< 2.87		27.0	330	27	0	90	1920	67	4280	119	2.4	0.80	0.8	0.1	0	1.3	1,11,34,41
NGC 4467	15.18	-5	0.10	< 0.56		27.0															
NGC 4472	9.32	-3	0.09	130.89	2.80	27.0	190	35	0	45	0	66	0	94	248.7		58.1	0.10	0	0.2	1,10,41
NGC 4473	11.07	-5	0.25	3.76	0.95	27.0	270	51	470	50	0	62	0	95	0	0.25	0	0.39	0	0.6	1,10,31,41
NGC 4474	12.70	-2	0.22	< 1.99		27.0	0	37	0	42	0	48	0	80	0	2.9	0	0.17	0	1.2	1,21,34,41
NGC 4479	13.21	-2	0.08	< 1.43		27.0	0	33	0	52	0	25	0	134			0	0.17	< 0.8		1,34,42
NGC 4526	10.59	-2	0.48	1.57	0.36	27.0	440	39	530	49	5720	47	21000	270			3.1	0.2	0	0.5	1,34,41
NGC 4507	12.80	-1	0.10	< 8.35		72.5	460	55	1410	169	4580	733	5600	896					11.0		5,42
NGC 4550	12.33	-3	0.55	< 1.83		27.0	0	29	0	63	140	31	220	80	0	0.25	0	0.17	0	1.5	1,10,34,41
NGC 4551	12.65	-5	0.10	< 2.77		27.0	0	28	0	69	0	38	0	137	0	0.33	0	0.17	0.13		1,12,31,42
NGC 4552	10.80	-2	0.04	9.60	0.74	27.0	120	52	0	49	160	47	470	52	108.0	2.00	107	3	0	0.5	1,11,25,41
NGC 4564	11.87	-5	0.38	< 1.79		27.0	0	35	0	43	0	61	0	168	0	0.25	0	0.17	0	0.4	1,10,34,41
NGC 4578	12.04	-2	0.13	< 2.78		27.0	0	40	0	38	0	34	0	98	0	4.1	0	0.17	0	0.4	1,21,34,41
NGC 4589	11.81	-5	0.09	< 1.65		48.2	0	31	0	21	210	31	590	136	23.5	0.12	21.0	0.7	0	6.0	1,10,34,41
NGC 4621	10.67	-5	0.16	< 3.10		27.0	220	41	0	40	0	51	0	83	6.0		0	0.23	0	1.0	1,10,31,41
NGC 4638	12.05	-2	0.21	1.91	0.56	27.0	0	21	0	32	0	45	0	66	0	0.33	0	0.17	0	0.9	2,10,34,41
NGC 4636	10.50	-3	0.11	108.94	5.91	27.3	190	48	0	52	140	43	0	152	45.0	9.00	27.3		0	1.0	1,11,28,41
NGC 4649	9.83	-2	0.09	46.98	1.83	27.0	360	80	360	68	900	65	2300	270	23.8	2.00	18.4		0	1.6	1,10,28,41
NGC 4645	12.56	-5	0.21	< 1.20		74.6	0	36	0	29	300	60	1490	227	0	4.00					1,11
NGC 4697	10.11	-5	0.19	5.58	0.76	37.4	270	38	0	38	470	23	1100	67	0	0.20	0	0.21	0	16.0	1,11,31,41
NGC 4754	11.41	-2	0.27	< 1.54		27.0	0	26	0	43	0	45	0	102			0	0.17	0	0.9	1,34,41
NGC 4753	10.85	-2	0.33	1.71	0.37	24.3	340	42	310	71	2640	60	8010	176	0	0.10	0	0.13	0	16.0	1,10,39,41
NGC 4756	13.28	-5	0.10	12.16	1.15	88.4	0	30	0	60	0	43	0	135	14.0	3.4					1,20
NGC 4762	11.26	-2	0.72	3.79	0.58	27.0	140	50	0	33	0	48	0	71	0	0.67	0	0.10	0	0.6	1,22,41
NGC 4782	12.75	-5	0.02	6.89	1.51	84.7	0	37	0	75	0	33	0	288	2540.0	75.0	1472		0	32.3	1,11,35,42
IC 3896	12.37	-5	0.12	< 5.87		48.5	0	26	0	30	0	70	0	242	0	4.00					1,11
NGC 4880	12.57	-2	0.11	< 2.73		25.2	0	17	0	57	0	34	0	129	0	0.33			0	0.3	1,11,41
NGC 5044	11.87	-5	0.00	315.01	9.56	62.5	140	35	0	75	140	57	130	65	30.0	3.00			0	2.2	1,11,41
NGC 5077	12.52	-5	0.11	2.32	0.45	65.2	0	45	0	83	410	38	3750	154	166.7		87	4	0	2.1	8,10,25,41
NGC 5084	11.95	-2	0.73	7.46	1.57	42.4	0	48	0	49	420	42	2300	330	34.0	3.00			84.8		1,11,41
NGC 5102	10.47	-2	0.49	< 3.44		5.6	80	31	170	33	940	35	2430	90	0.9	0.12	0	0.27	72.0		1,10,37,41
NGC 5128	6.62	-2	0.11	398.44	3.85	7.9	23000	460	24700	550	230500	560	492000	1880	124000		6984	210	230.		1,10,29,42
NGC 5195	10.50	-2	0.10	2.32	0.51	14.9	680	20	48330	14	39070	1261	0	454	0	26.7			< 42.4		1,11,42
IC 4296	11.43	-5	0.02	12.86	1.10	78.4	0	27	0	29	140	59	230	73	2060.1		224	45			1,10,30
IC 4329	12.48	-2	0.24	< 12.78		93.8	0	23	0	31	460	61	930	234	0.6	0.1	0.63	0.09			1,11,38
NGC 5322	10.91	-5	0.18	< 3.58		50.8	0	20	0	19	430	38	890	67	42.1		14	1	0	3.0	1,10,12,41
NGC 5318	13.40	-2	0.22	< 2.14		95.7	0	27	0	34	170	29	1240	112	86.3	0.17	60	3	0	1.0	1,10,25,42
NGC 5354	12.19	-2	0.04	< 4.33		63.9	0	47	0	30	420	50	1430	51	33.0	7.00	8.1	0.3	18.9	2.2	1,12,34,42
NGC 5353	12.05	-3	0.30	5.79	0.89	60.8	0	29	0	34	330	54	1290	100	35.0	2.00	34	2.0	17.6		1,11,12,41
NGC 5363	11.06	-2	0.19	4.02	1.31	36.0	190	36	220	50	1700	46	4450	45	95.0	3.00	77	3.0	1.9		1,11,18,41
NGC 5485	12.44	-2	0.08	< 3.59		52.7	0	20	0	19	150	34	850	88	0.9	0.10	0	0.33	0	5.0	1,10,34,41
IC 989	14.00	-5	0.07	< 2.39		157.9	0	38	0	50	120	45	390	79	70.1	0.12			0.54		1,10,42
NGC 5532	12.64	-2	0.00	2.99	0.89	154.6	70	27	0	34	0	38	480	89	1509.7		77		< 1.1		1,10,32,42
NGC 5576	11.76	-5	0.20	< 2.65		42.4	70	34	70	37	90	27	190	247	0	0.33	0	0.17	0	0.4	1,11,34,41
IC 1024	13.90	-2	0.39	< 2.37		40.1	310	24	480	26	4210	33	6930	95	11.0	1.00	11.3	1.0	7.58	0.89	1,13,34,42
NGC 5838	11.72	-2	0.45	1.42	0.27	45.8	120	28	90	41	750	40	1480	82	0	16.7	2.0	0.1	0	1.5	1,11,34,41
NGC 5846	11.13	-2	0.03	51.38	1.52	45.8	0	22	0	22	0	37	0	112	7.8	0.10	5.3	0.3	0	0.2	1,10,34,41
NGC 5866	10.86	-2	0.38	2.02	0.63	24.6	300	16	240	14	5210	21	16610	51	12.9	1.00	7.4	0.3	0	6.0	1,10,34,41
NGC 5982	12.03	-5	0.12	5.12	1.26	69.1	0	20	0	20	0	33	330	31	0	0.33	0	0.17			1,11,34
NGC 6027	14.23	-2	0.28	< 4.45		97.6	0	83	0	100	1030	124	2200	264					3.3		6,42
NGC 6034	14.60	-5	0.11	5.46	1.73	209.5									229.0	0.20	0	91.2			10
NGC 6146	13.50	-2	0.10	< 4.64		183.2	0	33	0	29	0	25	0	143	100.0	0.31	72	4	0	6.0	1,10,25,42
NGC 6876	12.45	-5	0.11	9.29	0.96	73.4	0	24	70	26	90	35	430	92	0	4.01					2,10
NGC 6880	14.00	-1	0.36	< 3.35		75.2	90	22	80	24	970	50	3030	136	0	3.7					1,21
NGC 6963	14.40	-5		< 1.88		89.1									0	16.7					14
NGC 6964	13.12	-5	0.12	< 1.80		79.0	250		254		401		1938		0	13.3					9,14
NGC 7236	14.08	-3	0.00	< 2.57		158.0									336	50			< 0.34		3,17,43
NGC 7237	14.33	-3	0.00	< 3.50		158.3									454	42	14		< 0.34		3,23,43
NGC 7332	11.58	-2	0.56	< 3.15		29.3	110	25	0	32	220	30	360	96	0	20.0			0	1.6	1,11,41
IC 1459	10.96	-5	0.14	8.23	1.16	32.1	160	27	300	41	520	31	1050	91	1066.9		1000		0	5.8	1,10,40,41
NGC 7562	12.28	-5	0.18	< 3.69		72.0	0	29	0	43	0	37	0	268	0	0.30	0	0.30	0.25		1,10,31,46
NGC 7619	12.17	-5	0.04	14.92	1.12	75.0	0	31	0	57	0	38	630	205	6.6		6.6		0	1.1	1,10,31,41
NGC 7626	12.17	-5	0.05	5.67	0.84	68.3	0	46	0	52	0	42	0	113	227.9		30		0	0.7	1,10,31,41

[a] The values listed as upper limits are 3 σ.

TABLE 1B

LUMINOSITY DATA

Name	$\log(L_B)$ erg/sec	$\log(L_X)$ erg/sec	$\log(L_X/L_B)$	$\log(L_{12})$ erg/sec	$\log(L_{100})$ erg/sec	$\log(L_6)$ erg/sec	$\log(L_{6co})$ erg/sec	$\log(M_{HI})$ $M_\odot$
NGC 127	42.84	< 41.52	< −1.33					
NGC 128	43.69	< 41.53	< −2.14	< 43.22	43.10	< 36.91		9.38
NGC 130	42.89	< 41.62	< −1.27					
NGC 205	41.15	< 38.02	< −3.13	39.01	39.26	< 31.47		5.58
NGC 221	41.08	37.73	−3.35	39.65	< 39.35	< 31.47		< 5.69
NGC 315	44.02	42.06	−1.96	< 43.25	42.63	38.80	38.52	< 9.50
NGC 499	43.74	42.45	−1.29	< 43.12	< 42.50	37.45		< 9.33
NGC 507	44.19	43.05	−1.15	< 42.64	< 42.22	< 37.55	< 37.25	< 10.07
NGC 533	43.87	42.64	−1.23	< 43.47	< 42.60	36.92		
NGC 584	43.57	< 40.69	< −2.88	< 42.55	41.95	< 34.93	< 34.92	< 9.33
NGC 596	43.32	< 40.63	< −2.69	< 42.44	< 41.72	< 34.94	< 34.92	
NGC 720	43.47	41.34	−2.13	42.26	< 41.33	< 34.81	< 34.74	< 9.04
NGC 984	42.91	< 41.62	< −1.29	< 43.02	42.04	37.56		10.15
NGC 1044	43.48	< 41.40	< −2.08			38.46	37.18	
NGC 1052	43.20	40.71	−2.49	42.54	42.14	37.79	37.78	9.03
NGC 1167	43.79	< 41.56	< −2.23	< 43.23	43.05	38.74	< 38.64	10.50
NGC 1172	42.64	< 40.22	< −2.42	< 42.11	< 41.35			< 9.04
NGC 1201	43.30	< 40.86	< −2.44	< 42.36	< 41.44	< 35.88		< 9.74
NGC 1316	44.04	41.25	−2.80	42.64	43.10	38.47	35.65	< 8.35
NGC 1332	43.29	40.81	−2.48	42.14	42.19	< 34.68		
NGC 1387	43.04	40.76	−2.28	42.35	42.73	< 35.73		
NGC 1389	42.82	< 40.36	< −2.46	< 42.01	< 41.37	< 34.65	< 34.64	
NGC 1395	43.44	41.14	−2.30	42.41	41.57	35.09	35.10	
NGC 1399	43.46	42.28	−1.18	42.10	41.38	37.01	36.69	< 8.90
NGC 1404	43.35	41.47	−1.88	42.10	41.33	< 34.49	< 34.49	
NGC 1400	41.88	< 39.58	< −2.30	< 41.12	41.35	33.88		< 7.93
NGC 1407	43.61	41.31	−2.30	42.40	41.79	36.50		< 9.19
NGC 1497	43.40	< 41.57	< −1.83		< 43.43	37.55	36.87	9.12
NGC 1510	42.05	< 40.14	< −1.91	< 42.17	42.55	< 35.54		8.02
NGC 1553	43.42	40.90	−2.52	42.18	41.75	< 35.52		< 9.52
NGC 1574	43.12	< 40.59	< −2.53	41.95	41.51	< 35.52		
NGC 1600	44.01	41.95	−2.06	< 42.82	42.22	37.03		< 10.59
NGC 1947	42.78	< 40.30	< −2.48	42.00	42.28	35.61		
NGC 2314	43.63	< 41.41	< −2.22	< 42.99	42.41	38.48	36.54	< 10.05
NGC 2300	43.50	41.51	−1.99	42.63	< 41.86	35.02	35.02	< 9.72
NGC 2444	43.39	< 41.65	< −1.74	< 43.53	43.73	< 37.15		< 10.17
NGC 2562	43.58	< 41.59	< −1.99	< 43.27	42.66	< 36.91		< 9.12
NGC 2563	43.70	42.12	−1.58	< 42.98	< 42.79	< 35.26		< 9.08
NGC 2629	43.40	< 41.24	< −2.17	< 42.89	42.51	37.30	37.25	
NGC 2685	42.99	< 40.46	< −2.53	42.11	42.13	35.13		9.71
NGC 2694	42.98	< 41.69	< −1.29			< 37.92		
NGC 2693	43.86	< 41.64	< −2.22	< 43.25	43.01	36.04	35.96	< 10.60
NGC 2716	43.48	< 40.99	< −2.49	43.16	42.78	< 36.51		
NGC 2832	44.25	42.74	−1.51	43.49	43.51	< 37.60		< 10.45
NGC 2859	43.43	< 40.38	< −3.05	< 42.43	42.22	< 35.00	< 34.71	< 8.75
NGC 2911	43.57	< 41.33	< −2.24	< 42.89	42.51	37.54	37.67	9.70
NGC 2974	43.55	40.92	−2.63	< 42.40	42.63	35.96	36.08	9.47
NGC 3078	43.60	41.17	−2.43			37.46	37.33	< 9.53
NGC 3065	43.18	41.38	−1.80	< 42.58	42.73			9.67
NGC 3115	43.01	< 39.95	< −3.06	41.81	< 40.82	< 33.36		< 7.71
NGC 3222	43.69	< 41.63	< −2.06			< 37.03		< 10.19
NGC 3258	43.47	41.49	−1.99	< 42.66	42.45	37.05	35.91	< 9.18
NGC 3377	42.69	< 39.44	< −3.25	41.51	40.80	< 33.78	< 33.78	< 6.99
NGC 3379	43.00	< 40.13	< −2.87	41.91	< 40.77	34.31	33.91	< 6.91
NGC 3384	42.85	< 39.88	< −2.97	41.76	40.91	< 35.07	< 33.71	< 7.26
NGC 3458	43.00	< 41.02	< −1.98	< 42.43	< 41.81		< 34.84	< 9.34
NGC 3516	43.56	42.16	−1.40	43.46	42.95	36.56	36.56	< 9.78
NGC 3585	43.66	40.37	−3.29	42.40	< 41.53	< 34.94		< 9.89
NGC 3607	43.48	40.88	−2.60			35.38	35.25	< 8.25
NGC 3608	43.30	40.50	−2.80			34.88	< 34.75	< 8.11
NGC 3818	43.00	< 40.98	< −2.03	< 42.62	< 41.70	< 34.99	< 34.81	< 9.59
NGC 3894	43.49	41.52	−1.97	< 42.85	42.46	38.24	38.29	
NGC 3923	43.82	41.35	−2.47	42.60	< 41.87	35.67	< 34.95	< 9.97
NGC 3990	42.53	< 40.43	< −2.11	< 41.99	41.56			
NGC 3998	43.38	41.94	−1.44	42.48	42.17	36.82	36.63	9.26
NGC 4105	43.48	40.91	−2.57	< 42.36	42.23	35.62		9.72
NGC 4168	42.88	40.30	−2.59	< 42.24	41.71	35.24	35.29	
NGC 4203	42.64	40.96	−1.68	< 41.74	41.75	35.33	35.23	9.20
NGC 4215	43.19	< 40.89	< −2.30	< 42.80	< 42.02	< 36.28	< 34.99	< 9.06
NGC 4251	42.64	< 39.55	< −3.09	< 41.65	< 40.85	< 34.24	< 33.87	< 7.50
NGC 4261	43.85	41.70	−2.15	43.01	41.70	39.20	37.78	< 10.03
NGC 4267	43.05	< 40.29	< −2.76	< 42.04	41.95	< 36.16	< 34.35	< 8.22
NGC 4291	43.35	41.34	−2.01	< 42.31	< 41.55	< 34.60	< 34.83	
NGC 4340	42.99	< 40.32	< −2.67	< 42.00	41.46		< 34.35	< 8.09
NGC 4350	43.01	< 40.16	< −2.85	42.29	41.93	< 35.61	< 34.35	< 8.16
NGC 4365	43.53	40.42	−3.11	42.32	41.70	< 34.34	< 34.29	< 7.90
NGC 4386	43.20	< 40.39	< −2.81	< 42.37	< 41.76		< 34.80	< 9.46
NGC 4374	43.67	41.16	−2.51	42.47	41.95	38.10	36.89	< 9.12
NGC 4382	43.73	40.72	−3.01	< 42.22	< 41.26	< 34.64	< 34.35	< 8.27
NGC 4387	42.67	< 40.53	< −2.14	< 42.14	< 41.62	< 34.64	< 34.37	< 7.77
NGC 4406	43.76	42.24	−1.52	42.32	41.40	< 34.42	< 34.37	8.35

TABLE 1B—*Continued*

Name	log(L_B) erg/sec	log(L_X) erg/sec	log(L_X/L_B)	log(L_{12}) erg/sec	log(L_{100}) erg/sec	log(L_6) erg/sec	log(L_{6co}) erg/sec	log(M_{HI}) $M_\odot$
NGC 4417	42.94	< 41.06	< −1.88	< 42.10	< 41.44	< 35.61	< 34.23	< 8.13
NGC 4425	42.65	< 40.25	< −2.40	< 42.14	< 41.58	< 35.59	< 34.35	< 7.98
NGC 4435	43.08	< 40.52	< −2.56	42.22	42.56		34.72	< 8.12
NGC 4458	42.69	40.22	−2.47	42.10	< 41.52	< 34.64	< 34.35	< 7.78
NGC 4459	43.17	< 40.40	< −2.77	42.66	42.57	35.02	34.54	< 8.42
NGC 4467	41.69	< 39.69	< −2.00					
NGC 4472	44.04	42.06	−1.98	42.42	< 41.39	37.04	36.40	< 7.89
NGC 4473	43.34	40.52	−2.82	42.57	< 41.40	< 34.52	< 34.71	< 8.14
NGC 4474	42.69	< 40.24	< −2.45	< 42.19	< 41.32	< 35.58	< 34.35	< 8.22
NGC 4479	42.48	< 40.10	< −2.38	< 42.14	< 41.54		< 34.35	< 8.14
NGC 4526	43.53	40.14	−3.39	42.79	43.26		35.13	< 8.12
NGC 4507	43.50	< 41.72	< −1.78	43.66	43.55			10.14
NGC 4550	42.83	< 40.20	< −2.63	< 41.90	41.28	< 34.52	< 34.35	< 8.37
NGC 4551	42.71	< 40.38	< −2.33	< 42.07	< 41.56	< 34.64	< 34.35	7.35
NGC 4552	43.45	40.92	−2.53	42.22	41.61	36.67	36.67	< 8.10
NGC 4564	43.02	< 40.19	< −2.83	< 42.16	< 41.64	< 34.52	< 34.35	< 7.86
NGC 4578	42.95	< 40.39	< −2.57	< 42.22	< 41.41	< 35.73	< 34.35	< 7.83
NGC 4589	43.55	< 40.66	< −2.89	< 42.62	42.22	36.51	36.47	< 9.71
NGC 4621	43.50	< 40.43	< −3.07	42.49	< 41.34	35.42	< 34.48	< 8.41
NGC 4638	42.95	40.22	−2.73	< 41.94	< 41.24	< 34.64	< 34.35	< 8.18
NGC 4636	43.58	41.99	−1.59	42.43	< 41.61	36.30	36.09	< 8.45
NGC 4649	43.83	41.61	−2.22	42.70	42.30	36.02	35.91	< 8.73
NGC 4645	43.63	< 40.90	< −2.73	< 43.06	43.00	< 36.60		
NGC 4697	44.01	40.97	−3.04	42.86	42.27	< 34.70	< 34.72	< 10.07
NGC 4754	43.20	< 40.13	< −3.07	< 42.04	< 41.43		< 34.35	< 8.27
NGC 4753	43.34	40.08	−3.26	42.58	42.75	< 34.03	< 34.14	< 9.47
NGC 4756	43.48	42.06	−1.42	< 43.13	< 42.58	36.82		
NGC 4762	43.26	40.52	−2.74	42.29	< 41.27	< 34.94	< 34.12	< 8.11
NGC 4782	43.66	41.77	−1.89	< 43.18	< 42.87	39.04	38.80	< 10.97
IC 3896	43.33	< 41.22	< −2.11	< 42.54	< 42.31	< 36.23		
NGC 4880	42.68	< 40.32	< −2.36	< 41.79	< 41.47	< 34.58		< 7.56
NGC 5044	43.75	43.17	−0.58	43.02	41.78	36.85		< 9.57
NGC 5077	43.52	41.07	−2.45	< 43.04	43.28	37.63	37.35	< 9.51
NGC 5084	43.38	41.21	−2.17	< 42.69	42.70	36.56		10.56
NGC 5102	42.21	< 39.11	< −3.10	40.68	40.96	33.23	< 33.18	8.73
NGC 5128	44.05	41.47	−2.58	43.44	43.57	38.67	37.42	9.53
NGC 5195	43.05	39.79	−3.26	42.46	< 41.56	< 36.03		< 9.35
IC 4296	44.12	41.98	−2.14	< 42.98	42.23	38.88	37.92	
IC 4329	43.86	< 42.13	< −1.73	< 43.06	42.99	35.50	35.52	
NGC 5322	43.95	< 41.04	< −2.91	< 42.47	42.44	36.81	36.34	< 9.59
NGC 5318	43.51	< 41.37	< −2.14	< 43.15	43.13	37.68	37.52	< 9.51

Name	log(L_B) erg/sec	log(L_X) erg/sec	log(L_X/L_B)	log(L_{12}) erg/sec	log(L_{100}) erg/sec	log(L_6) erg/sec	log(L_{6co}) erg/sec	log(M_{HI}) $M_\odot$
NGC 5354	43.64	< 41.33	< −2.31	< 43.04	42.85	36.91	36.30	10.26
NGC 5353	43.65	41.41	−2.24	< 42.60	42.76	36.89	36.88	10.19
NGC 5363	43.59	40.80	−2.80	42.67	42.84	36.87	36.78	8.76
NGC 5485	43.37	< 41.08	< −2.29	< 42.50	42.45	35.18	< 35.22	< 9.65
IC 989	43.70	< 41.85	< −1.85	< 43.73	43.07	38.02		9.50
NGC 5532	44.23	41.93	−2.30	43.50	43.14	39.33	38.04	< 9.79
NGC 5576	43.45	< 40.76	< −2.69	42.38	41.61	< 35.03	< 34.74	< 8.39
IC 1024	42.55	< 40.66	< −1.89	42.98	43.13	36.03	36.04	9.46
NGC 5838	43.54	40.55	−2.99	42.68	42.57	< 36.80	35.40	< 9.06
NGC 5846	43.77	42.11	−1.66	< 42.42	< 41.93	35.99	35.82	< 8.27
NGC 5866	43.34	40.17	−3.18	42.54	43.08	35.67	35.43	< 9.06
NGC 5982	43.77	41.47	−2.30	< 42.74	42.28	< 35.46	< 35.16	
NGC 6027	43.19	< 41.71	< −1.49	< 43.66	43.40			9.87
NGC 6034	43.71	42.46	−1.25			38.78	< 38.86	
NGC 6146	44.03	< 42.27	< −1.76	< 43.80	< 43.24	38.30	38.16	< 11.03
NGC 6876	43.66	41.78	−1.88	< 42.87	42.44	< 36.59		
NGC 6880	43.06	< 41.36	< −1.70	42.99	43.31	< 36.58		
NGC 6963	43.04	< 41.25	< −1.79			< 37.38		
NGC 6964	43.45	< 41.13	< −2.32	43.47	43.16	< 37.17		
NGC 7236	43.67	< 41.89	< −1.79			38.70		< 9.30
NGC 7237	43.57	< 42.02	< −1.55			38.83	37.32	< 9.30
NGC 7332	43.21	< 40.51	< −2.70	42.26	41.57	< 36.49		< 8.59
IC 1459	43.53	41.01	−2.52	42.50	42.11	37.82	37.79	< 9.34
NGC 7562	43.71	< 41.36	< −2.35	< 42.75	< 42.70	< 35.45	< 35.45	8.49
NGC 7619	43.79	42.00	−1.79	< 43.00	42.63	36.35	36.35	< 9.44
NGC 7626	43.70	41.50	−2.20	< 43.09	< 42.28	37.80	36.92	< 9.13

TABLE 1C

REFERENCES TO TABLE 1A

IRAS references:

1. Knapp *et al.*, 1989
2. Knapp *et al.*, 1989, blended:
   NGC 2832 with NGC 2831
   NGC 4638 with NGC 4637
   NGC 6876 with NGC 6877
3. Not observed by IRAS - Lonsdale *et al.*, 1985
4. Rice *et al.*, 1988
5. Fullmer and Lonsdale 1989
6. Fullmer and Lonsdale 1989, blended:
   NGC 1510 with NGC 1512
   NGC 2444 with NGC 2445
   NGC 6027 in a Zwicky Group
   NGC 127, NGC 130 and NGC 128
7. Condon *et al.*, 1991
8. Haynes *et al.*, 1990
9. Vereshchagin *et al.*, 1989

Radio continuum references:

10. FGT
11. Roberts *et al.*, 1991
12. Wrobel 1991
13. Wrobel and Heeschen 1988
14. Ekers and Ekers 1973
15. Fabbiano *et al.*, 1987
16. Wright 1974
17. Sulentic 1976
18. Hummel *et al.*, 1984
19. Haynes *et al.*, 1975
20. Disney and Wall 1977
21. Calvani *et al.*, 1989
22. Hummel *et al.*, 1991
23. Condon *et al.*, 1991

Radio core references:

24. Bridle and Fomalont 1978
25. Wrobel and Heeschen 1984
26. Geldzahler and Fomalont 1978
27. Killeen *et al.*, 1988
28. Stanger and Warwick 1986
29. Burns *et al.*, 1983
30. Killeen *et al.*, 1986
31. Birkinshaw and Davies 1985
32. Fabbiano *et al.*, 1984
33. Feretti *et al.*, 1984
34. Wrobel and Heeschen 1991
35. Bridle and Perley 1984
36. Impey and Gregorini, 1993
37. Sadler *et al.*, 1989
38. Wilkinson *et al.*, 1987
39. Neff and Hutchings 1992
40. Ekers *et al.*, 1989

HI references:

41. Roberts *et al.*, 1991
42. Huchtmeier and Richter 1989
43. Huchtmeier and Richter 1989:
    NGC 7236 blended with NGC 7237
44. Eder *et al.*, 1991
45. van Gorkom *et al.*, 1989: HI in absorption
46. Bottinelli *et al.*, 1990

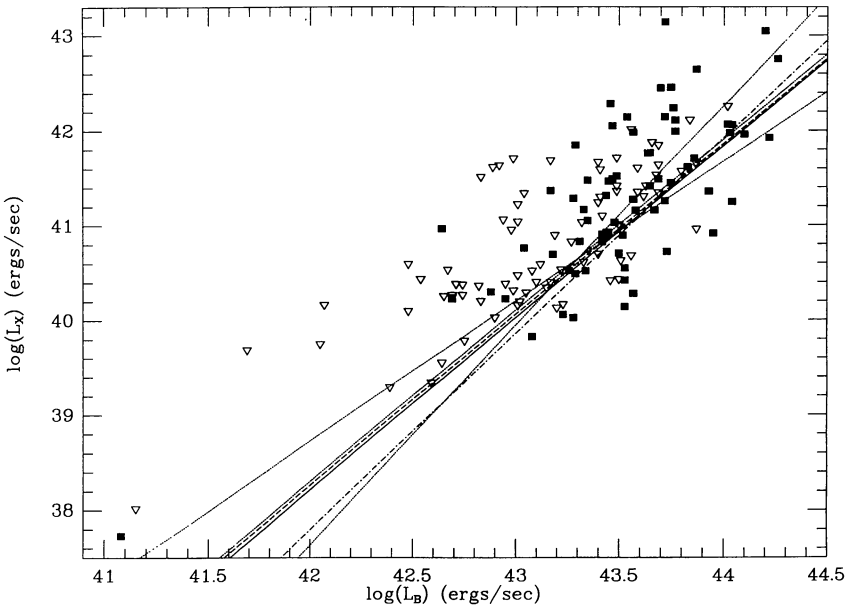

FIG. 1.—L_X vs. L_B for all E and S0 galaxies observed by *Einstein*. Filled squares show X-ray detections; open downward-pointing triangles show 3 σ X-ray upper limits. Fit lines are from the E-M algorithm (*solid line*), the Buckley-James (B-J) algorithm (*dashed line*), Schmitt's binning method (*dotted lines,* showing both fits—L_X on L_B and L_B on L_X—as well as their bisector), and the E-M algorithm applied to the sample with Local Group dE galaxies removed (*dot-dash line*).

TABLE 2A

CORRELATION TESTS ON THE E+S0 SAMPLE

Parameter	L_X		L_B		L_X/L_B	
	N_{tot}[a]	N_{lim}[b]	N_{tot}[a]	N_{lim}[b]	N_{tot}[a]	N_{lim}[b]
L_X[c]	...	...	148	78	148	78
			63.555	$<10^{-4}$	48.283	$<10^{-4}$
			8.656	$<10^{-4}$	7.449	$<10^{-4}$
			0.687	$<10^{-4}$	0.619	$<10^{-4}$
L_X	...	...	146	77	146	77
			76.136	$<10^{-4}$	56.671	$<10^{-4}$
			8.520	$<10^{-4}$	7.283	$<10^{-4}$
			0.695	$<10^{-4}$	0.608	$<10^{-4}$
L_B	...	...	...	...	146	77
					28.642	$<10^{-4}$
					5.358	$<10^{-4}$
					0.446	$<10^{-4}$
L_{12}	132	27, 19, 48	132	75	132	27, 19, 48
	...	...	51.002	$<10^{-4}$	...	...
	4.569	$<10^{-4}$	5.918	$<10^{-4}$	2.499	0.0124
	0.412	$<10^{-4}$	0.486	$<10^{-4}$	0.238	0.0064
L_{12}/L_B	132	27, 19, 48	132	75	132	27, 19, 48
	...	...	2.943	0.0863	...	...
	1.403	0.1605	1.607	0.1080	0.846	0.3977
	−0.091	0.2952	−0.156	0.0736	−0.081	0.3513
L_{100}	133	21, 42, 26	133	47	133	21, 42, 26
	...	...	17.992	$<10^{-4}$	...	...
	1.700	0.0891	4.425	$<10^{-4}$	0.720	0.4715
	0.198	0.0227	0.383	$<10^{-4}$	0.105	0.2277
L_{100}/L_B	133	21, 42, 26	133	47	133	21, 42, 26
	...	...	0.064	0.8004	...	...
	1.665	0.0959	0.202	0.8399	1.263	0.2065
	−0.105	0.2255	−0.014	0.8714	−0.091	0.2949
L_6	131	23, 26, 38	131	61	131	23, 26, 38
	...	...	32.121	$<10^{-4}$	...	...
	5.646	$<10^{-4}$	6.535	$<10^{-4}$	4.472	$<10^{-4}$
	0.492	$<10^{-4}$	0.541	$<10^{-4}$	0.425	$<10^{-4}$
L_6/L_B	131	23, 26, 38	131	61	131	23, 26, 38
	...	...	14.349	0.0002	...	...
	4.778	$<10^{-4}$	4.870	$<10^{-4}$	4.061	$<10^{-4}$
	0.401	$<10^{-4}$	0.393	$<10^{-4}$	0.384	$<10^{-4}$
L_{6cm}	99	17, 17, 30	99	47	99	17, 17, 30
	...	...	31.506	$<10^{-4}$	...	...
	5.398	$<10^{-4}$	5.775	$<10^{-4}$	4.436	$<10^{-4}$
	0.565	$<10^{-4}$	0.585	$<10^{-4}$	0.481	$<10^{-4}$
L_6[d]	99	15, 21, 26	99	41	99	15, 21, 26
	...	...	35.657	$<10^{-4}$	...	...
	5.406	$<10^{-4}$	6.473	$<10^{-4}$	4.171	$<10^{-4}$
	0.534	$<10^{-4}$	0.608	$<10^{-4}$	0.441	$<10^{-4}$
M_{HI}	115	45, 15, 44	115	89	115	45, 15, 44
	...	...	0.898	0.3434	...	...
	1.097	0.2728	1.049	0.2940	1.226	0.2202
	0.204	0.0294	0.177	0.0582	0.208	0.0265
M_{HI}/L_B	115	45, 15, 44	115	89	115	45, 15, 44
	...	...	0.894	0.3584	...	...
	0.109	0.9135	1.242	0.2143	0.769	0.4422
	0.018	0.8507	−0.076	0.4199	0.102	0.2778

[a] The values in rows 2–4 of each group in these columns are the test scores for the Cox-Hazard, Kendall's τ, and Spearman rank correlation tests, respectively.

[b] The three values for N_{lim} in the first row of each group in these columns are respectively the number of limit points in the row variable, the number in the column variable, and the number of double limits. The numbers listed in rows 2–4 are probabilities.

[c] This entry shows the analysis for the sample including M32 and NGC 205, as an example of the effects of these two galaxies. They are not included in the remaining analysis in the table.

[d] Correlations with total 6 cm luminosity using only the 6 cm core sample.

TABLE 2B

CORRELATION TESTS ON THE ELLIPTICAL GALAXIES

	L_X		L_B		L_X/L_B	
	N_{tot}	N_{lim}	N_{tot}	N_{lim}	N_{tot}	N_{lim}
L_X	...	...	72	30	72	30
			32.925	$<10^{-4}$	23.027	$<10^{-4}$
			5.973	$<10^{-4}$	5.128	$<10^{-4}$
			0.687	$<10^{-4}$	0.600	$<10^{-4}$
L_B	...	...	...	...	72	30
					12.062	0.0005
					3.754	0.0002
					0.443	0.0002
L_{12}	62	18, 5, 18	62	36	62	18, 5, 18
	...	...	25.291	$<10^{-4}$	...	...
	3.236	0.0012	4.109	$<10^{-4}$	1.816	0.0693
	0.468	0.0003	0.518	0.0001	0.269	0.0359
L_{12}/L_B	62	18, 5, 18	62	36	62	18, 5, 18
	...	...	4.615	0.0317	...	...
	0.826	0.4089	1.778	0.0755	0.176	0.8599
	−0.098	0.4448	−0.230	0.0730	−0.060	0.6393
L_{100}	62	14, 14, 9	62	23	62	14, 14, 9
	...	...	7.782	0.0053	...	...
	1.224	0.2211	3.236	0.0012	0.471	0.6379
	0.196	0.1262	0.430	0.0008	0.109	0.3942
L_{100}/L_B	62	14, 14, 9	62	23	62	14, 14, 9
	...	...	0.675	0.4113	...	...
	1.510	0.1310	0.115	0.9086	1.129	0.2587
	−0.177	0.1669	−0.010	0.9382	−0.133	0.3005
L_6	69	12, 12, 15	69	27	69	12, 12, 15
	...	...	18.327	$<10^{-4}$	...	...
	3.796	0.0001	4.665	$<10^{-4}$	2.951	0.0032
	0.492	0.0001	0.551	$<10^{-4}$	0.380	0.0017
L_6/L_B	69	12, 12, 15	69	27	69	12, 12, 15
	...	...	7.534	0.0061	...	...
	3.264	0.0011	3.322	0.0009	2.836	0.0046
	0.387	0.0014	0.385	0.0015	0.340	0.0051

NOTE.—Table entries as defined in notes to Table 2A.

to be addressed is whether one can identify "dependent" and "independent" variables. We refer readers to the work of Isobe et al. (1990) and Feigelson & Babu (1992a) for general discussions of this and other issues relating to the application of linear regression to various sorts of data. Our use of the survival analysis regression algorithms has led us to conclude that it is best to treat the uncensored variable as the "independent" variable when using the E-M or B-J algorithms on singly censored data sets. These algorithms are explicitly designed to address problems in which there is censoring in the dependent variable. If the censored variable is used as the independent variable, the algorithms will yield zero points that are seriously in error (the slope computations, however, appear quite robust). When using Schmitt's method (on either singly or doubly censored data sets), we do not define an "independent" variable. Instead, we use the bisector of the fits of $(X \mid Y)$ and $(Y \mid X)$ (see Isobe et al. 1990 for background).

There are two objects relatively isolated in the lower left corner of Figure 1. These are the Local Group dwarf galaxies M32 and NGC 205. It is fairly clear that these objects are quite different sorts of galaxies, in terms of their fundamental physical properties, than the more luminous systems that dominate our sample (Kormendy 1985; Bender, Paquet, & Nieto 1991). They are also positioned in the L_X-L_B plane so as to have a large statistical leverage on our analysis. We have therefore repeated our analysis without these systems. The results of the correlation tests (see Table 2A) show somewhat stronger statistical relationships with the Local Group dwarf ellipticals (dE's) removed. The results of the regression analysis are shown in Table 3A, and the E-M line is plotted in Figure 1. While the L_X-L_B slope is steeper if the dwarfs are excluded, the difference is only at the $\sim 1\ \sigma$ level. In general, we find no significant differences in our results with or without the Local Group dwarfs. Since they are fundamentally different sorts of galaxies than the bulk of our sample, we choose to exclude them in the rest of our analysis. Also, for these reasons, we will not use these two objects in comparisons between the E and S0 subsamples below.

Another useful way of presenting the relationship between optical and X-ray emission for our sample is to plot log L_X

TABLE 2C

CORRELATION TESTS ON THE S0 GALAXIES

	L_X		L_B		L_X/L_B	
	N_{tot}	N_{lim}	N_{tot}	N_{lim}	N_{tot}	N_{lim}
L_X	...	...	74	47	74	47
			38.461	$<10^{-4}$	28.350	$<10^{-4}$
			5.016	$<10^{-4}$	4.174	$<10^{-4}$
			0.611	$<10^{-4}$	0.528	$<10^{-4}$
L_B	...	...	...	...	74	47
					10.984	0.0009
					2.652	0.0080
					0.351	0.0027
L_{12}	70	9, 14, 30	70	39	70	9, 14, 30
	...	...	22.851	$<10^{-4}$	...	...
	3.259	0.0011	4.257	$<10^{-4}$	1.424	0.1544
	0.376	0.0018	0.454	0.0002	0.198	0.0994
L_{12}/L_B	70	9, 14, 30	70	39	70	9, 14, 30
	...	...	0.158	0.6907	...	...
	0.385	0.7005	0.089	0.9288	0.225	0.8223
	−0.004	0.9733	−0.025	0.8338	−0.050	0.6774
L_{100}	71	7, 28, 17	71	24	71	7, 28, 17
	...	...	15.590	0.0001	...	...
	2.255	0.0242	4.328	$<10^{-4}$	1.142	0.2533
	0.313	0.0087	0.470	0.0001	0.185	0.1225
L_{100}/L_B	71	7, 28, 17	71	24	71	7, 28, 17
	...	...	1.606	0.2051	...	...
	0.555	0.5791	1.359	0.1743	0.415	0.6784
	0.131	0.2745	0.162	0.1743	0.045	0.7037
L_6	62	11, 14, 23	62	34	62	11, 14, 23
	...	...	12.309	0.0005	...	...
	3.568	0.0004	3.767	0.0002	2.254	0.0242
	0.454	0.0004	0.426	0.0009	0.355	0.0056
L_6/L_B	62	11, 14, 23	62	34	62	11, 14, 23
	...	...	5.241	0.0221	...	...
	3.069	0.0021	2.724	0.0064	1.968	0.0491
	0.393	0.0021	0.303	0.0181	0.337	0.0085

NOTE.—Table entries as defined in notes to Table 2A.

against log (L_X/L_B). There is an obvious trend in such a plot (see Fig. 2) for L_X to increase with increasing L_X/L_B. Our statistical analysis confirms this (see Table 2A). The results of the regressions are given in Table 3A and plotted in Figure 2. We find that the relationship between X-ray and optical emission from early-type systems is steep [$L_X \propto (L_X/L_B)^{\sim 1.8}$], and is close to the relationship expected from the L_X-L_B relationship [$L_X \propto (L_X/L_B)^2$]. The slopes are steeper than slope 1 by more than 6 σ. The slope 0 case, appropriate for L_X/L_B = constant (i.e., slope 1 in the L_X-L_B plane) is ruled out at more than 13 σ.

We have also tested for a possible relationship between L_B and L_X/L_B. There is statistical evidence for a correlation between these parameters (see Table 2), but it is weaker than that between L_X and L_X/L_B. Furthermore, it appears to be driven by the relatively small range in L_B among the X-ray detections in our sample, and the typically larger values of L_X for the optically brightest galaxies. There appears to be no additional information in this plane that is not more apparent in the L_X-L_B or L_X-L_X/L_B planes.

To investigate this point further, we must move beyond simple bivariate analysis. This study deals with a large, multiparametric data set. Given this, it is important to examine the interrelationships between the various observables for our sample. A number of different multivariate analysis tools have been applied to astrophysical problems in the last five or six years (see Feigelson & Babu 1992b). One, that was applied to a preliminary sample of *Einstein*-selected galaxies (Fabbiano et al. 1988), is the partial Spearman rank analysis (Kendall & Stuart 1976). This analysis builds a matrix of bivariate Spearman rank statistics, and then tests the correlation between subsamples of the parameters in the matrix set while holding all other variables in the matrix set constant. Because our sample contains upper limits for many variables, we generally use the results from the modified Spearman rank analysis to provide inputs for the matrices of bivariate Spearman rank statistics. These matrices are then subject to the partial rank analysis as detailed in Kendall & Stuart (1976).

In this initial case, we tested the triplet of L_X, L_B, and L_X/L_B. The numerical results of the partial rank analysis are shown in

TABLE 3A

REGRESSION ANALYSIS ON E+S0 SAMPLE

X	Y	Slope[a]	σ_S	Intercept	σ_I
L_B[b] ($N = 148$, $N_{ul} = 0$)	L_X ($N_{ul} = 78$)	1.81	0.15	−37.80	6.31
		1.80	0.16	−37.29	...
		1.80	0.11	−37.30	3.87
L_B ($N = 146$, $N_{ul} = 0$)	L_X ($N_{ul} = 77$)	2.01	0.18	−46.68	7.93
		2.00	0.22	−46.17	...
		2.02	0.13	−46.61	4.52
L_X/L_B ($N = 146$, $N_{ul} = 0$)	L_X ($N_{ul} = 77$)	1.79	0.13	+45.08	0.29
		1.84	0.12	+45.11	...
		1.75	0.09	+45.30	0.21
L_B ($N = 132$, $N_{ul} = 0$)	L_{12} ($N_{ul} = 75$)	0.83	0.11	+6.33	4.59
		0.81	0.13	+7.36	...
		1.05	0.10	−3.20	3.46
L_{12} ($N = 132$, $N_{ul} = 75$)	L_X ($N_{ul} = 67$)	...	...	...	...
		...	...	...	...
		1.53	0.12	−23.95	3.89
L_X/L_B ($N = 132$, $N_{ul} = 67$)	L_{12} ($N_{ul} = 75$)	...	...	...	...
		...	...	...	...
		0.82	0.17	+44.27	3.44
L_B ($N = 131$, $N_{ul} = 0$)	L_{12} ($N_{ul} = 75$)	2.79	0.40	−85.68	17.26
		2.87	0.33	−89.20	...
		3.67	0.38	−123.63	12.20
L_X ($N = 131$, $N_{ul} = 64$)	L_6 ($N_{ul} = 61$)	...	...	...	...
		...	...	...	...
		1.61	0.06	−29.72	4.00
L_X/L_B ($N = 131$, $N_{ul} = 64$)	L_6 ($N_{ul} = 61$)	...	...	...	...
		...	...	...	...
		2.32	0.28	+41.63	2.16
L_B ($N = 131$, $N_{ul} = 0$)	L_6/L_B ($N_{ul} = 61$)	1.72	0.39	−82.41	16.82
		1.81	0.33	−86.46	...
		2.73	0.54	−126.31	16.88
L_X ($N = 131$, $N_{ul} = 64$)	L_6/L_B ($N_{ul} = 61$)	...	...	...	...
		...	...	...	...
		1.18	0.18	−55.72	5.51
L_X/L_B ($N = 131$, $N_{ul} = 64$)	L_6/L_B ($N_{ul} = 61$)	...	...	...	...
		...	...	...	...
		2.23	0.38	−2.30	0.79
L_X ($N = 99$, $N_{ul} = 47$)	L_{6co} ($N_{ul} = 47$)	...	...	...	...
		...	...	...	...
		1.53	0.12	−26.86	3.72
L_X/L_B ($N = 99$, $N_{ul} = 47$)	L_{6co} ($N_{ul} = 47$)	...	...	...	...
		...	...	...	...
		2.92	0.33	+42.77	2.49
L_X ($N = 99$, $N_{ul} = 47$)	L_6[c] ($N_{ul} = 41$)	...	...	...	...
		...	...	...	...
		1.57	0.21	−28.11	6.41
L_X/L_B ($N = 99$, $N_{ul} = 47$)	L_6[c] ($N_{ul} = 41$)	...	...	...	...
		...	...	...	...
		2.76	0.43	+40.81	2.46

[a] Numbers in rows 1–3 of each group in the following columns refer to results using the E-M algorithm, the B-J algorithm, and the Schmitt method, respectively.

[b] This entry shows the analysis for the sample including M32 and NGC 205, as an example of the effects of these two galaxies. They are not included in the remaining analysis in the table.

[c] Regressions with total 6 cm luminosity using only the 6 cm core sample.

TABLE 3B

REGRESSION ANALYSIS ON THE ELLIPTICAL GALAXIES

X	Y	Slope	σ_S	Intercept	σ_I
L_B ($N = 72$, $N_{ul} = 0$)	L_X ($N_{ul} = 30$)	1.95	0.25	−43.94	11.04
		1.93	0.29	−42.99	...
		1.84	0.16	−39.26	5.44
L_X/L_B ($N = 72$, $N_{ul} = 0$)	L_X ($N_{ul} = 30$)	1.88	0.19	+45.30	0.42
		1.90	0.17	+45.31	...
		1.75	0.19	+45.26	0.37
L_B ($N = 62$, $N_{ul} = 0$)	L_{12} ($N_{ul} = 36$)	0.84	0.12	+5.87	5.36
		0.84	0.18	+5.97	...
		0.94	0.10	+1.63	3.83
L_{12} ($N = 62$, $N_{ul} = 36$)	L_X ($N_{ul} = 23$)	...	...	...	...
		...	...	...	...
		1.93	0.21	−40.73	6.87
L_B ($N = 69$, $N_{ul} = 0$)	L_6 ($N_{ul} = 27$)	3.09	0.60	−98.56	26.30
		3.20	0.53	−103.31	...
		3.62	0.48	−121.31	15.93
L_X ($N = 69$, $N_{ul} = 27$)	L_6 ($N_{ul} = 27$)	...	...	...	...
		...	...	...	...
		1.75	0.19	−35.75	6.04
L_X/L_B ($N = 69$, $N_{ul} = 27$)	L_6 ($N_{ul} = 27$)	...	...	...	...
		...	...	...	...
		2.19	0.65	+41.11	3.47
L_B ($N = 69$, $N_{ul} = 0$)	L_6/L_B ($N_{ul} = 27$)	1.87	0.59	−81.15	25.89
		1.98	0.52	−93.91	...
		2.44	0.60	−113.76	18.98
L_X ($N = 69$, $N_{ul} = 27$)	L_6/L_B ($N_{ul} = 27$)	...	...	...	...
		...	...	...	...
		1.06	0.24	−50.77	7.19
L_X/L_B ($N = 69$, $N_{ul} = 27$)	L_6/L_B ($N_{ul} = 27$)	...	...	...	...
		...	...	...	...
		1.64	0.47	−3.50	0.96

NOTE.—Table entries as defined in notes to Table 3A.

Table 4A. In brief, they confirm the results of the bivariate tests that there are strong relationships between L_X and L_B and between L_X and L_X/L_B, but no significant relationship between L_B and L_X/L_B.

3.1.2. *Luminosity Dependence of the Correlations*

The recent study of Kim, Fabbiano, & Trinchieri (1992a,b) shows that high-luminosity early-type galaxies typically have X-ray spectra best fitted by thermal emission from a ~1 keV gas. The emission from lower luminosity ellipticals, however, is better fitted by a harder (≳3 keV) bremsstrahlung spectrum, similar to that seen for spirals (Kim et al. 1992b). The lowest L_X/L_B group also has a very soft (~0.2 keV) component (Kim et al. 1992b; Fabbiano, Kim, & Trinchieri 1994), the nature of which is still unclear (see Pellegrini & Fabbiano 1994). A plausible explanation for this is that only the high-luminosity systems are massive enough to retain their hot ISM (Canizares, Fabbiano, & Trinchieri 1987; FGT). The X-ray emission from low-luminosity systems would thus be largely due to stellar X-ray sources. In this case it seems likely that the functional dependence of L_B on L_X will change with increasing luminosity. To test this point, we made subsamples of our data set by imposing limits from both above and below on L_X and L_B, and made fits to the resulting subsamples. The clearest results came from imposing decreasing maxima on L_X. Decreasing the maximum log L_X (in ergs s^{-1}) from 43.2 (the full sample) down to 40.5 results in a decrease in the slope of the L_X-L_B relation from 1.8 ± 0.15 to 1.0 ± 0.2. These values are different at roughly the 3 σ level, arguing strongly that there are at least two distinct physical processes producing the X-ray emission from low-luminosity (log $L_X \lesssim 40.5$) and high-luminosity (log $L_X \gtrsim 40.5$) systems (see also FGT). This conclusion is reinforced by the spectral differences found by Kim et al. (1992b) between high- and low-L_X systems. We note that evaluating the L_X-L_B relation for only the more luminous galaxies results in an even steeper slope ($\approx 2.0 \pm 0.2$ for log $L_B \gtrsim 42$), as expected from the above result. This steepening is statistically marginal (~1 σ). It is nonetheless interesting that this slope 2 behavior at high L_B is predicted by the instability-cycle models of Kritsuk (1992). However, a steep L_X-L_B trend is also reproduced for very different physical reasons by the hydrodynami-

TABLE 3C

REGRESSION ANALYSIS ON THE S0 GALAXIES

X	Y	Slope	σ_S	Intercept	σ_I
$L_B (N = 74, N_{ul} = 0)$	$L_X (N_{ul} = 47)$	1.87	0.26	−40.63	11.45
		1.83	0.35	−38.98	...
		1.92	0.20	−42.51	6.91
$L_X/L_B (N = 74, N_{ul} = 0)$	$L_X (N_{ul} = 47)$	2.15	0.39	+46.65	1.22
		2.20	0.60	+46.73	...
		1.83	0.18	+45.64	0.47
$L_B (N = 70, N_{ul} = 0)$	$L_{12} (N_{ul} = 39)$	0.88	0.17	+3.95	7.50
		0.86	0.20	+4.98	...
		1.33	0.19	−15.27	6.30
$L_{12} (N = 70, N_{ul} = 39)$	$L_X (N_{ul} = 44)$	...	...	...	...
		...	...	...	...
		1.17	0.15	−8.86	4.98
$L_{100} (N = 71, N_{ul} = 24)$	$L_X (N_{ul} = 45)$	...	...	...	...
		...	...	...	...
		0.85	0.23	+7.85	6.94
$L_B (N = 62, N_{ul} = 0)$	$L_6 (N_{ul} = 34)$	2.32	0.52	−65.19	22.41
		2.37	0.43	−67.21	...
		3.24	0.72	−104.80	22.86
$L_X (N = 62, N_{ul} = 37)$	$L_6 (N_{ul} = 34)$	...	...	...	...
		...	...	...	...
		1.61	0.28	−29.75	8.58
$L_X/L_B (N = 62, N_{ul} = 37)$	$L_6 (N_{ul} = 34)$	...	...	...	...
		...	...	...	...
		2.52	0.41	+42.16	4.35
$L_B (N = 62, N_{ul} = 0)$	$L_6/L_B (N_{ul} = 34)$	1.38	0.49	−68.02	21.44
		1.42	0.42	−69.75	...
		2.27	0.90	−106.85	27.96
$L_X (N = 62, N_{ul} = 37)$	$L_6/L_B (N_{ul} = 34)$	...	...	...	...
		...	...	...	...
		1.34	0.46	−62.49	13.68
$L_X/L_B (N = 62, N_{ul} = 37)$	$L_6/L_B (N_{ul} = 34)$	...	...	...	...
		...	...	...	...
		1.90	0.62	−2.87	1.27

NOTE.—Table entries as defined in notes to Table 3A.

cal evolution models of Ciotti et al. (1991) for X-ray emission arising from hot gaseous halos around massive early-type galaxies. Both these theories are much more physically developed than the hypothesis presented by Forman et al. (1985) in the first paper to recognize the slope 2 behavior of the L_X-L_B correlation for the most X-ray–luminous early-type galaxies.

We noted above that the relationship between L_X and L_B is shallower for lower maximum L_X values, becoming consistent with slope 1 for galaxies with log $L_X < 40.5$. The simple interpretation of this predicts that the relationship between L_X and L_X/L_B should disappear for a subsample with a maximum L_X of about this value. This is the case: for a sample with log $L_X <$ 40.5, the slope of the regression with log (L_X/L_B) is 1.56 ± 1.38. By evaluating samples of progressively higher minimum L_X, we find that this regression slope converges to unity. This is apparently because the L_B for our sample is more or less constant for the most luminous X-ray galaxies. While systems exist with L_X up to 1.2 dex larger that the cutoff at log $L_X = 42$, the dispersion of log L_B for this sample is only 0.24.

3.1.3. *Comparison with* 7S *Distances*

Donnelly et al. (1990) suggested that use of the D_n-σ distances derived from the work of Faber et al. (1989, hereafter 7S) caused a decrease in the scatter and increases in both the strength of correlation and the slope of the L_X-L_B relationship. Roughly half of our sample (75 of 148) have 7S velocity distances. In Figure 3 we show a plot of our distances taken from P0, and distances from the 7S velocity distances with $H_0 = 50$ km s^{-1} Mpc^{-1}. The best fit (*solid line*), and both individual fits (*dashed lines*), are consistent with the slope 1, intercept 0 line (*dotted line*). There is thus no evidence for a systematic difference between the two sets of distance estimates.

We derived X-ray and optical luminosities for this subsample, using both our distances and the 7S distances, and then tested both samples for correlation between L_X and L_B. For both samples, all three tests indicate a statistical correlation with $P < 10^{-4}$. In keeping with the findings of Donnelly et al., the scores for the correlation tests are higher for the sample

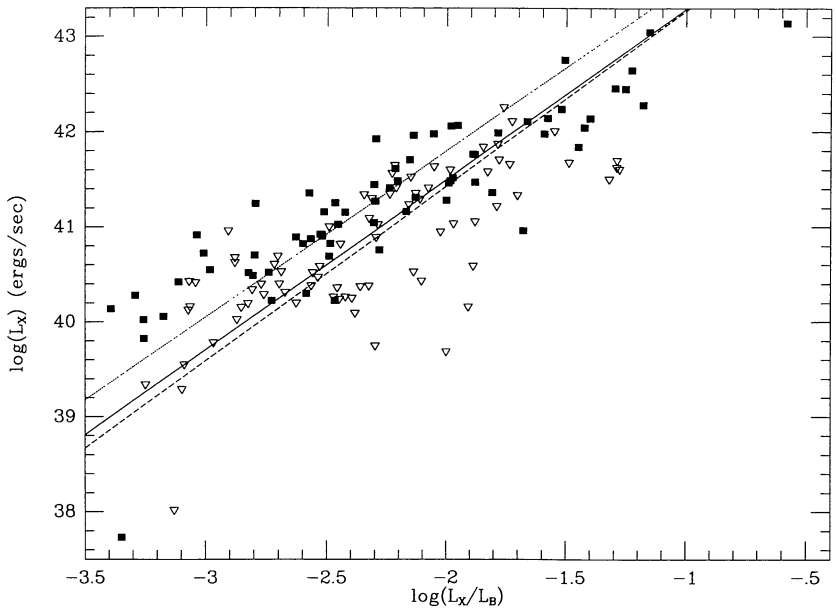

FIG. 2.—L_X vs. L_X/L_B for E and S0 galaxies observed by *Einstein*. Symbols as in Fig. 1. Fit lines are from the E-M algorithm (*solid line*), the B-J algorithm (*dashed line*), and the bisector from Schmitt's method (*dotted line*), all for the sample without the Local Group dwarfs.

with 7S distances. We also computed regression lines for the L_X-L_B relationship using both sets of distances, and both the E-M and B-J algorithms. Figure 4 shows the two scatter plots along with these fits. For distances from P0 we find

$$\log L_X = 2.08(\pm 0.23) \log L_B - 49.45(\pm 10.03), \quad \sigma = 0.61\,, \quad (1a)$$

TABLE 4A

PARTIAL SPEARMAN RANK ANALYSIS: X-RAY PROPERTIES, E+S0 SAMPLES

Test Pair	Held Parameters	Size	Partial Spearman Rank	Probability
L_B-L_X	L_X/L_B	146	0.596	<0.005
	C_{21}	39	0.469	<0.005
	L_X/L_B, C_{21}	39	0.896	<0.005
L_B-L_X/L_B	L_X	146	0.041	0.314
	C_{21}	39	0.021	>0.400
	L_X, C_{21}	39	−0.864	<0.005
L_X-L_X/L_B	L_B	146	0.463	<0.005
	C_{21}	39	0.309	0.032
	L_B, C_{21}	39	0.965	<0.005
L_B-C_{21}	L_X	39	−0.032	>0.400
	L_X/L_B	39	0.179	0.152
	L_X, L_X/L_B	39	−0.226	0.092
L_X-C_{21}	L_B	39	0.398	0.008
	L_X/L_B	39	0.309	0.032
	L_B, L_X/L_B	39	0.336	0.022
L_X/L_B-C_{21}	L_B	39	0.328	0.023
	L_X	39	−0.098	0.279
	L_B, L_X	39	−0.244	0.077

$$\log L_X = 2.07(\pm 0.25) \log L_B - 48.96, \quad \sigma = 0.55\,, \quad (1b)$$

while for distances from 7S we find

$$\log L_X = 2.36(\pm 0.24) \log L_B - 61.62(\pm 10.47), \quad \sigma = 0.58\,, \quad (2a)$$

$$\log L_X = 2.34(\pm 0.25) \log L_B - 60.92, \quad \sigma = 0.50\,, \quad (2b)$$

for the two regression algorithms. Again, we confirm the findings of Donnelly et al. that the scatter about the fit line decreases using the 7S distances, and that the slope of the regression line is formally steeper. We note that the increase in slope is not statistically significant for either method ($\Delta_{EM} = 0.28 \pm 0.33$, $\Delta_{BJ} = 0.27 \pm 0.35$). Thus, while the 7S distances do appear to give marginally better results, this is more than offset by their being available for only half of our sample.

3.1.4. *Correlations with X-Ray Colors*

Detailed analysis of *Einstein* imaging proportional counter (IPC) data for a number of the brightest early-type galaxies has led to the suggestion that these systems have N_H values in excess of the standard Galactic values (Kim et al. 1992a). Kim et al. (1992b) have defined the index C_{21}, the ratio of the counts in the energy range 0.8–1.36 keV (C_2) to the counts in the energy range 0.16–0.8 keV (C_1). Thus it measures the strength of the low-energy cutoff, and should therefore directly measure N_H in the absence of large ranges in the temperatures or abundances of the X-ray–emitting gas from galaxy to galaxy. However, it would also be sensitive to differences in spectral shape due to abundance variations, or multiple temperature components for a fixed N_H. Recent *ROSAT* results reveal differing spectral shapes for early-type galaxies over a range in

TABLE 4B

PARTIAL SPEARMAN RANK ANALYSIS: X-RAY PROPERTIES, SEPARATE E AND S0 SAMPLES

Test Pair	Held Parameters	Sample	Size	Partial Spearman Rank	Probability
L_B-L_X	L_X/L_B	E	72	0.587	<0.005
	L_X/L_B	S0	74	0.535	<0.005
	C_{21}	E	24	0.486	0.010
	C_{21}	S0	15	0.278	0.181
	L_X/L_B, C_{21}	E	24	0.880	<0.005
	L_X/L_B, C_{21}	S0	15	0.594	0.018
L_B-L_X/L_B	L_X	E	72	0.053	0.332
	L_X	S0	74	0.042	0.362
	C_{21}	E	24	0.127	0.282
	C_{21}	S0	15	−0.095	0.375
	L_X, C_{21}	E	24	−0.842	<0.005
L_X-L_X/L_B	L_B	E	72	0.454	<0.005
	L_B	S0	74	0.423	<0.005
	C_{21}	E	24	0.905	<0.005
	C_{21}	S0	15	0.789	<0.005
	L_B, C_{21}	E	24	0.973	<0.005
L_B-C_{21}	L_X	E	24	−0.240	0.144
	L_X	S0	15	0.249	0.207
	L_X/L_B	E	24	−0.085	0.351
	L_X, L_X/L_B	E	24	−0.242	0.151
	L_X, L_X/L_B	S0	15	0.484	0.048
L_X-C_{21}	L_B	E	24	0.433	0.021
	L_B	S0	15	0.485	0.041
	L_X/L_B	E	24	0.038	>0.400
	L_X/L_B	S0	15	0.457	0.050
	L_B, L_X/L_B	E	24	0.230	0.164
	L_B, L_X/L_B	S0	15	0.613	0.014
L_X/L_B-C_{21}	L_B	E	24	0.397	0.032
	L_X	E	24	0.132	0.275
	L_X	S0	15	−0.119	0.345
	L_B, L_X	E	24	−0.134	0.276
	L_B, L_X	S0	15	0.092	0.384

L_X and L_X/L_B, confirming the "softening" of the spectrum already seen by Kim et al. (1992b) for the lowest luminosity detected X-ray galaxies. Similar effects are seen in some slightly more luminous X-ray galaxies (Fabbiano et al. 1994; Fabbiano and Schweizer 1994). Also, *ROSAT* data do not show excess absorption in the X-ray–luminous galaxies analyzed to date (e.g., Trinchieri et al. 1994; Kim & Fabbiano 1994) despite these data being more sensitive to low X-ray energies than the *Einstein* data.

There are a total of 39 objects in our sample with more than 3 σ detections in both C_1 and C_2. In Table 5 we show the results of bivariate analysis on the C_{21} color, L_B, L_X, and L_X/L_B for this subsample of objects. There is a strong correlation found between L_X and C_{21}, and a somewhat weaker ($\sim$3%) correlation found between L_X/L_B and C_{21}. There is no evidence for correlation between L_B and C_{21}. In Figure 5 we show plots of C_{21} against both L_X and L_X/L_B. The *ROSAT* results noted above would indicate that these trends are the result of differences in the intrinsic spectral shape as a function of L_X, rather than differences in N_H.

We conducted a partial rank analysis of the C_{21} sample, using L_B, L_X, L_X/L_B, and C_{21} as inputs. The results are shown in Table 4A. Briefly, we recover the relationship between L_X and C_{21} found in the bivariate analysis at the $\lesssim$3% level for all combinations including these two variables. The evidence for a relationship between L_X/L_B and C_{21} varies from the $\sim$2% level to nonexistent, depending on the combination examined. Since the worst case is the three-way case including L_X as the frozen variable, we conclude that the relationship between L_X/L_B and C_{21} seen in the bivariate analysis is driven by an underlying relationship between L_X and C_{21}. We find no evidence for a relationship between L_B and C_{21} for any combination.

3.2. *Type Separation*

Our sample is large enough that we can make the crude separation between E ($T \leq -3$) and S0 ($-2 \leq T < 0$) systems and still have statistically interesting numbers of galaxies.

3.2.1. *The Elliptical Galaxies*

There are 72 E galaxies in our sample. Our bivariate statistical analysis shows that L_X is correlated with L_B for this subsample (see Table 2B). The results of the regression analysis are given in Table 3B. The fits, along with the data, are shown in

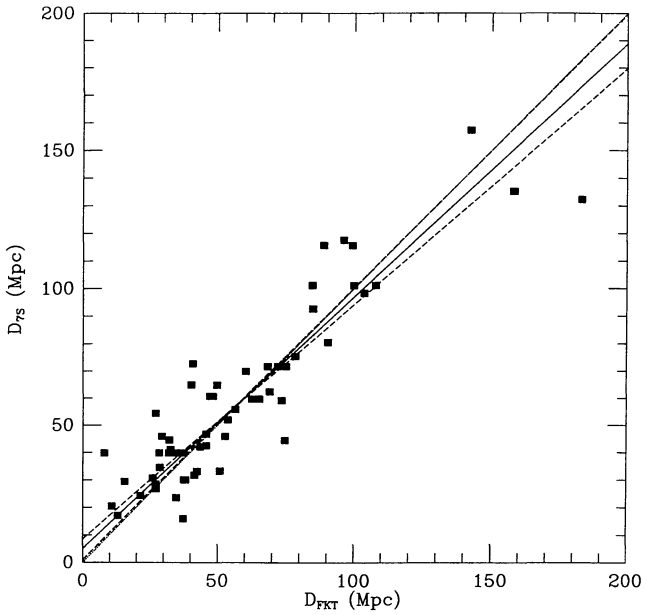

FIG. 3.—Distances from P0 plotted against distances determined from 7S velocity distances. The dotted line has slope 1 and intercept 0. The best fit [linear bisector of $(X|Y)$ and $(Y|X)$] is shown as a solid line. The fits $(X|Y)$ and $(Y|X)$ are shown as dashed lines. All the fits are consistent with the dotted line.

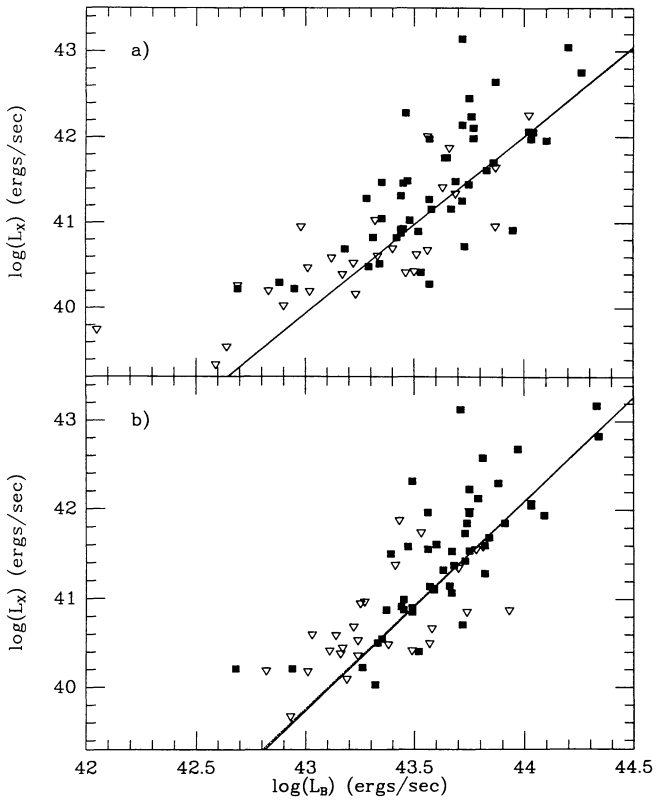

FIG. 4.—L_X vs. L_B for the subset of galaxies with distances from 7S, (*a*) for distances from P0 and (*b*) for distances from 7S. In both cases we show fit lines from the E-M (*solid line*) and B-J (*dotted line*) algorithms.

Figure 6*a*. Although the analysis of just the E galaxies gives slightly shallower regression lines than does the full sample, the differences are not statistically significant. We also find a strong L_X-L_X/L_B relationship for the elliptical galaxies (Table 2B). The results of the regression algorithms (Table 3B) along with the data are shown in Figure 6*b*. The results are consistent with those found for the full sample. The most discrepant slopes (in this case, those from the B-J algorithm and from Schmitt's method) differ by only 0.6 σ. The correlations found between C_{21} and X-ray emission become much weaker if we test only the E galaxies (see Table 5).

The results of a three-way partial rank analysis on L_B, L_X, and L_X/L_B for the elliptical galaxies (see Table 4B) confirm the L_B-L_X, and L_X-L_X/L_B correlations found in the bivariate analysis. For the C_{21} sample of elliptical galaxies, partial rank analysis yields results consistent with the bivariate analysis: the correlations found are the same as for the full sample, but the strengths of the correlations are decreased.

TABLE 5

CORRELATION TESTS ON THE C_{21} SAMPLE

	L_X		L_B		L_X/L_B		L_{12}		L_{100}		$L_{6\,cm}$	
SAMPLE	N_{tot}	N_{lim}	N_{tot}	N_{lim}	N_{tot}	N_{lim}	N_{tot}	N_{lim}	N_{tot}	N_{lim}	N_{tot}	N_{lim}
E+S0	39	0	39	0	39	0	38	13	38	11	39	14
	6.630	0.0100	1.277	0.2585	6.003	0.0143	0.511	0.4749	0.090	0.7637	3.526	0.0604
	2.891	0.0038	1.186	0.2357	2.141	0.0323	0.215	0.8295	0.743	0.4572	1.803	0.0713
	0.434	0.0075	0.191	0.2402	0.334	0.0394	0.075	0.6499	−0.071	0.6653	0.274	0.0911
E	24	0	24	0	24	0	24	8	24	7	24	8
	1.641	0.2002	0.191	0.6620	2.753	0.0971	0.112	0.7374	0.026	0.8709	1.441	0.2300
	1.885	0.0594	0.273	0.7849	1.836	0.0664	1.128	0.2594	0.859	0.3905	1.111	0.2666
	0.373	0.0415	−0.039	0.8527	0.391	0.0365	−0.170	0.4159	−0.141	0.4986	0.223	0.2858
S0	15	0	15	0	15	0	14	5	14	4	15	6
	6.017	0.0142	4.486	0.0342	4.602	0.0319	0.730	0.3929	0.099	0.7535	2.509	0.1132
	2.326	0.0200	1.930	0.0536	1.732	0.0833	0.884	0.3766	0.606	0.5448	1.219	0.2230
	0.596	0.0159	0.457	0.0465	0.443	0.0496	0.313	0.2584	0.137	0.6210	0.348	0.1933

NOTE.—Table entries as defined in notes to Table 2A.

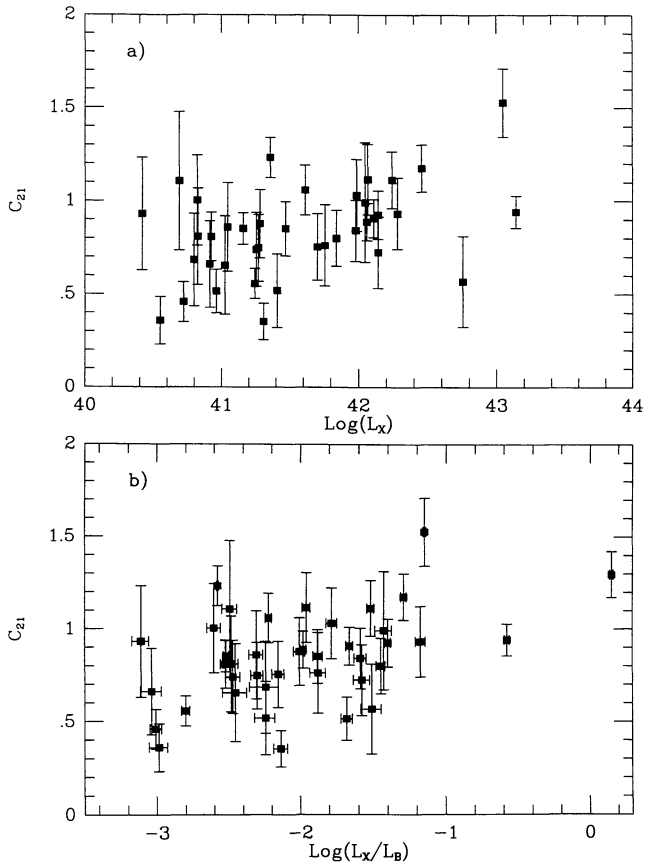

FIG. 5.—C_{21} vs. (*a*) L_X and (*b*) L_X/L_B for the 39 systems with well-determined C_{21} colors. There are weak but statistically significant trends toward higher C_{21} with higher L_X and L_X/L_B.

3.2.2. *The S0 Galaxies*

There are also 74 S0 galaxies in our sample. For these galaxies the results of the correlation tests (Table 2C) indicate that L_X is strongly correlated with L_B. The regression analyses are given in Table 3C. The L_X-L_X/L_B correlation is strongly upheld (Table 2C). The results from the various regression methods are given in Table 3C. The results for both the slopes and the zero points are statistically indistinguishable from those for the elliptical galaxies, although the zero points for the S0 galaxies are consistently smaller than those for the ellipticals. The data, along with the regression lines, are shown in Figure 7. Partial rank analysis of this sample confirms the correlations found in the bivariate analysis and shows no evidence of any L_B-L_X/L_B correlation for the S0 sample (see Table 4B).

As for the E galaxies, the correlation between C_{21} and L_X and L_X/L_B is weaker for the S0 galaxies only than for the full sample (see Table 5). Still, despite a fairly small number of objects (only 15), the correlation with L_X is at the 1%–2% level. It thus appears from this small sample that the relationship between X-ray emission and C_{21} is a function of morphological type, with a stronger correlation found for the S0 than for the E galaxies. The results of the partial rank analysis (see Table 4B) support this conclusion. The sample sizes make this finding tentative at best, but interesting nonetheless. This could be a consequence of S0 galaxies being less X-ray–luminous than E galaxies on average (see § 3.2.3 below). As noted above, recent *ROSAT* results indicate that soft excesses are more significant in less X-ray–luminous galaxies (e.g., Fabbiano et al. 1994).

3.2.3. *Comparison of the E and S0 Samples*

Another way of searching for potential differences between the E and the S0 galaxies is to compare the distribution functions (DFs) of each sample for the various observables. The integral Kaplan-Meier (K-M; see Feigelson & Nelson 1985) DFs of L_B for the E and S0 samples are shown in Figure 8*a*. The mean values are given in Table 6. These values differ by 1.9 σ, the E galaxies being more luminous, on average, than the S0s (consistent with the lower zero points in the fits for the S0s noted above). The results of a variety of two-sample tests (discussed in Feigelson & Nelson 1985 and LaValley et al. 1992), shown in Table 6, indicate that the null hypothesis (that the two samples are drawn from the same distribution) is supported at roughly the 2% level at most. This is consistent with existing studies of field and cluster luminosity function studies of E and S0 galaxies, as reviewed by Binggeli, Sandage, & Tammann (1988).

The difference between the elliptical and the S0 galaxies becomes more clear upon examining the DFs of the X-ray luminosity. The integral K-M DFs of L_X for the E and S0 galaxies

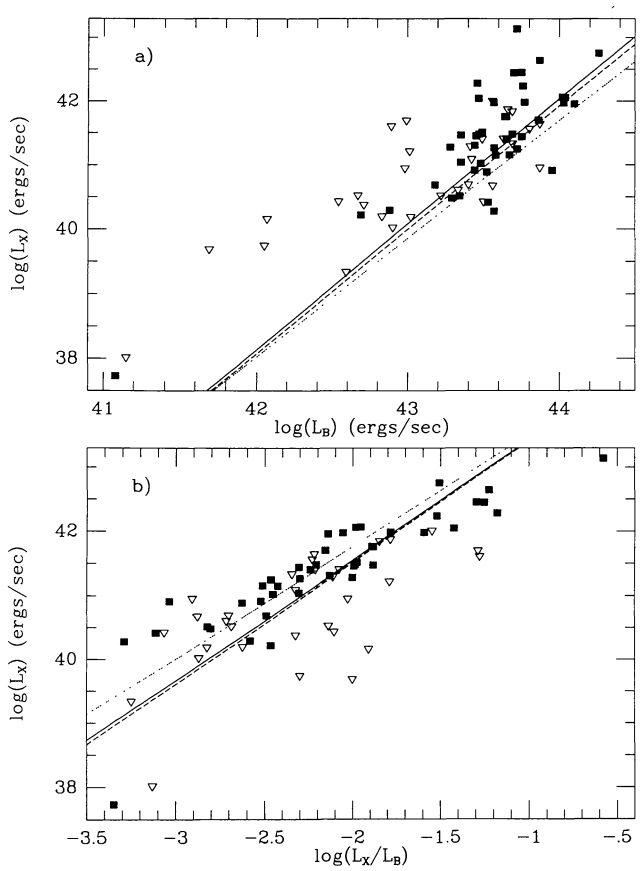

FIG. 6.—L_X vs. (*a*) L_B and (*b*) L_X/L_B for the E galaxies only. Symbols and line coding as in Fig. 2.

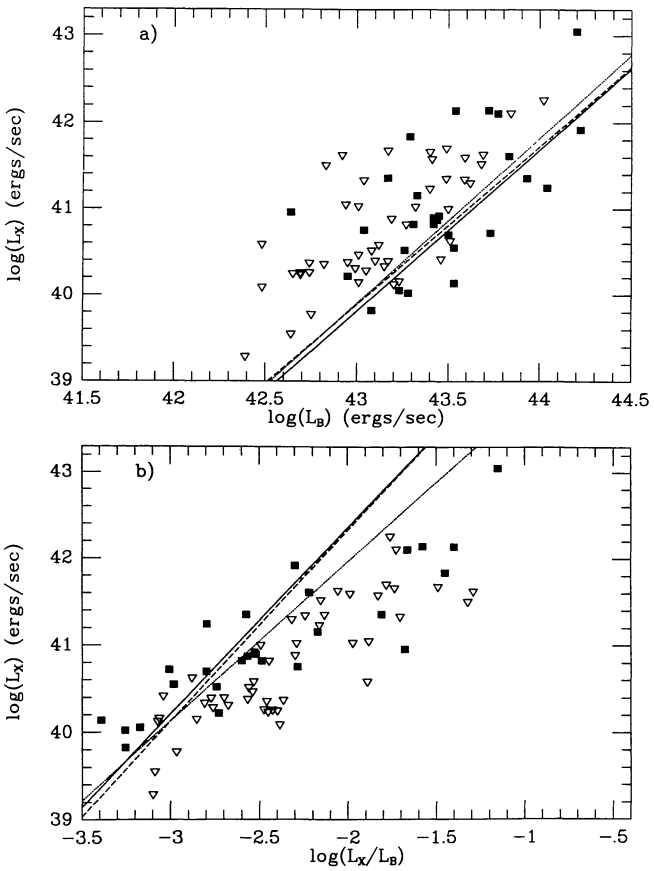

FIG. 7.—L_X vs. (*a*) L_B and (*b*) L_X/L_B for the S0 galaxies only. Symbols and line coding as in Fig. 1.

are shown in Figure 8*b*. The mean values for the two samples are given in Table 6. They differ by 2.8 σ, in the sense that the E galaxies tend to be more X-ray–luminous than the S0s. As the X-ray DFs are substantially more discrepant than the optical DFs, it is unlikely that the difference is wholly the result of a bias in our sample toward optically more luminous elliptical galaxies. As shown in Table 6, the two-sample tests uphold the difference between the samples, with probability $P = 0.0004$–0.0016 that the null hypothesis is upheld. Extending this comparison to the DFs of L_X/L_B argues more strongly that this difference is real. The DFs are shown in Figure 8*c*. The mean values (see Table 6) are distinct at the 3.5 σ level, in the sense that E galaxies tend to have higher X-ray luminosity per unit optical luminosity than do S0 galaxies. This difference is supported by the two-sample tests, which give $P = 0.0005$–0.0012 that the null hypothesis is upheld. Given the results of the regression analysis above, it appears that the slopes of the L_X-L_B relationships are the same for E and S0 galaxies, but that the S0 galaxies are systematically shifted to lower X-ray luminosities than the ellipticals.

Our conclusion that the DF of L_X/L_B is clearly shifted to higher values for the E galaxies compared to the S0s is at odds with the conclusion of Bregman et al. (1992), who found no differences in the X-ray properties of their E and S0 samples. However, they tested for differences in the DFs of R_{ex}, where $R_{ex} = L_X/L_X(\text{best fit})$, and $L_X(\text{best fit}) \propto L_B^{1.75}$. This approach reduces the intrinsic difference between the samples. Moreover, Bregman et al. interpret their results in terms of a cooling flow model with an intrinsic underlying $L_X \propto L_B^{1.7}$ scaling (see also Trinchieri & Fabbiano 1985). However, both the large scatter in this correlation (see Fabbiano 1989) and the luminosity dependence we find for the power-law exponent (see

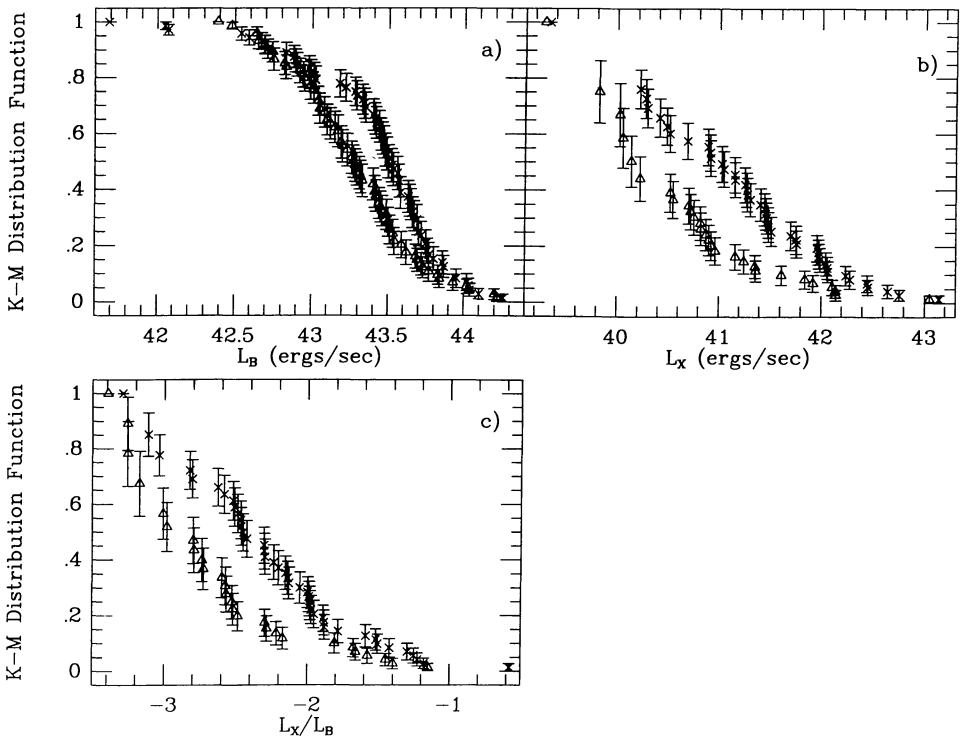

FIG. 8.—Integral K-M DFs for our samples of E and S0 galaxies. The Local Group dE galaxies have not been included. Crosses mark E galaxies; triangles, S0 galaxies. Error bars are 1 σ. (*a*) DFs of L_B. (*b*) DFs of L_X. (*c*) DFs of L_X/L_B.

TABLE 6

COMPARISON BETWEEN E AND S0 SAMPLES

Parameter	Elliptical[a] Sample Size	S0[a] Sample Size	Difference (σ)	Gehan Permutation[b]	Gehan Hypergeometric	logrank	Peto-Peto	Peto-Prentice
L_B	43.403 ± 0.057 (N = 72)	43.262 ± 0.047 (N = 74)	1.9	2.774 (0.0055)	2.794 (0.0052)	2.313 (0.0207)	2.313 (0.0207)	... ...
L_X	40.836 ± 0.138 (N = 72)	40.303 ± 0.130 (N = 74)	2.8	3.525 (0.0004)	3.546 (0.0004)	3.155 (0.0016)	3.469 (0.0005)	3.493 (0.0005)
L_X/L_B	−2.425 ± 0.082 (N = 72)	−2.813 ± 0.076 (N = 74)	3.5	3.349 (0.0008)	3.361 (0.0008)	3.239 (0.0012)	3.443 (0.0006)	3.463 (0.0005)
L_{12}	42.164 ± 0.091 (N = 62)	42.018 ± 0.129 (N = 70)	0.9	0.123 (0.9018)	0.124 (0.9015)	0.726 (0.4676)	0.475 (0.6349)	0.456 (0.6481)
L_{12}/L_B	−1.140 ± 0.046 (N = 62)	−1.025 ± 0.060 (N = 70)	1.5	2.109 (0.0349)	2.103 (0.0354)	1.142 (0.2535)	1.801 (0.0717)	1.810 (0.0702)
L_{100}	41.832 ± 0.105 (N = 62)	42.006 ± 0.111 (N = 71)	1.1	1.638 (0.1015)	1.633 (0.1026)	0.853 (0.3938)	1.446 (0.1481)	1.442 (0.1493)
L_{100}/L_B	−1.604 ± 0.094 (N = 62)	−1.254 ± 0.102 (N = 71)	2.5	2.939 (0.0033)	2.940 (0.0033)	2.295 (0.0217)	2.817 (0.0048)	2.846 (0.0044)
L_6	35.964 ± 0.228 (N = 69)	35.123 ± 0.238 (N = 62)	2.6	2.264 (0.0236)	2.262 (0.0237)	1.786 (0.0742)	2.146 (0.0319)	2.137 (0.0326)
L_6/L_B	−7.454 ± 0.199 (N = 69)	−8.038 ± 0.206 (N = 62)	2.0	1.916 (0.0553)	1.913 (0.0557)	1.361 (0.1735)	1.774 (0.0761)	1.775 (0.0759)

[a] The first row of each pair of values in these columns gives the mean value of the DF for either the E or the S0 sample. The second gives the number of objects in the sample.

[b] The first row of each pair of values in these columns gives the test score for the comparison of the E and S0 samples. The second row gives the probability (in parentheses) that the two samples are drawn from the same parent distribution.

§ 3.1.2 above) suggest that more complex explanations (e.g., Ciotti et al. 1991) of the L_X-L_B diagram are required.

We suggest that the likely cause for this is the influence of the disk in S0 galaxies. The initial mechanism for the heating of gas from photospheric to coronal temperatures in early-type galaxies is simple virial heating, due to the velocity dispersion of the stars in the galaxy. Because a large fraction of the internal energy in S0 galaxies is due to ordered rotation, this heating mechanism will be significantly suppressed. Furthermore, again due to the influence of the disk, the shape of the central potential well is significantly shallower for an S0 galaxy of a given mass than for an elliptical of comparable mass (Binney & Tremaine 1987, §§ 2.1 and 2.6).

4. THE RELATIONSHIP OF L_X WITH OTHER ISM TRACERS

As noted in § 1, the classic problem of what has become of the ISM in early-type galaxies has, in general, been answered by the discovery of X-ray luminous halos of material associated with, at least, the most luminous early-type galaxies. The physical details controlling whether a galaxy can retain its ISM as an X-ray halo are a matter of current vigorous theoretical debate (e.g., Ciotti et al. 1991; David, Forman, & Jones 1991; Bertin, Pignatelli, & Saglia 1993). Our sample is large enough that we can address the issue of relationships between various phases of the ISM in early-type galaxies. The largest and most homogeneous comparison sample is drawn from the *IRAS* data. Large but more heterogeneous samples can be constructed with radio continuum and H I data from the literature.

This analysis is similar in scope to that presented by Roberts et al. (1991) and Bregman et al. (1992), but uses an explicitly X-ray–selected sample, and differs substantially in analytic approach. We thus believe the two studies complement each other very usefully.

4.1. L_X *versus* 12 μm *Data*

4.1.1. *The Full Sample*

The available *IRAS* 12 μm data for the *Einstein* sample are presented in Table 1. They are taken mainly from the work of Knapp et al. (1989), supplemented by a number of other sources. There are data for a total of 134 of the 148 galaxies in the *Einstein* sample. The 12 μm flux from early-type galaxies has typically been ascribed to either photospheric emission or emission from dust created in outer atmospheres of red giants (e.g., Jura et al. 1987; Knapp, Gunn, & Wynn-Williams 1992). Given the ostensibly simple stellar populations of early-type galaxies, one would thus expect $\log(L_{12})$ to show a strong, linear, slope 1 correlation with $\log(L_B)$. This expectation is, in fact, confirmed by our analysis (see Tables 2A and 3A). The fit lines are displayed with the data in Figure 9*a*.

Naively, one would thus expect the relationship between L_X and L_{12} to be similar to that found above between L_X and L_B. The results of the experiment are, however, ambiguous. The two applicable correlation tests for doubly censored samples both indicate that L_X is strongly correlated with L_{12} (see Table 2A). The Schmitt's regression is given in Table 3A. The data and the fit line are shown in Figure 9*b*. If the slope of the L_B-L_{12} relationship is exactly unity, then L_X should scale the same with both L_B and L_{12}. An examination of Table 3A shows this to be ruled out at the 2.7 σ level ($\Delta_{m,2} = 0.49 \pm 0.18$). If one

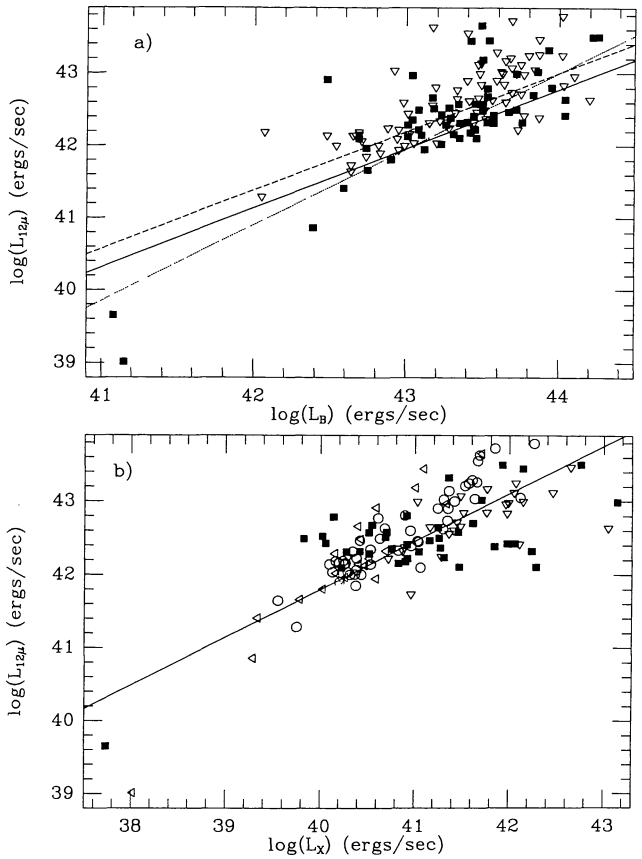

FIG. 9.—L_{12} vs. (*a*) L_B and (*b*) L_X for our sample with 12 μm *IRAS* data. Symbols and line coding as in Fig. 2. Additionally, open left-pointing triangles are 3 σ X-ray upper limits and 12 μm detections, and open circles are 3 σ upper limits in both X-rays and 12 μm. The fit displayed in (*b*) is from Schmitt's method for the sample without the Local Group dE galaxies (*solid line*).

takes the slopes from Schmitt's regression of L_B against L_{12} at face value, then the expected slope for the relationship between L_X and L_{12} would be 1.92 ± 0.16. These differ from the actual values determined at the 2.0 σ level ($\Delta_{m,4} = 0.39 \pm 0.20$). To explore this problem further, we have searched for trends between L_{12}/L_B and L_B, L_X, and L_X/L_B. In no case do we find any evidence for such trends (see Table 2A).

This discrepancy may be no more than a statistical fluke. It may also be driven by a systematic effect, such as the use of unmatched apertures for the various flux measurements, as discussed in Jura et al. (1987) and Knapp et al. (1992). However, we argue that it is likely to be real, based on evidence (see § 4.1.2 below) that the discrepancy is driven by a difference in the 12 μm properties of the E and S0 galaxies in our sample. The results of the partial rank analysis on L_B-L_X-L_X/L_B-L_{12} are presented in Table 7A. For all combinations of variables that include L_B, we find strong correlation between L_B and L_{12}. The only case in which we find evidence for correlation between L_X and L_{12} is the three-way sample not including L_B. It appears that the bivariate L_X-L_{12} correlation is driven mainly by the mutual dependence of both these parameters on L_B.

There is no evidence for correlation between L_{12} and C_{21} for the 38 galaxies with well-determined C_{21} values and *IRAS* measurements (see Table 5). This conclusion is fully supported by a partial rank analysis including these variables (see Table 7A).

4.1.2. *Type Separation*

We have analyzed the data for E and S0 galaxies separately to search for possible systematic differences between the galaxy types. Knapp et al. (1989) found significant differences in the *IRAS* 60 and 100 μm (FIR) properties for E and S0 galaxies, although there was no significant difference between the two classes in the *IRAS* 12 and 25 μm (mid-IR[MIR]) data. We have a sample of 62 elliptical galaxies. Our analysis for this sample is given in Tables 2B and 3B. We find no compelling evidence for any correlations with L_{12}/L_B. The L_B-L_{12} and L_X-L_{12} results are shown in Figures 10*a* and 11*a*. A partial rank analysis on L_B-L_X-L_X/L_B-L_{12} for the E sample gives results fully consistent with those for the full sample (see Table 7B). A partial rank analysis on L_B-L_X-L_X/L_B-L_{12}-C_{21} on the E subsamples reveals no trends not found for the full sample.

There are 70 S0 galaxies in the 12 μm sample. Our bivariate analysis for this sample is given in Tables 2C and 3C. There is no evidence for correlations between L_{12} and L_X/L_B, or between L_{12}/L_B and any tested quantity for the S0 sample. The fits and data for the L_{12}-L_B relationships for the S0 galaxies are shown in Figure 10*b*. Those for the L_{12}-L_X relation are displayed in Figure 11*b*. The integral K-M DFs for the 12 μm luminosities and the 12 μm to *B* ratio are shown in Figure 12. The mean values, along with the results of the two-sample tests, are given in Table 6. In agreement with earlier work by Knapp et al. (1989), we find no statistically significant difference in the 12 μm properties of E and S0 galaxies in our sample. We do, however, find the S0s to have marginally higher (at the 1.5 σ level) L_{12}/L_B than do the Es. A partial rank analysis on L_B-L_X-L_X/L_B-L_{12} for the S0 sample yields qualitatively similar results to those for the E sample: The weight of evidence is for an underlying L_B-L_{12} relation driving the bivariate correlation between L_{12} and L_X (see Table 7B). Having only 14 objects for a L_B-L_X-L_X/L_B-L_{12}-C_{21} partial rank analysis, we have not conducted this test.

We note that the ~ 2 σ discrepancy between the expected and derived slopes of the L_X-L_{12} relationship for the full sample, discussed in § 4.1.1 above, appears to be entirely driven by the S0 galaxies (see Tables 3B, 3C, and 6). There is growing evidence that S0 galaxies are more able to retain significant quantities of "spiral-like" ISM than are ellipticals (e.g., Thronson et al. 1989; Knapp et al. 1989). Many S0 galaxies are also known to be undergoing current massive star formation (Pogge & Eskridge 1987, 1993). We thus speculate that a possible cause for the discrepancy in the slope of the L_X-L_{12} relationship for the S0 galaxies is due to a significant contribution from dust heated in star-forming regions. While our results are consistent with this interpretation, we caution the reader that we find no difference between the two samples at greater than the 2 σ level. However, additional support for this hypothesis is found in our analysis of optical-IR colors for our sample (§ 4.3 below).

4.2. L_X *versus* 100 μm *Data*

The *IRAS* 100 μm data for 135 of the galaxies in the *Einstein* sample are also given in Table 1, again mainly taken from Knapp et al. (1989) with some additional sources. There are

TABLE 7A

PARTIAL SPEARMAN RANK ANALYSIS: *IRAS* 12 MICRON PROPERTIES, E+S0 SAMPLES

Test Pair	Held Parameters	Size	Partial Spearman Rank	Probability
L_B-L_X	L_{12}	132	0.625	<0.005
	L_X/L_B, L_{12}	132	0.531	<0.005
	L_{12}, C_{21}	38	0.430	<0.005
	L_X/L_B, L_{12}, C_{21}	38	0.855	<0.005
L_B-L_X/L_B	L_{12}	132	0.392	<0.005
	L_X, L_{12}	132	0.043	0.316
	L_{12}, C_{21}	38	0.026	>0.400
	L_X, L_{12}, C_{21}	38	−0.818	<0.005
L_B-L_{12}	L_X	132	0.304	<0.005
	L_X/L_B	132	0.437	<0.005
	L_X, L_X/L_B	132	0.305	<0.005
	C_{21}	38	0.515	<0.005
	L_X, C_{21}	38	0.495	<0.005
	L_X/L_B, C_{21}	38	0.515	<0.005
	L_X, L_X/L_B, C_{21}	38	0.208	0.120
L_B-C_{21}	L_{12}	38	0.197	0.129
	L_X, L_{12}	38	−0.017	>0.400
	L_X/L_B, L_{12}	38	0.173	0.168
	L_X, L_X/L_B, L_{12}	38	−0.108	0.268
L_X-L_X/L_B	L_{12}	132	0.583	<0.005
	L_B, L_{12}	132	0.471	<0.005
	L_{12}, C_{21}	38	0.879	<0.005
	L_B, L_{12}, C_{21}	38	0.962	<0.005
L_X-L_{12}	L_B	132	0.116	0.095
	L_X/L_B	132	0.347	<0.005
	L_B, L_X/L_B	132	0.118	0.093
	C_{21}	38	0.179	0.156
	L_B, C_{21}	38	−0.072	0.340
	L_X/L_B, C_{21}	38	0.485	<0.005
	L_B, L_X/L_B, C_{21}	38	0.068	0.351
L_X-C_{21}	L_{12}	38	0.453	<0.005
	L_B, L_{12}	38	0.417	0.006
	L_X/L_B, L_{12}	38	0.264	0.063
	L_B, L_X/L_B, L_{12}	38	0.229	0.095
L_X/L_B-L_{12}	L_B	132	0.026	0.384
	L_X	132	−0.021	>0.400
	L_B, L_X	132	−0.033	0.357
	C_{21}	38	−0.095	0.289
	L_B, C_{21}	38	−0.094	0.292
	L_X, C_{21}	38	−0.466	<0.005
	L_B, L_X, C_{21}	38	−0.091	0.301
L_X/L_B-C_{21}	L_{12}	38	0.385	0.010
	L_B, L_{12}	38	0.375	0.014
	L_X, L_{12}	38	−0.056	0.376
	L_B, L_X, L_{12}	38	−0.120	0.246
L_{12}-C_{21}	L_B	38	−0.039	>0.400
	L_X	38	−0.015	>0.400
	L_X/L_B	38	0.105	0.268
	L_B, L_X	38	−0.005	>0.400
	L_B, L_X/L_B	38	0.000	>0.400
	L_X, L_X/L_B	38	−0.039	>0.400
	L_B, L_X, L_X/L_B	38	−0.016	>0.400

two main sources of 100 μm emission recognized in normal spiral galaxies: emission from cirrus, and emission from dust heated by nearby regions of massive star formation (e.g., Soifer et al. 1989). In either case, the dominant source of 100 μm emission from late-type galaxies clearly appears to be interstellar dust. The relative amount of dust per unit stellar mass is ostensibly much smaller in early-type galaxies than it is in late-type galaxies. To the extent that this dust is traced by FIR emission, the work of Knapp et al. (1989) demonstrates this quite well. They report detections at 100 μm for only ~45% of ellip-

TABLE 7B

PARTIAL SPEARMAN RANK ANALYSIS: *IRAS* 12 MICRON PROPERTIES, SEPARATE E AND S0 SAMPLES

Test Pair	Held Parameters	Sample	Size	Partial Spearman Rank	Probability
L_B-L_X	L_{12}	E	62	0.543	<0.005
	L_{12}	S0	70	0.553	<0.005
	L_X/L_B, L_{12}	E	62	0.471	<0.005
	L_X/L_B, L_{12}	S0	70	0.475	<0.005
L_B-L_X/L_B	L_{12}	E	62	0.308	0.008
	L_{12}	S0	70	0.326	<0.005
	L_X, L_{12}	E	62	0.018	>0.400
	L_X, L_{12}	S0	70	0.064	0.305
L_X-L_{12}	L_X	E	62	0.317	0.007
	L_X	S0	70	0.302	0.006
	L_X/L_B	E	62	0.466	<0.005
	L_X/L_B	S0	70	0.418	<0.005
	L_X, L_X/L_B	E	62	0.318	0.007
	L_X, L_X/L_B	S0	70	0.303	0.007
L_X-L_X/L_B	L_{12}	E	62	0.543	<0.005
	L_{12}	S0	70	0.508	<0.005
	L_B, L_{12}	E	62	0.470	<0.005
	L_B, L_{12}	S0	70	0.416	<0.005
L_X-L_{12}	L_B	E	62	0.200	0.064
	L_B	S0	70	0.132	0.152
	L_X/L_B	E	62	0.398	<0.005
	L_X/L_B	S0	70	0.326	<0.005
	L_B, L_X/L_B	E	62	0.183	0.084
	L_B, L_X/L_B	S0	70	0.129	0.158
L_X/L_B-L_{12}	L_B	E	62	0.083	0.263
	L_B	S0	70	0.034	0.391
	L_X	E	62	−0.009	>0.400
	L_X	S0	70	−0.005	>0.400
	L_B, L_X	E	62	−0.014	>0.400
	L_B, L_X	S0	70	−0.024	>0.400

tical galaxies. The percentage for S0 galaxies is higher, but still only 68%. For comparison, Bothun, Lonsdale, & Rice (1989) find that more than 90% of UGC spirals with $m_B \leq 13.5$ are detected by *IRAS* in the FIR. One currently favored hypothesis is that the material responsible for FIR emission in early-type galaxies is accreted material (e.g., Forbes 1991). If this is the case, and the X-ray emission is due to a gravitationally bound thermal plasma, there should not necessarily be any relationship between L_X and L_{100}, the 100 μm luminosity. Alternatively, the dust could be intrinsic to the host galaxy, but interaction with the X-ray plasma and interstellar radiation field (ISRF) could then evaporate the grains (e.g., Boulanger et al. 1988; Knapp et al. 1992). How this would manifest itself in terms of global luminosity correlations would depend on the balance between the grain formation (or accretion) and evaporation timescales. The correlation tests uphold the null hypothesis at the $\approx$5% level (Table 2A). Also, we find no correlation between L_{100} and either L_X/L_B (Table 2A) or C_{21} (Table 5), and no correlations of L_{100}/L_B with any tested parameter (Table 2A).

The results of a partial rank analysis on L_B-L_X-L_X/L_B-L_{100} confirm that there is no significant correlation between L_X and L_{100} for our sample. They do reveal a correlation between L_B and L_{100} (see Table 8A). We also tested the combination L_B-L_X-L_X/L_B-L_{100}-C_{21}. No new trends were uncovered by this analysis.

We now consider the L_X-L_{100} relations for the E and S0 subsamples. There are 62 elliptical galaxies in the subsample. The data are shown in Figure 13. As for the full sample, there is no significant correlation between L_{100} and either L_X or L_X/L_B, and none between L_{100}/L_B and L_B, L_X, or L_X/L_B (Table 2B). A four-component partial rank analysis on L_B-L_X-L_X/L_B-L_{100} for the E galaxies is similar to that for the full sample. The one significant difference is that the (*weak*) evidence for an L_X-L_{100} trend in the full sample disappears completely when only the E galaxies are considered. Adding L_{12} to the partial rank analysis, we note that there is no evidence for a correlation between L_{12} and L_{100} for the E galaxies (such a trend *does* appear for the full sample). Thus, for the E galaxies alone, the sources of 12 and 100 μm radiation are apparently uncoupled. These results are shown in Table 8B.

Turning to the S0 sample ($N = 71$), we find somewhat different results (see Table 2C). Taking the more pessimistic of the correlation test results, there is evidence for a correlation between L_X and L_{100} for the S0 sample at the $\approx$2.3 σ level (although there is no evidence for a correlation between L_{100} and L_X/L_B). Accepting the relationship between L_{100} and L_X as real, we derive a regression line from Schmitt's method

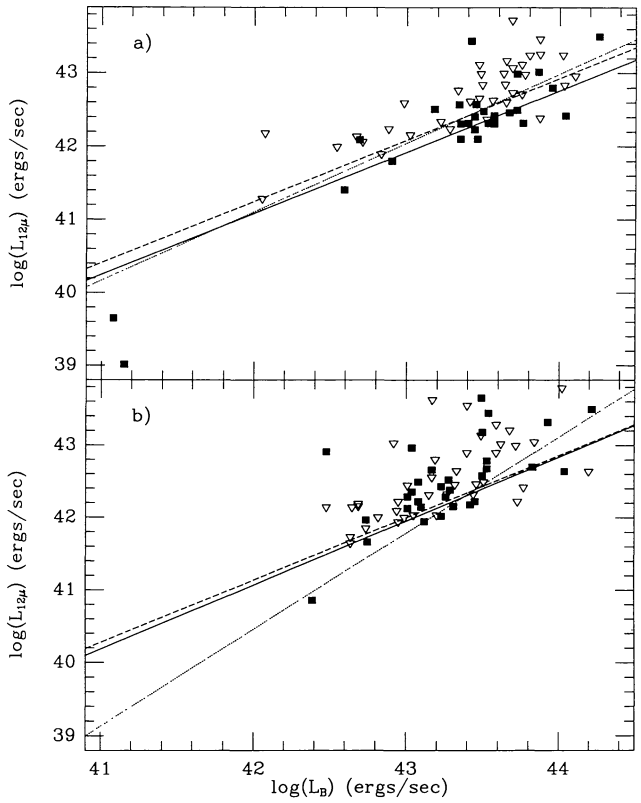

FIG. 10.—L_{12} vs. L_B for (*a*) E and (*b*) S0 galaxies in our sample with 12 μm *IRAS* data. Symbols and line coding as in Fig. 2.

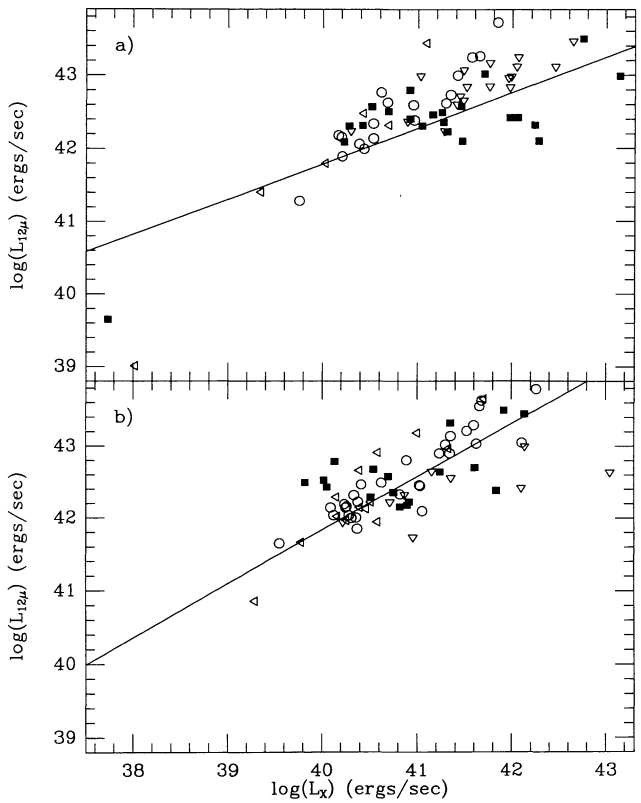

FIG. 11.—L_{12} vs. L_X for (*a*) E and (*b*) S0 galaxies in our sample with 12 μm *IRAS* data. Symbols and line coding as in Fig. 9.

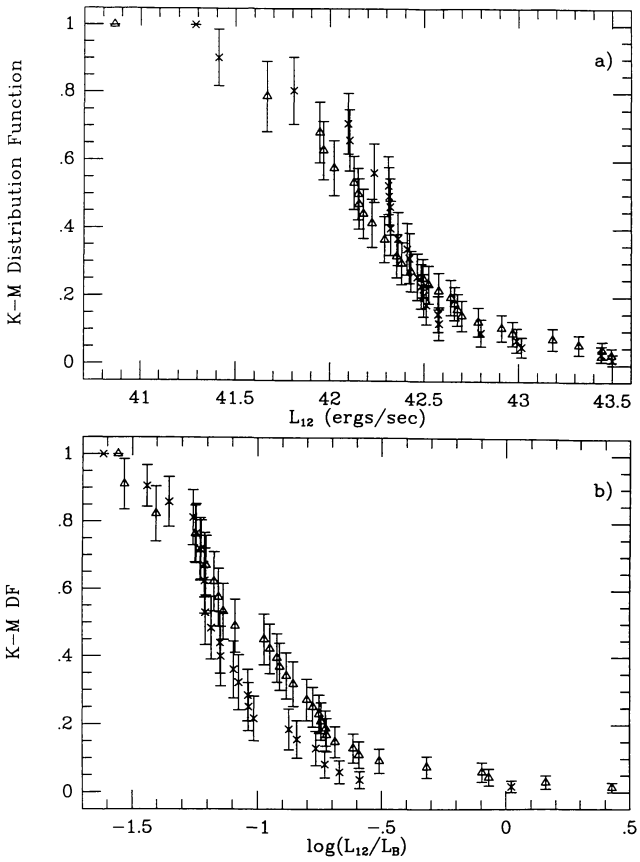

FIG. 12.—Integral K-M DFs of (*a*) L_{12} and (*b*) L_{12}/L_B for our samples of E and S0 galaxies. Symbols and error bars as in Fig. 8.

(Table 3C and Figure 13). The slope of this relationship (0.85 ± 0.23) does not differ significantly from unity. Thus, if the effect is real, it is an example of a "bright things are bright" relationship and does not necessarily indicate any direct connection between the X-ray– and FIR-emitting materials. We find no evidence of any trend with L_{100}/L_B (Table 2C). A partial rank analysis of L_B-L_X-L_X/L_B-L_{100} on just the S0 galaxies (Table 8B) suggests that the bivariate L_X-L_{100} relationship is driven by the mutual dependence of both these parameters on L_B. Including L_{12} in the partial rank analysis, we find that the L_{12}-L_{100} correlation found for the full sample (Table 8A) is driven entirely by the S0 galaxies. Indeed, there is a *stronger* correlation between L_{12} and L_{100} for the S0 sample than between L_B and L_{100}. Thus, in distinction to the E galaxies, the 12 μm and 100 μm emission from S0 galaxies do appear coupled for our sample.

A comparison of the 100 μm properties of the two subsamples reveals that the L_{100} DFs for the E and S0 galaxies are not significantly different, while the S0 galaxies tend to have larger L_{100}/L_B than the E galaxies at the 2.5 σ level. This is quite in keeping with earlier results (e.g., Knapp et al. 1989) showing S0 galaxies to have relatively more FIR emission than E galaxies. These results are given in Table 6 and displayed in Figure 14.

A number of physical factors may be involved in causing the differences between the E and S0 samples. First, it appears that

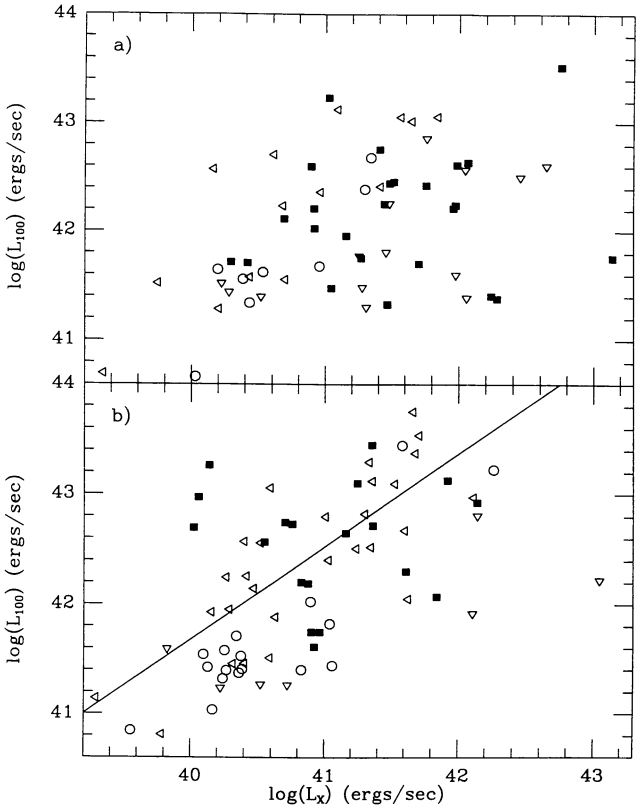

FIG. 13.—L_{100} vs. L_X for (*a*) E and (*b*) S0 galaxies in our sample with *IRAS* 100 μm data. Symbols and line coding as in Fig. 9.

a larger fraction of the X-ray emission from S0 galaxies is due to the same sort of stellar X-ray sources that provide the X-ray emission from spiral galaxies (Kim et al. 1992b), for which there is known to be a strong correlation between X-ray and 100 μm emission (Fabbiano et al. 1988). Second, while the FIR emission from elliptical galaxies may be due to accreted material (although the L_B-L_{100} correlation for the E galaxies shown in Table 8B argues against this), the evidence that the cool ISM in S0 galaxies is accreted is far less convincing (e.g., Jura 1986; Thronson & Bally 1987; Bertola et al. 1988; Marston 1988; Véron-Cetty & Véron 1988; Kim 1989; Knapp et al. 1989; Eskridge & Pogge 1991; Goudfrooij 1991; Shields 1991). Instead, it appears that a significant fraction of the FIR emission from S0 galaxies is due to radiation from dust intrinsic to the disk.

4.3. *L_X versus IRAS Colors*

We have examined our data to see whether there are any significant trends between X-ray emission and *IRAS* colors. A number of the possible FIR colors have been used by previous authors (e.g., Helou 1986; Soifer et al. 1987; Soifer et al. 1989; Rowan-Robinson & Crawford 1989; Helou, Ryter, & Soifer 1991) to generate diagnostic diagrams for separating AGNs, starbursts, and ISM heated by an ambient ISRF. Figure 15 shows histograms of the same flux ratios for our sample as are used by Soifer et al. (1989, their Fig. 2) for the *IRAS* Bright Galaxy Sample (IBGS). This sample is dominated by late-type

TABLE 8A

PARTIAL SPEARMAN RANK ANALYSIS: *IRAS* 100 MICRON PROPERTIES, E+S0 SAMPLES

Test Pair	Held Parameters	Size	Partial Spearman Rank	Probability
L_B-L_X	L_{100}	133	0.686	<0.005
	L_X/L_B, L_{100}	133	0.585	<0.005
	L_{12}, L_{100}	132	0.636	<0.005
	L_X/L_B, L_{12}, L_{100}	132	0.541	<0.005
L_B-L_X/L_B	L_{100}	133	0.444	<0.005
	L_X, L_{100}	133	0.046	0.304
	L_{12}, L_{100}	132	0.401	<0.005
	L_X, L_{12}, L_{100}	132	0.048	0.295
L_B-L_{12}	L_{100}	132	0.374	<0.005
	L_X, L_{100}	132	0.180	0.021
	L_X/L_B, L_{100}	132	0.318	<0.005
	L_X, L_X/L_B, L_{100}	132	0.181	0.021
L_B-L_{100}	L_X	133	0.345	<0.005
	L_X/L_B	133	0.378	<0.005
	L_{12}	132	0.198	0.013
	L_X, L_X/L_B	133	0.346	<0.005
	L_X, L_{12}	132	0.248	<0.005
	L_X/L_B, L_{12}	132	0.219	0.007
	L_X, L_X/L_B, L_{12}	132	0.249	<0.005
L_X-L_X/L_B	L_{100}	133	0.609	<0.005
	L_B, L_{100}	133	0.466	<0.005
	L_{12}, L_{100}	132	0.583	<0.005
	L_B, L_{12}, L_{100}	132	0.464	<0.005
L_X-L_{12}	L_{100}	132	0.367	<0.005
	L_B, L_{100}	132	0.164	0.033
	L_X/L_B, L_{100}	132	0.305	<0.005
	L_B, L_X/L_B, L_{100}	132	0.154	0.042
L_X-L_{100}	L_B	133	−0.099	0.139
	L_X/L_B	133	0.175	0.023
	L_{12}	132	0.007	>0.400
	L_B, L_X/L_B	133	−0.069	0.224
	L_B, L_{12}	132	−0.153	0.043
	L_X/L_B, L_{12}	132	0.015	>0.400
	L_B, L_X/L_B, L_{12}	132	−0.123	0.086
L_X/L_B-L_{12}	L_{100}	132	0.215	0.007
	L_B, L_{100}	132	0.059	0.254
	L_X, L_{100}	132	−0.012	>0.400
	L_B, L_X, L_{100}	132	−0.020	>0.400
L_X/L_B-L_{100}	L_B	133	−0.081	0.190
	L_X	133	−0.025	0.389
	L_{12}	132	−0.009	>0.400
	L_B, L_X	133	−0.039	0.331
	L_B, L_{12}	132	−0.096	0.148
	L_X, L_{12}	132	−0.016	>0.400
	L_B, L_X, L_{12}	132	−0.028	0.377
L_{12}-L_{100}	L_B	132	0.358	<0.005
	L_X	132	0.439	<0.005
	L_X/L_B	132	0.466	<0.005
	L_B, L_X	132	0.374	<0.005
	L_B, L_X/L_B	132	0.361	<0.005
	L_X, L_X/L_B	132	0.439	<0.005
	L_B, L_X, L_X/L_B	132	0.373	<0.005

TABLE 8B

PARTIAL SPEARMAN RANK ANALYSIS: *IRAS* 100 MICRON PROPERTIES, SEPARATE E AND S0 SAMPLES

Test Pair	Held Parameters	Sample	Size	Partial Spearman Rank	Probability
L_B-L_X	L_{100}	E	62	0.642	<0.005
	L_{100}	S0	71	0.570	<0.005
	L_X/L_B, L_{100}	E	62	0.557	<0.005
	L_X/L_B, L_{100}	S0	71	0.495	<0.005
	L_{12}, L_{100}	E	62	0.547	<0.005
	L_{12}, L_{100}	S0	70	0.542	<0.005
	L_X/L_B, L_{12}, L_{100}	E	62	0.473	<0.005
	L_X/L_B, L_{12}, L_{100}	S0	70	0.464	<0.005
L_B-L_X/L_B	L_{100}	E	62	0.386	<0.005
	L_{100}	S0	71	0.329	<0.005
	L_X, L_{100}	E	62	0.020	>0.400
	L_X, L_{100}	S0	71	0.054	0.333
	L_{12}, L_{100}	E	62	0.312	0.008
	L_{12}, L_{100}	S0	70	0.322	<0.005
	L_X, L_{12}, L_{100}	E	62	0.023	>0.400
	L_X, L_{12}, L_{100}	S0	70	0.066	0.298
L_B-L_{12}	L_{100}	E	62	0.477	<0.005
	L_{100}	S0	70	0.175	0.080
	L_X, L_{100}	E	62	0.280	0.017
	L_X, L_{100}	S0	70	0.079	0.261
	L_X/L_B, L_{100}	E	62	0.425	<0.005
	L_X/L_B, L_{100}	S0	70	0.151	0.114
	L_X, L_X/L_B, L_{100}	E	62	0.280	0.018
	L_X, L_X/L_B, L_{100}	S0	70	0.080	0.262
L_B-L_{100}	L_X	E	62	0.407	<0.005
	L_X	S0	71	0.370	<0.005
	L_X/L_B	E	62	0.424	<0.005
	L_X/L_B	S0	71	0.440	<0.005
	L_{12}	E	62	0.373	<0.005
	L_{12}	S0	70	0.286	0.009
	L_X, L_X/L_B	E	62	0.407	<0.005
	L_X, L_X/L_B	S0	71	0.369	<0.005
	L_X, L_{12}	E	62	0.380	<0.005
	L_X, L_{12}	S0	70	0.256	0.019
	L_X/L_B, L_{12}	E	62	0.377	<0.005
	L_X/L_B, L_{12}	S0	70	0.280	0.011
	L_X, L_X/L_B, L_{12}	E	62	0.380	<0.005
	L_X, L_X/L_B, L_{12}	S0	70	0.257	0.020
L_X-L_X/L_B	L_{100}	E	62	0.581	<0.005
	L_{100}	S0	71	0.510	<0.005
	L_B, L_{100}	E	62	0.472	<0.005
	L_B, L_{100}	S0	71	0.416	<0.005
	L_{12}, L_{100}	E	62	0.541	<0.005
	L_{12}, L_{100}	S0	70	0.505	<0.005
	L_B, L_{12}, L_{100}	E	62	0.466	<0.005
	L_B, L_{12}, L_{100}	S0	70	0.416	<0.005
L_X-L_{12}	L_{100}	E	62	0.443	<0.005
	L_{100}	S0	70	0.198	0.054
	L_B, L_{100}	E	62	0.203	0.063
	L_B, L_{100}	S0	70	0.123	0.171
	L_X/L_B, L_{100}	E	62	0.377	<0.005
	L_X/L_B, L_{100}	S0	70	0.172	0.085
	L_B, L_X/L_B, L_{100}	E	62	0.186	0.083
	L_B, L_X/L_B, L_{100}	S0	70	0.115	0.189

TABLE 8B—*Continued*

Test Pair	Held Parameters	Sample	Size	Partial Spearman Rank	Probability
L_X-L_{100}	L_B	E	62	−0.124	0.182
	L_B	S0	71	0.028	>0.400
	L_X/L_B	E	62	0.164	0.105
	L_X/L_B	S0	71	0.258	0.018
	L_{12}	E	62	0.103	0.223
	L_{12}	S0	70	0.134	0.146
	L_B, L_X/L_B	E	62	−0.102	0.225
	L_B, L_X/L_B	S0	71	0.025	>0.400
	L_B, L_{12}	E	62	−0.128	0.176
	L_B, L_{12}	S0	70	−0.030	>0.400
	L_X/L_B, L_{12}	E	62	0.090	0.248
	L_X/L_B, L_{12}	S0	70	0.117	0.183
	L_B, L_X/L_B, L_{12}	E	62	−0.107	0.218
	L_B, L_X/L_B, L_{12}	S0	70	−0.019	>0.400
L_X/L_B-L_{12}	L_{100}	E	62	0.252	0.026
	L_{100}	S0	70	0.100	0.216
	L_B, L_{100}	E	62	0.084	0.262
	L_B, L_{100}	S0	70	0.045	0.359
	L_X, L_{100}	E	62	−0.007	>0.400
	L_X, L_{100}	S0	70	−0.002	>0.400
	L_B, L_X, L_{100}	E	62	−0.014	>0.400
	L_B, L_X, L_{100}	S0	70	−0.007	>0.400
L_X/L_B-L_{100}	L_B	E	62	−0.072	0.291
	L_B	S0	71	0.012	>0.400
	L_X	E	62	−0.008	>0.400
	L_X	S0	71	0.022	>0.400
	L_{12}	E	62	0.050	0.351
	L_{12}	S0	70	0.066	0.295
	L_B, L_X	E	62	−0.015	>0.400
	L_B, L_X	S0	71	0.001	>0.400
	L_B, L_{12}	E	62	−0.073	0.290
	L_B, L_{12}	S0	70	−0.030	>0.400
	L_X, L_{12}	E	62	−0.007	>0.400
	L_X, L_{12}	S0	70	−0.002	>0.400
	L_B, L_X, L_{12}	E	62	−0.015	>0.400
	L_B, L_X, L_{12}	S0	70	−0.019	>0.400
L_{12}-L_{100}	L_B	E	62	0.009	>0.400
	L_B	S0	70	0.603	<0.005
	L_X	E	62	0.160	0.114
	L_X	S0	70	0.646	<0.005
	L_X/L_B	E	62	0.210	0.054
	L_X/L_B	S0	70	0.680	<0.005
	L_B, L_X	E	62	0.035	0.393
	L_B, L_X	S0	70	0.602	<0.005
	L_B, L_X/L_B	E	62	0.016	>0.400
	L_B, L_X/L_B	S0	70	0.603	<0.005
	L_X, L_X/L_B	E	62	0.160	0.117
	L_X, L_X/L_B	S0	70	0.646	<0.005
	L_B, L_X, L_X/L_B	E	62	0.035	0.395
	L_B, L_X, L_X/L_B	S0	70	0.602	<0.005

galaxies, many of which are starbursts, are interacting, or have prominent active nuclei. The dotted histograms in Figure 15 are for the IBGS, scaled to our sample size. The distribution of the 60 μm/100 μm ratios peaks at lower values for our sample than for the IBGS. This would appear to indicate overall lower dust temperature in our sample relative to the IBGS, possibly because the dust in our sample is more like Galactic cirrus than like dust heated by H II regions. This is in keeping with the differences in morphology between the two samples. The distributions of the 12 μm/25 μm, 12 μm/60 μm, and 25 μm/60 μm ratios are shifted to larger values for our sample than for the IBGS. This makes sense if the relative contribution of photospheric emission to dust emission in the MIR is greater for our sample than for the IBGS.

Helou et al. (1991) have introduced the Γ parameter [$\Gamma = \nu f_\nu(12)/\mathrm{FIR}$] to be used in conjunction with Θ (the ratio of the 60 μm and 100 μm fluxes) as a diagnostic of the contribution as a function of grain size to the overall *IRAS* flux of a source. They give distributions in this "Γ-Θ" plane for regions associated with Galactic disk stars, Virgo spirals, and the IBGS, and for a sample of "cold" galaxies in their Figure 1. We show the distribution of our sample in the Γ-Θ plane in Figure 16, along

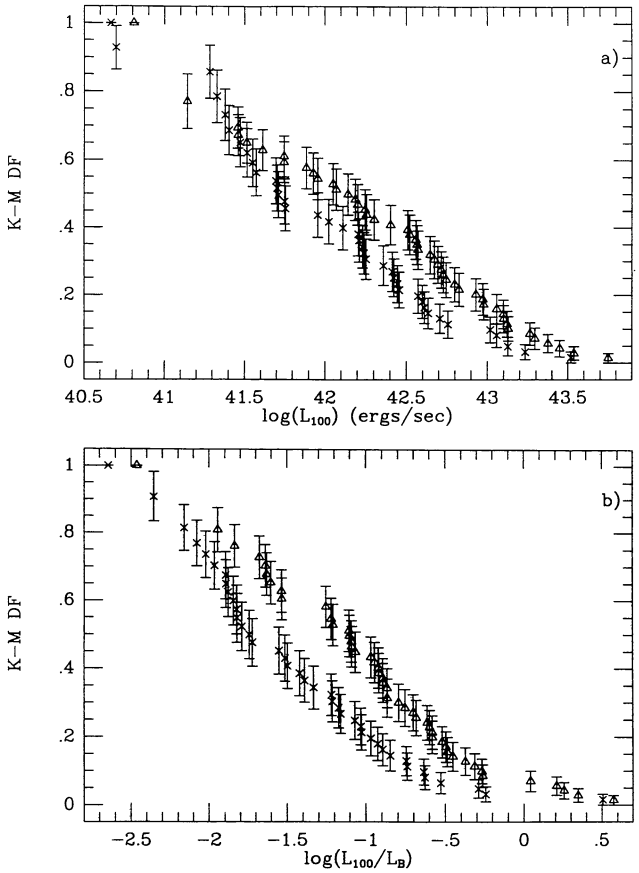

FIG. 14.—Integral K-M DFs of (*a*) L_{100} and (*b*) L_{100}/L_B for our samples of E and S0 galaxies. Symbols and error bars as in Fig. 8.

with outlines of the regions occupied by the various samples from Helou et al. (1991) as labeled in the figure caption. An examination of Figure 16 points out two particularly interesting features. First, the distribution of our sample in Γ goes to far higher values than are found for any of the Helou et al. late-type galaxy or stellar samples. Virtually all the E galaxies are high-Γ objects. Second, while our sample has no objects with Θ as large as the largest values found either in the IBGS or in regions near Galactic stars, it has many objects with Θ-values larger than those found for the cold galaxy sample. The first of these distinctions is reasonably explained by assuming that a significant fraction of the 12 μm flux from our sample comes from stars or AGNs, and by noting that the FIR is typically much lower for early-type galaxies than for spirals (Knapp et al. 1989). It could also be due to a grain-size spectrum strongly skewed to small grains due to efficient sputtering by the harder ISRF of early-type galaxies. The second distinction indicates that, while the overall FIR flux from E/S0 galaxies is not due to emission from dust as warm as that associated with major starbursts, the dust in early-type galaxies is heated as effectively as that in normal spirals.

Returning to the morphological segregation in Figure 16, we note that nearly all the objects that fall into the region occupied by the Virgo spiral sample and the circumstellar ISM are S0 galaxies. There is no evidence for any significant difference in the typical Θ values of the E and S0 galaxies: the separation is entirely due to the S0 galaxies having typically lower Γ-values than the E galaxies. Recalling that we find no compelling evidence for a difference in the 12 μm DFs of the E and S0 galaxies (§ 4.1.2 above), the separation in Γ seems driven by the larger relative amount of FIR radiation from S0s than from Es—a result fully in keeping with the study of Knapp et al. (1989),

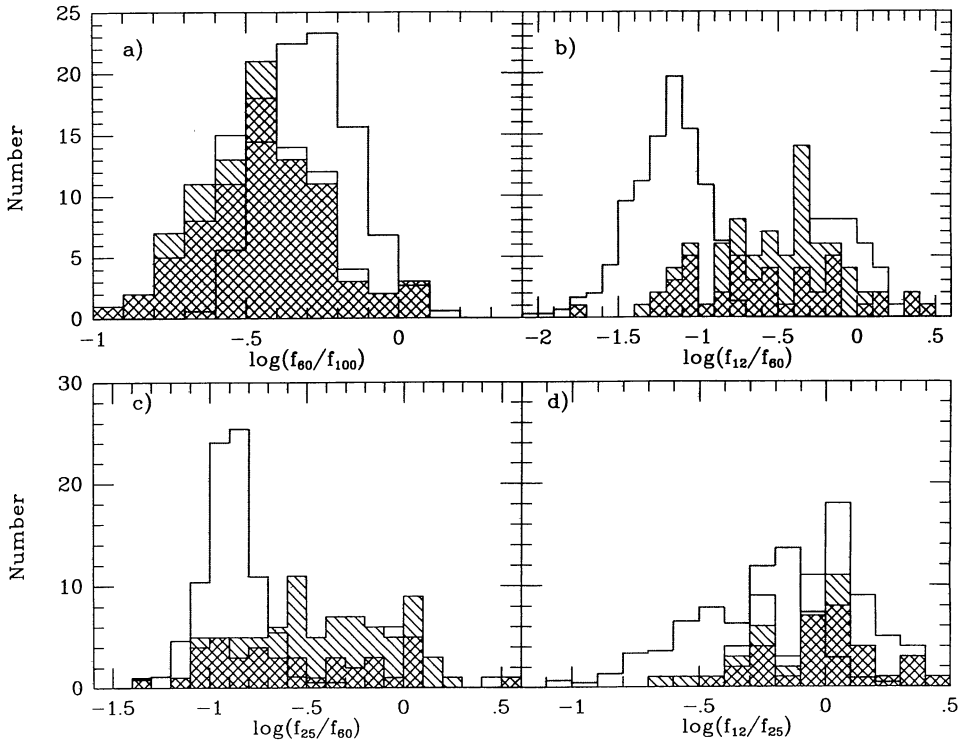

FIG. 15.—Histograms of various infrared colors for our sample, following Soifer et al. (1989). Cross-hatched areas show detections; hatched areas include upper limits; and open areas also include lower limits. Dotted histograms are for the IBGS (Soifer et al. 1989) scaled to our sample size.

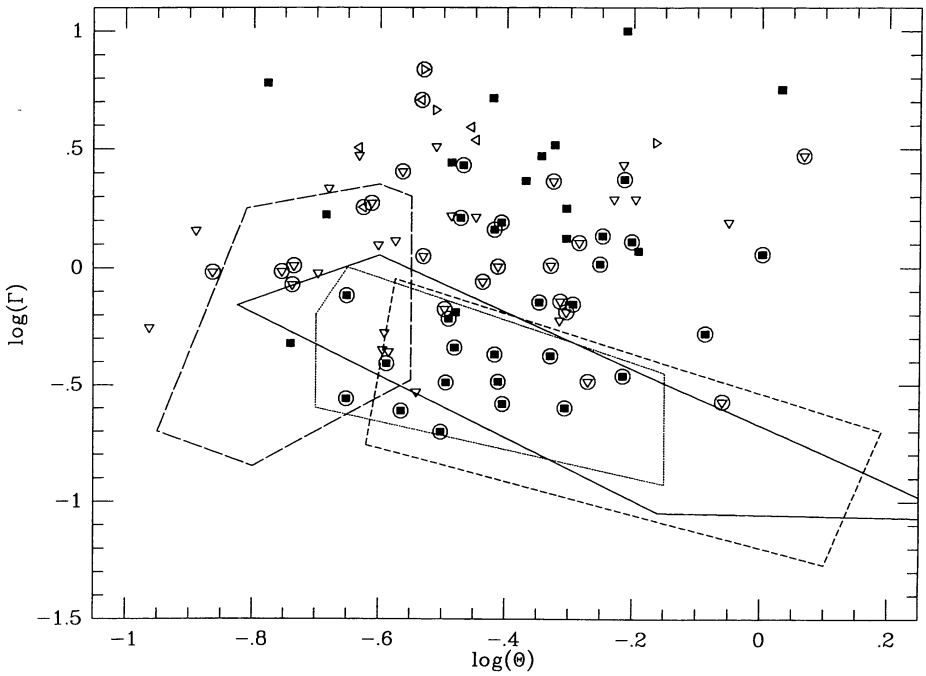

FIG. 16.—"Γ-Θ" plot for our sample, following Helou et al. (1991), showing a significant number of objects with much larger Γ-values than are found for spiral samples. Symbols as in Fig. 9. Circled objects are S0 galaxies. Outlined regions are the areas occupied by the various samples of Helou et al. (1991): *Solid outline:* ISM near Galactic disk stars. *Dotted outline:* Virgo spirals. *Dashed outline:* IBGS. *Long-dashed outline:* "Cold" galaxies and diffuse Galactic ISM.

and consistent with the higher values of L_{100}/L_B that we found for the S0 sample compared with the E sample in § 4.1.2.

Plots of the *IRAS* colors against L_X and L_X/L_B do not define any clear correlations. There is a vague tendency for the systems with the largest L_X/L_B to have the highest Θ-values, but no trend is apparent at all over the lowest 2 dex in L_X/L_B. There also appears to be a trend of increasing Θ with increasing L_X. However, given the scarcity of points with log $L_X < 40$ in our sample, this could easily be a selection effect. Plots of these two distributions are shown in Figure 17. We note that these are the *best* trends we find between X-ray emission and *IRAS* colors. Given the existence of both lower and upper limits in the FIR colors, there are no statistical tests of correlation that can be applied to these samples.

Finally, we have examined two *IRAS*-optical color-color plots to search for evidence of extinction in our sample. In Figure 18 we plot L_{12}/L_{100} against L_B/L_{100}. The circled points are the S0 galaxies. If the 12 μm flux is due to photospheric emission, and there is no substantial optical extinction, the data should scatter about a line of slope 1. Such a line is drawn (with an arbitrary zero point) in the figure. The bulk of the points are consistent with such a relationship. If there is a significant amount of dust extinction, then the B flux will be decreased more than the 12 μm flux, and there will be an increase in the 100 μm emission. These effects will cause dusty systems to lie substantially to the left of the slope 1 line (due to both the decrease in B and the increase in 100 μm), and to lie in the lower part of the plot (mainly due to the 100 μm enhancement). A number of objects do lie in this region. They are labeled in the figure. Note that virtually all these anomalous objects are S0 galaxies. The one E galaxy that is highly deviant is the dwarf elliptical NGC 1510 ($M_B \sim -18$). Recent work (e.g., Bender et al. 1991) indicates that such galaxies do not fall along a simple extension of the properties of giant ellipticals. Additionally, NGC 1510 is known to have an H II region–like nuclear spectrum (Phillips, Charles, & Baldwin 1983). We also note that most of the deviant S0 galaxies are known to be not entirely "normal" S0s. NGC 2444 is the early-type component of Arp 143, and is paired with a highly distorted ring galaxy (Arp 1966). NGC 6964 is also in an interacting pair with the starburst system NGC 6962 (Bernlohr 1993). NGC 6027 is the brightest member of Seyfert's Quintet (Hickson group 79; Hickson 1982). NGC 4507 has a weak Seyfert 2 nucleus (Phillips et al. 1983). Finally, NGC 6880 has optical dust lanes (Corwin, de Vaucouleurs, & de Vaucouleurs 1985).

In Figure 19 we plot L_{12}/L_{100} against L_{12}/L_B. In this case, the standard assumptions that the 12 μm flux is due to photospheric emission, and that there is no substantial optical extinction, would result in the points scattering about some constant value of L_{12}/L_B. Objects with significant extinction will tend to populate the lower right area of the plot. Once again, a number of points lie in this regime. They are the same objects as in Figure 18. Three of these galaxies are in the "spiral" region of Figure 16 (NGC 2444, NGC 6880, and IC 1024). Note that the one object in the elliptical sample that lies at the lower left in the plot is the Local Group nucleated dwarf elliptical NGC 205. This object is clearly very different from normal giant ellipticals in its structural properties (e.g., Kormendy 1985; Bender et al. 1991), its stellar populations (e.g., Wilcots et al. 1990; Davidge 1992), and its ISM (e.g., Johnson & Gottesman 1983; Fich & Hodge 1991). The above findings reinforce the results of §§ 4.1.2 and 4.2 that the S0 galaxies are the objects driving the discrepancy between our results for the L_{12}-L_B correlation and our expectations, that S0 galaxies have a

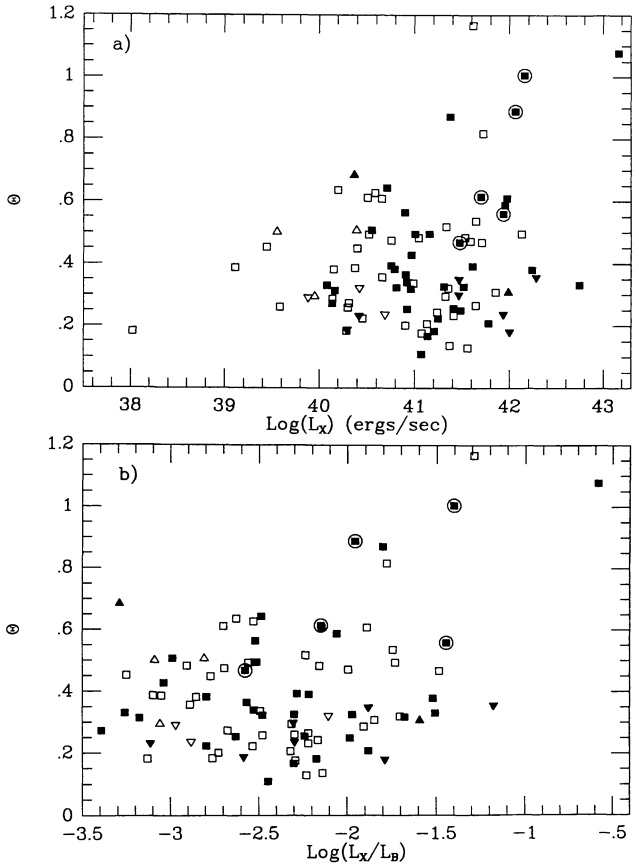

FIG. 17.—Θ-parameter for objects in our sample plotted against (*a*) L_X and (*b*) L_X/L_B. Filled symbols are X-ray detections; open symbols are X-ray upper limits. Squares are 60 and 100 μm detections, upward-pointing triangles are Θ lower limits, and downward-pointing triangles are Θ upper limits. Circled points are known AGNs.

significantly larger nonphotospheric contribution to their 12 μm flux than do E galaxies, and that S0 galaxies have larger FIR-to-optical and FIR-to-MIR ratios than do E galaxies. We note that an actual enhancement of the 12 μm flux from S0 galaxies (rather than just a decrease in the *B*-band flux due to extinction) would cause the observed difference in slope between the L_{12}-L_X relationships for the E and S0 galaxies determined in § 4.1.2.

4.4. *L_X versus Radio Emission*

There are published integrated 6 cm radio continuum measurements for 133 of our sample (see Table 1). Unfortunately, these data are very heterogeneous, having been collected by a large number of workers with many telescope/receiver combinations over the last ~20 years. The relationship between radio power and X-ray emission from early-type galaxies has been studied previously with smaller samples (e.g., FGT). The standard hypothesis (see Fabbiano 1989 and references therein) is that the X-ray gas acts as a confining medium for outflowing material from an active nuclear source. There also could be a connection in the opposite sense: the central source could be fueled by cooling flow gas (FGT). We have analyzed both the relationship between X-ray and total radio emission and, where the data are available, that between X-ray and core radio emission.

4.4.1. *Total Radio Emission*

There are strong statistical correlations between the 6 cm radio luminosity (L_6) and L_X, L_B, and L_X/L_B for our sample (see Table 2A). Strong correlations also exist between the radio-to-optical ratio (L_6/L_B) and the X-ray and optical data. We derive L_6 by summing the radio power over a ~1% bandwidth of 50 MHz. The regressions are given in Table 3A. The

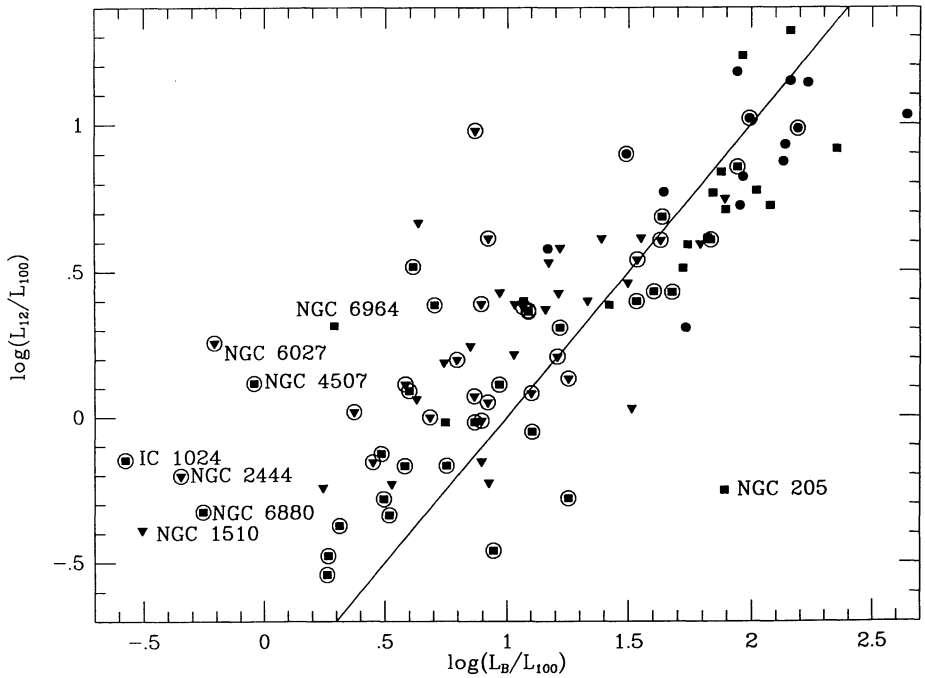

FIG. 18.—L_{12}/L_{100} vs. L_B/L_{100} for our sample. The squares are objects detected in both 12 and 100 μm. Downward-pointing triangles are objects with 12 μm upper limits. Filled circles are objects with 100 μm upper limits (and are thus double lower limits in this plot). Circled points are S0 galaxies. The line has slope 1 with an arbitrary zero point. Objects that deviate from this trend are labeled.

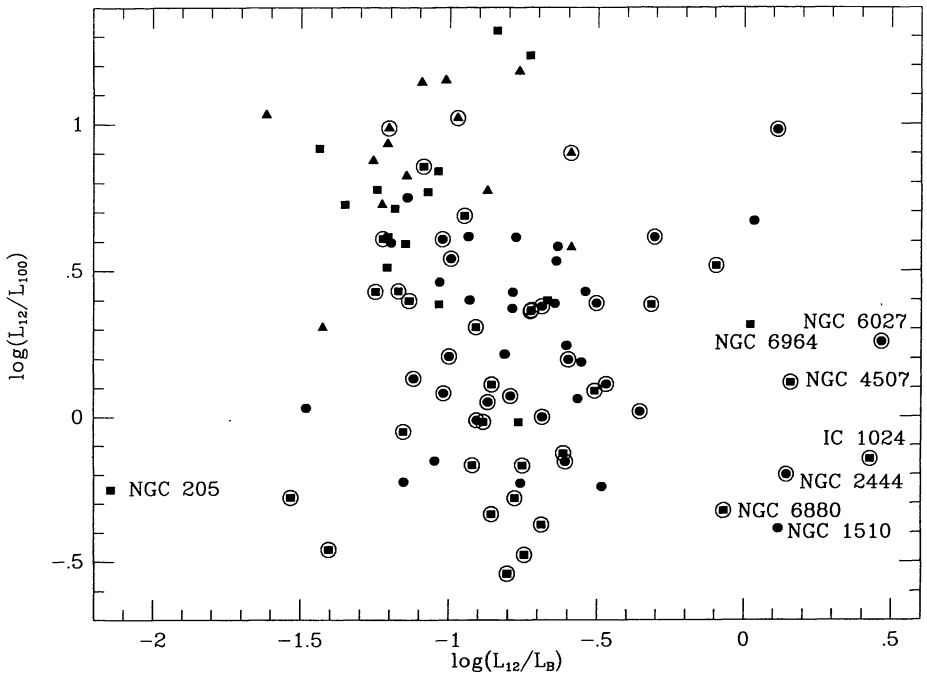

FIG. 19.—L_{12}/L_{100} vs. L_{12}/L_B for our sample. Filled squares are objects detected in both 12 and 100 μm. Upward-pointing triangles are objects with 100 μm upper limits (lower limits in this plot). Filled circles are objects with 12 μm upper limits (double upper limits in this plot). Circled points are S0 galaxies. Objects that deviate from the typical L_{12}/L_B are labeled.

fits for L_B, L_X and L_X/L_B are shown along with the data in Figures 20 (for L_6) and 21 (for L_6/L_B). We note that the regressions on the current sample yield slopes that are consistent in all cases with those given by FGT. It is clear that there is a relationship between the X-ray and radio emission in our sample that cannot be explained as a "bright-things-are-bright" correlation: The L_6-L_X relationship is steeper than slope 1 at nearly the 8 σ level, while the relationship between L_X and L_6/L_B is almost exactly slope 1. Given this, and the slopes of the L_B-L_6 and L_X-L_6 regressions (Table 3A), one might argue that the relationship we derive between L_X and L_6 is a statistical fluke, entirely driven by the (statistically stronger; see Table 2A) relationships between L_B and both L_X and L_6. However, we also derive strong statistical relationships between L_6 and L_X/L_B, L_6/L_B and L_X, and L_6/L_B and L_X/L_B. Thus for a given L_B, those objects with higher X-ray luminosities also tend to have higher radio luminosities. Furthermore, the X-ray luminosity scales linearly with the radio-to-optical ratio.

A partial rank analysis on L_B-L_X-L_X/L_B-L_6 shows the L_B-L_6 relationship to be the dominant statistical relationship. It *does* appear to drive the bivariate correlation between L_X and L_6 (see Table 9A). However, there is also a strong correlation between L_X/L_B and L_6, even accounting for the L_B-L_6 correlation. Thus there appears to be an underlying physical relationship between the total radio power and the X-ray–to–optical ratio for our sample. Including L_{12} in the partial rank analysis does not change any of these results. We also tested the combination L_B-L_X-L_X/L_B-L_{100}-L_6. This revealed a strong correlation between L_{100} and L_6 (see Table 9A). Among the six luminosity pairs in the test, it is second only to L_B-L_X in strength (stronger than any L_X- or L_X/L_B-L_6 trend): the presence of FIR emission appears strongly coupled to the ability of early-type galaxies to generate nonthermal radio emission. This point is investigated further in § 4.4.2 below.

Because of the known differences in radio emission from E and S0 galaxies (Walsh et al. 1989; Wrobel & Heeschen 1991), we have examined the results for our morphological subsamples. There are 69 elliptical galaxies in our 6 cm sample. Our bivariate analyses of these samples are given in Tables 2B and 3B. The regression lines against L_B, L_X, and L_X/L_B are statistically identical to the fits for the full sample and to those given in FGT. The fits are shown with the data in Figures 22 (for L_6) and 23 (for L_6/L_B).

A partial rank analysis on the variables L_B-L_X-L_X/L_B-L_6 for the E galaxies only gives substantially weaker results for correlations between L_6 and both L_X and L_X/L_B than were obtained for the full sample (see Table 9B). The inclusion of L_{12} in the analysis reveals no new trends. Including L_{100}, we find, as for the full sample, that a strong correlation exists between L_{100} and L_6 for the E galaxies. This is in keeping with the result of Walsh et al. (1989) that powerful radio galaxies tend to also have significant FIR emission.

There are 62 S0 galaxies in our 6 cm sample. The bivariate analysis is given in Tables 2C and 3C. Although the statistical case for correlation is a bit less strong than for the E galaxies, it is still quite good. The fits and the generating data are shown in Figures 24 (for L_6) and 25 (for L_6/L_B). Once again, these results are consistent with those of FGT. There is no evidence from the fits for a statistically significant difference between the E and S0 galaxies in their radio to X-ray properties.

A partial rank analysis on the variables L_B-L_X-L_X/L_B-L_6 for the S0 galaxies shows a weaker relation between L_B and L_6 than

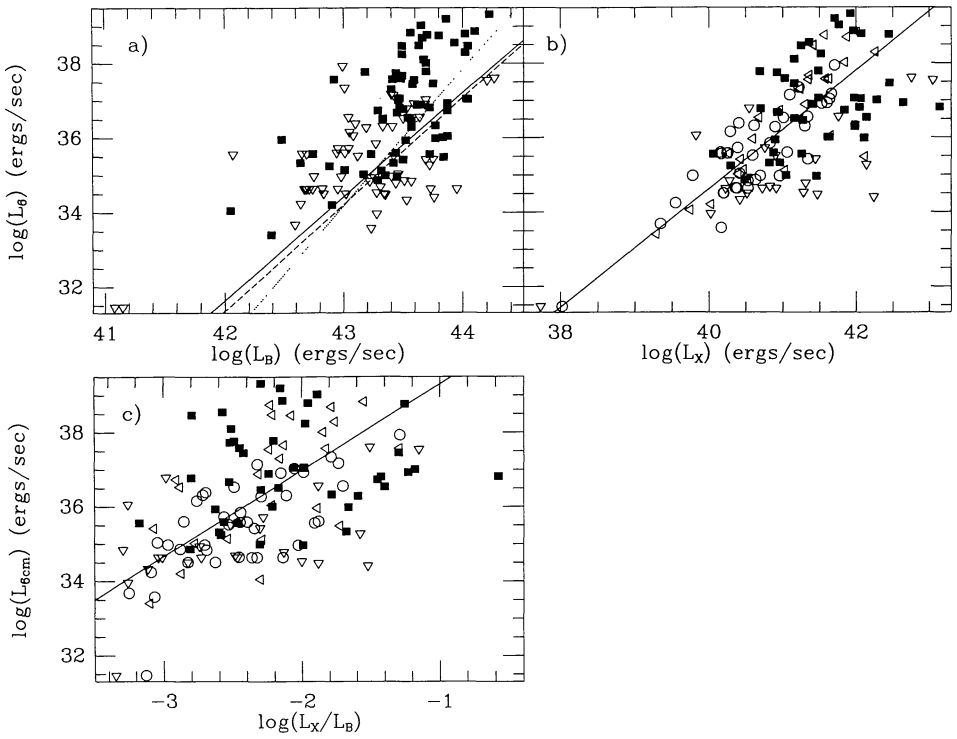

FIG. 20.—Radio luminosity at 6 cm for the full sample plotted against (*a*) L_B, (*b*) L_X, and (*c*) L_X/L_B. Symbols and line coding as in Fig. 9.

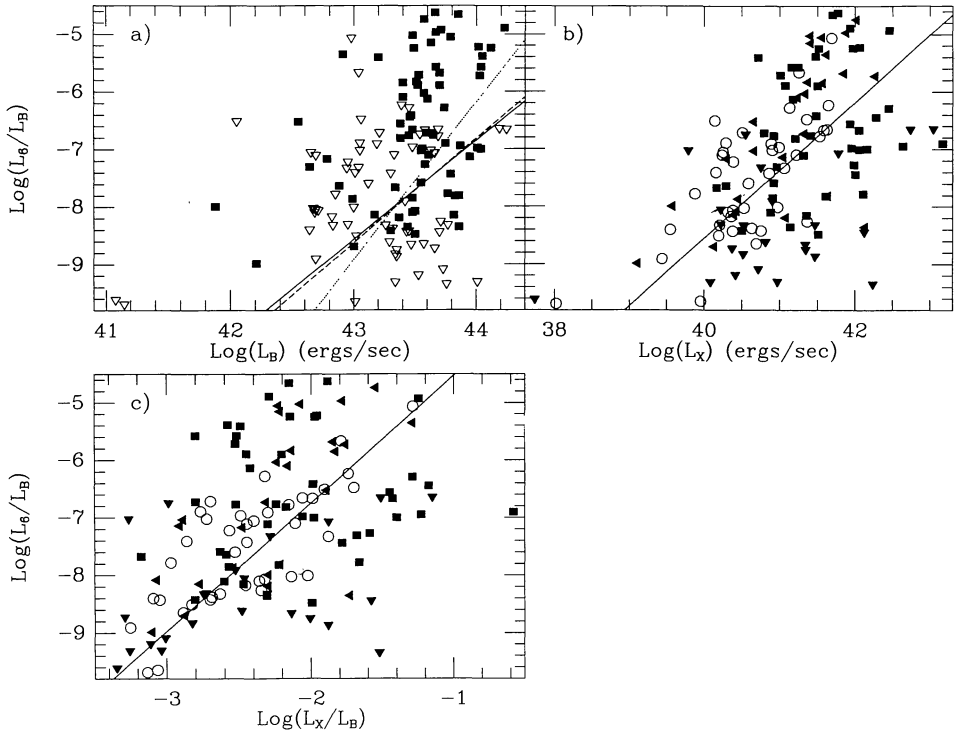

FIG. 21.—L_6/L_B vs. (*a*) L_B, (*b*) L_X, and (*c*) L_X/L_B for the full sample. Symbols and line coding as in Fig. 9.

TABLE 9A

PARTIAL SPEARMAN RANK ANALYSIS: 6 CENTIMETER PROPERTIES, E+S0 SAMPLES

Test Pair	Held Parameters	Size	Partial Spearman Rank	Probability
L_B-L_X	L_6	131	0.583	<0.005
	L_X/L_B, L_6	131	0.532	<0.005
	L_{12}, L_6	120	0.533	<0.005
	L_{100}, L_6	121	0.611	<0.005
	L_X/L_B, L_{12}, L_6	120	0.483	<0.005
	L_X/L_B, L_{100}, L_6	121	0.551	<0.005
L_B-L_X/L_B	L_6	131	0.281	<0.005
	L_X, L_6	131	−0.023	0.397
	L_{12}, L_6	120	0.258	<0.005
	L_{100}, L_6	121	0.316	<0.005
	L_X, L_{12}, L_6	120	−0.029	0.378
	L_X, L_{100}, L_6	121	−0.014	>0.400
L_B-L_{12}	L_6	120	0.362	<0.005
	L_X, L_6	120	0.242	<0.005
	L_X/L_B, L_6	120	0.349	<0.005
	L_X, L_X/L_B, L_6	120	0.239	<0.005
L_B-L_{100}	L_6	121	0.189	0.020
	L_X, L_6	121	0.280	<0.005
	L_X/L_B, L_6	121	0.238	<0.005
	L_X, L_X/L_B, L_6	121	0.277	<0.005
L_B-L_6	L_X	131	0.319	<0.005
	L_X/L_B	131	0.434	<0.005
	L_{12}	120	0.474	<0.005
	L_{100}	121	0.443	<0.005
	L_X, L_X/L_B	131	0.318	<0.005
	L_X, L_{12}	120	0.289	<0.005
	L_X, L_{100}	121	0.178	0.027
	L_X/L_B, L_{12}	120	0.379	<0.005
	L_X/L_B, L_{100}	121	0.309	<0.005
	L_X, L_X/L_B, L_{12}	120	0.289	<0.005
	L_X, L_X/L_B, L_{100}	121	0.178	0.028
L_X-L_X/L_B	L_6	131	0.510	<0.005
	L_B, L_6	131	0.444	<0.005
	L_{12}, L_6	120	0.524	<0.005
	L_{100}, L_6	121	0.532	<0.005
	L_B, L_{12}, L_6	120	0.472	<0.005
	L_B, L_{100}, L_6	121	0.451	<0.005
L_X-L_{12}	L_6	120	0.299	<0.005
	L_B, L_6	120	0.117	0.106
	L_X/L_B, L_6	120	0.290	<0.005
	L_B, L_X/L_B, L_6	120	0.131	0.083
L_X-L_{100}	L_6	121	−0.063	0.249
	L_B, L_6	121	−0.219	0.009
	L_X/L_B, L_6	121	0.008	>0.400
	L_B, L_X/L_B, L_6	121	−0.146	0.059
L_X-L_6	L_B	131	0.193	0.015
	L_X/L_B	131	0.324	<0.005
	L_{12}	120	0.431	<0.005
	L_{100}	121	0.476	<0.005
	L_B, L_X/L_B	131	0.091	0.164
	L_B, L_{12}	120	0.195	0.019
	L_B, L_{100}	121	0.262	<0.005
	L_X/L_B, L_{12}	120	0.269	<0.005
	L_X/L_B, L_{100}	121	0.291	<0.005
	L_B, L_X/L_B, L_{12}	120	0.085	0.191
	L_B, L_X/L_B, L_{100}	121	0.141	0.067
L_X/L_B-L_{12}	L_6	120	0.103	0.143
	L_B, L_6	120	0.003	>0.400
	L_X, L_6	120	−0.068	0.236
	L_B, L_X, L_6	120	−0.059	0.264
L_X/L_B-L_{100}	L_6	121	−0.130	0.082
	L_B, L_6	121	−0.195	0.018
	L_X, L_6	121	−0.114	0.112
	L_B, L_X, L_6	121	−0.106	0.135
L_X/L_B-L_6	L_B	131	0.245	<0.005
	L_X	131	0.180	0.021
	L_{12}	120	0.387	<0.005
	L_{100}	121	0.433	<0.005
	L_B, L_X	131	0.178	0.023
	L_B, L_{12}	120	0.248	<0.005
	L_B, L_{100}	121	0.293	<0.005
	L_X, L_{12}	120	0.177	0.029
	L_X, L_{100}	121	0.196	0.018
	L_B, L_X, L_{12}	120	0.178	0.029
	L_B, L_X, L_{100}	121	0.195	0.018
L_{12}-L_6	L_B	120	0.105	0.135
	L_X	120	0.161	0.042
	L_X/L_B	120	0.269	<0.005
	L_B, L_X	120	0.080	0.205
	L_B, L_X/L_B	120	0.101	0.147
	L_X, L_X/L_B	120	0.170	0.034
	L_B, L_X, L_X/L_B	120	0.089	0.182
L_{100}-L_6	L_B	121	0.333	<0.005
	L_X	121	0.445	<0.005
	L_X/L_B	121	0.479	<0.005
	L_B, L_X	121	0.371	<0.005
	L_B, L_X/L_B	121	0.369	<0.005
	L_X, L_X/L_B	121	0.456	<0.005
	L_B, L_X, L_X/L_B	121	0.382	<0.005

for either the full sample or the E galaxies. However, the evidence for a relation between L_X and L_6 is somewhat stronger for the S0 than for the E galaxies (see Tables 9B and 9C). Including L_{12} in the analysis weakens most trends with L_6, and shows a strong trend between L_{12} and L_6 not seen for either the full sample or the E galaxies (see Table 9C). This is another indication that the 12 μm emission in S0 galaxies is not due only to photospheric and circumstellar dust emission. Including L_{100}, we find evidence for an L_{100}-L_6 correlation as for the E galaxies.

The Kaplan-Meier DFs of L_6 and L_6/L_B of the two morphological subsamples do suggest a difference. These are plotted in integral form in Figure 26. The means of the distributions are given in Table 6. The mean luminosities differ at the 2.6 σ level, while the mean radio-to-optical ratios differ at the 2.0 σ level. In both cases, the S0 galaxies are more radio-weak than the Es. The results of the two-sample tests, also shown in Table 6, maintain evidence for differences at about this level of significance. As was found for the L_X-L_B relationship, the slope of the relation between L_X and L_6 is the same for both E and S0

TABLE 9B

PARTIAL SPEARMAN RANK ANALYSIS: 6 CENTIMETER PROPERTIES, SEPARATE E AND S0 SAMPLES

Test Pair	Held Parameters	Sample	Size	Partial Spearman Rank	Probability
L_B-L_X	L_6	E	69	0.522	<0.005
	L_6	S0	62	0.561	<0.005
	L_X/L_B, L_6	E	69	0.474	<0.005
	L_X/L_B, L_6	S0	62	0.502	<0.005
	L_{12}, L_6	E	61	0.428	<0.005
	L_{12}, L_6	S0	59	0.527	<0.005
	L_{100}, L_6	E	61	0.547	<0.005
	L_{100}, L_6	S0	60	0.563	<0.005
	L_X/L_B, L_{12}, L_6	E	61	0.396	<0.005
	L_X/L_B, L_{12}, L_6	S0	59	0.467	<0.005
	L_X/L_B, L_{100}, L_6	E	61	0.498	<0.005
	L_X/L_B, L_{100}, L_6	S0	60	0.493	<0.005
L_B-L_X/L_B	L_6	E	69	0.247	0.023
	L_6	S0	62	0.293	0.012
	L_X, L_6	E	69	−0.014	>0.400
	L_X, L_6	S0	62	0.034	0.296
	L_{12}, L_6	E	61	0.177	0.092
	L_{12}, L_6	S0	59	0.278	0.020
	L_{100}, L_6	E	61	0.262	0.024
	L_{100}, L_6	S0	60	0.317	0.008
	L_X, L_{12}, L_6	E	61	−0.013	>0.400
	L_X, L_{12}, L_6	S0	59	0.037	0.393
	L_X, L_{100}, L_6	E	61	0.042	>0.400
	L_X, L_{100}, L_6	S0	60	0.057	0.339
L_B-L_{12}	L_6	E	61	0.410	<0.005
	L_6	S0	59	0.280	0.018
	L_X, L_6	E	61	0.290	0.014
	L_X, L_6	S0	59	0.184	0.089
	L_X/L_B, L_6	E	61	0.392	<0.005
	L_X/L_B, L_6	S0	59	0.266	0.023
	L_X, L_X/L_B, L_6	E	61	0.290	0.015
	L_X, L_X/L_B, L_6	S0	59	0.185	0.089
L_B-L_{100}	L_6	E	61	0.277	0.018
	L_6	S0	60	0.299	0.011
	L_X, L_6	E	61	0.359	<0.005
	L_X, L_6	S0	60	0.311	0.009
	L_X/L_B, L_6	E	61	0.311	0.009
	L_X/L_B, L_6	S0	60	0.320	0.008
	L_X, L_X/L_B, L_6	E	61	0.358	<0.005
	L_X, L_X/L_B, L_6	S0	60	0.314	0.009
L_B-L_6	L_X	E	69	0.349	<0.005
	L_X	S0	62	0.195	0.070
	L_X/L_B	E	69	0.471	<0.005
	L_X/L_B	S0	62	0.332	<0.005
	L_{12}	E	61	0.452	<0.005
	L_{12}	S0	59	0.341	<0.005
	L_{100}	E	61	0.400	<0.005
	L_{100}	S0	60	0.253	0.028
	L_X, L_X/L_B	E	69	0.348	<0.005
	L_X, L_X/L_B	S0	62	0.189	0.078
	L_X, L_{12}	E	61	0.282	0.017
	L_X, L_{12}	S0	59	0.172	0.101
	L_X, L_{100}	E	61	0.131	0.173
	L_X, L_{100}	S0	60	0.060	0.328
	L_X/L_B, L_{12}	E	61	0.386	<0.005
	L_X/L_B, L_{12}	S0	59	0.264	0.024
	L_X/L_B, L_{100}	E	61	0.290	0.014
	L_X/L_B, L_{100}	S0	60	0.161	0.120
	L_X, L_X/L_B, L_{12}	E	61	0.281	0.018
	L_X, L_X/L_B, L_{12}	S0	59	0.166	0.116
	L_X, L_X/L_B, L_{100}	E	61	0.128	0.180
	L_X, L_X/L_B, L_{100}	S0	60	0.052	0.352

TABLE 9B—*Continued*

Test Pair	Held Parameters	Sample	Size	Partial Spearman Rank	Probability
L_X-L_X/L_B	L_6	E	69	0.493	<0.005
	L_6	S0	62	0.478	<0.005
	L_B, L_6	E	69	0.441	<0.005
	L_B, L_6	S0	62	0.396	<0.005
	L_{12}, L_6	E	61	0.439	<0.005
	L_{12}, L_6	S0	59	0.476	<0.005
	L_{100}, L_6	E	61	0.471	<0.005
	L_{100}, L_6	S0	60	0.491	<0.005
	L_B, L_{12}, L_6	E	61	0.408	<0.005
	L_B, L_{12}, L_6	S0	59	0.404	<0.005
	L_B, L_{100}, L_6	E	61	0.406	<0.005
	L_B, L_{100}, L_6	S0	60	0.398	<0.005
L_X-L_{12}	L_6	E	61	0.344	<0.005
	L_6	S0	59	0.236	0.040
	L_B, L_6	E	61	0.173	0.096
	L_B, L_6	S0	59	0.100	0.234
	L_X/L_B, L_6	E	61	0.317	0.008
	L_X/L_B, L_6	S0	59	0.221	0.050
	L_B, L_X/L_B, L_6	E	61	0.163	0.115
	L_B, L_X/L_B, L_6	S0	59	0.106	0.225
L_X-L_{100}	L_6	E	61	−0.062	0.320
	L_6	S0	60	0.076	0.286
	L_B, L_6	E	61	−0.245	0.033
	L_B, L_6	S0	60	−0.115	0.204
	L_X/L_B, L_6	E	61	0.010	>0.400
	L_X/L_B, L_6	S0	60	0.099	0.234
	L_B, L_X/L_B, L_6	E	61	−0.187	0.084
	L_B, L_X/L_B, L_6	S0	60	−0.073	0.296
L_X-L_6	L_B	E	69	0.211	0.044
	L_B	S0	62	0.259	0.023
	L_X/L_B	E	69	0.360	<0.005
	L_X/L_B	S0	62	0.330	<0.005
	L_{12}	E	61	0.440	<0.005
	L_{12}	S0	59	0.361	<0.005
	L_{100}	E	61	0.491	<0.005
	L_{100}	S0	60	0.347	<0.005
	L_B, L_X/L_B	E	69	0.132	0.155
	L_B, L_X/L_B	S0	62	0.185	0.082
	L_B, L_{12}	E	61	0.261	0.024
	L_B, L_{12}	S0	59	0.212	0.060
	L_B, L_{100}	E	61	0.336	<0.005
	L_B, L_{100}	S0	60	0.252	0.029
	L_X/L_B, L_{12}	E	61	0.322	0.007
	L_X/L_B, L_{12}	S0	59	0.249	0.033
	L_X/L_B, L_{100}	E	61	0.345	<0.005
	L_X/L_B, L_{100}	S0	60	0.230	0.043
	L_B, L_X/L_B, L_{12}	E	61	0.173	0.098
	L_B, L_X/L_B, L_{12}	S0	59	0.139	0.164
	L_B, L_X/L_B, L_{100}	E	61	0.233	0.041
	L_B, L_X/L_B, L_{100}	S0	60	0.174	0.099
L_X/L_B-L_{12}	L_6	E	61	0.144	0.147
	L_6	S0	59	0.089	0.255
	L_B, L_6	E	61	0.061	0.326
	L_B, L_6	S0	59	0.008	>0.400
	L_X, L_6	E	61	−0.017	>0.400
	L_X, L_6	S0	59	−0.029	>0.400
	L_B, L_X, L_6	E	61	−0.012	>0.400
	L_B, L_X, L_6	S0	59	−0.036	0.396
L_X/L_B-L_{100}	L_6	E	61	−0.112	0.206
	L_6	S0	60	−0.022	>0.400
	L_B, L_6	E	61	−0.185	0.084
	L_B, L_6	S0	60	−0.121	0.193
	L_X, L_6	E	61	−0.094	0.241
	L_X, L_6	S0	60	−0.068	0.308
	L_B, L_X, L_6	E	61	−0.090	0.251
	L_B, L_X, L_6	S0	60	−0.082	0.273

TABLE 9B—*Continued*

Test Pair	Held Parameters	Sample	Size	Partial Spearman Rank	Probability
L_X/L_B-L_6	L_B	E	69	0.209	0.046
	L_B	S0	62	0.223	0.044
	L_X	E	69	0.131	0.155
	L_X	S0	62	0.137	0.158
	L_{12}	E	61	0.350	<0.005
	L_{12}	S0	59	0.301	0.011
	L_{100}	E	61	0.406	<0.005
	L_{100}	S0	60	0.300	0.011
	L_B, L_X	E	69	0.128	0.163
	L_B, L_X	S0	62	0.128	0.177
	L_B, L_{12}	E	61	0.249	0.030
	L_B, L_{12}	S0	59	0.205	0.066
	L_B, L_{100}	E	61	0.299	0.011
	L_B, L_{100}	S0	60	0.230	0.043
	L_X, L_{12}	E	61	0.156	0.126
	L_X, L_{12}	S0	59	0.138	0.165
	L_X, L_{100}	E	61	0.174	0.196
	L_X, L_{100}	S0	60	0.142	0.155
	L_B, L_X, L_{12}	E	61	0.153	0.133
	L_B, L_X, L_{12}	S0	59	0.130	0.182
	L_B, L_X, L_{100}	E	61	0.171	0.100
	L_B, L_X, L_{100}	S0	60	0.138	0.164
L_{12}-L_6	L_B	E	61	0.087	0.255
	L_B	S0	59	0.286	0.016
	L_X	E	61	0.130	0.173
	L_X	S0	59	0.298	0.012
	L_X/L_B	E	61	0.259	0.024
	L_X/L_B	S0	59	0.375	<0.005
	L_B, L_X	E	61	0.037	0.388
	L_B, L_X	S0	59	0.257	0.028
	L_B, L_X/L_B	E	61	0.069	0.303
	L_B, L_X/L_B	S0	59	0.279	0.020
	L_X, L_X/L_B	E	61	0.131	0.173
	L_X, L_X/L_B	S0	59	0.299	0.013
	L_B, L_X, L_X/L_B	E	61	0.039	0.386
	L_B, L_X, L_X/L_B	S0	59	0.259	0.028
L_{100}-L_6	L_B	E	61	0.319	0.007
	L_B	S0	60	0.455	<0.005
	L_X	E	61	0.455	<0.005
	L_X	S0	60	0.512	<0.005
	L_X/L_B	E	61	0.489	<0.005
	L_X/L_B	S0	60	0.555	<0.005
	L_B, L_X	E	61	0.374	<0.005
	L_B, L_X	S0	60	0.467	<0.005
	L_B, L_X/L_B	E	61	0.354	<0.005
	L_B, L_X/L_B	S0	60	0.468	<0.005
	L_X, L_X/L_B	E	61	0.462	<0.005
	L_X, L_X/L_B	S0	60	0.515	<0.005
	L_B, L_X, L_X/L_B	E	61	0.382	<0.005
	L_B, L_X, L_X/L_B	S0	60	0.472	<0.005

galaxies, but the S0s are shifted to lower radio luminosity. This is consistent with the findings of Wrobel & Heeschen (1991) based on radio observations of a purely optically selected sample of E and S0 galaxies. Since both the size and significance of the offsets in L_X and L_6 for the E and S0 galaxies are comparable, we have also investigated the DF of the quantity L_X/L_6. There are upper limits in both quantities. No statistical methods are available that can robustly determine a distribution function with upper and lower limits (and many limit ratios!), so we have simply tested the sample of objects detected both in X-rays and at 6 cm. For these galaxies there is no evidence that the DFs of L_X/L_6 of the E and S0 galaxies differ: the mean values differ by 0.096 ± 0.370; the two-sample tests all support the null hypothesis at higher than 75%. Whatever governs the relationship between radio continuum and X-ray emission does not appear to differ between E and S0 galaxies from these data.

4.4.2. *X-Ray–FIR–Radio Correlation*

A previous analysis of a smaller sample of early-type galaxies led to the suggestion of a relationship between the distribution

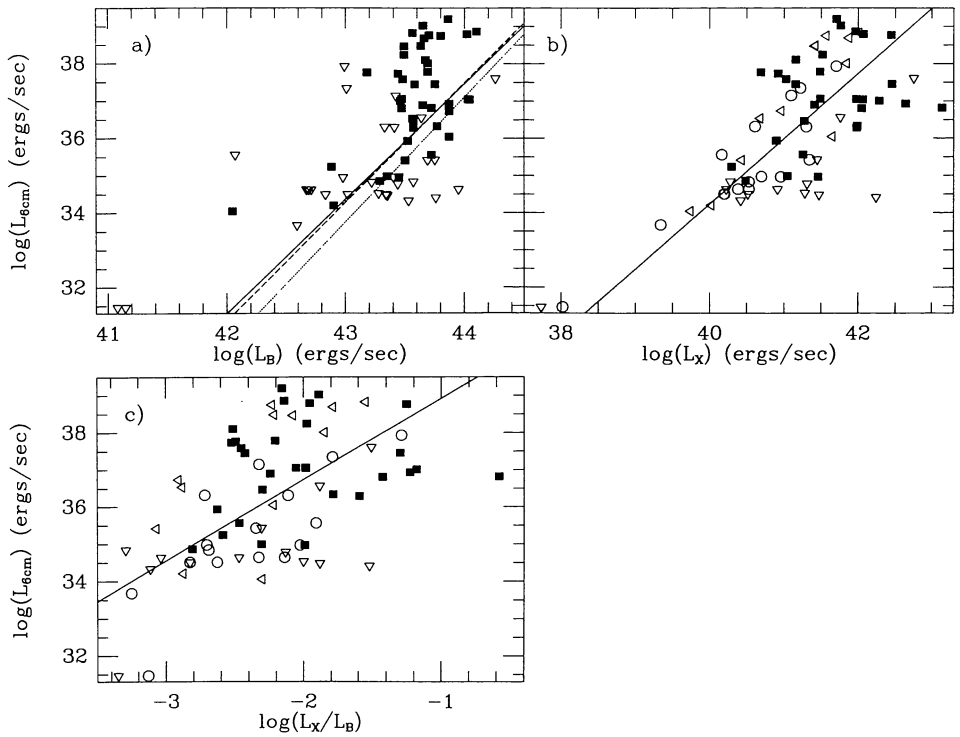

FIG. 22.—L_6 vs. (*a*) L_B, (*b*) L_X, and (*c*) L_X/L_B, for elliptical galaxies only. Symbols and line coding as in Fig. 9.

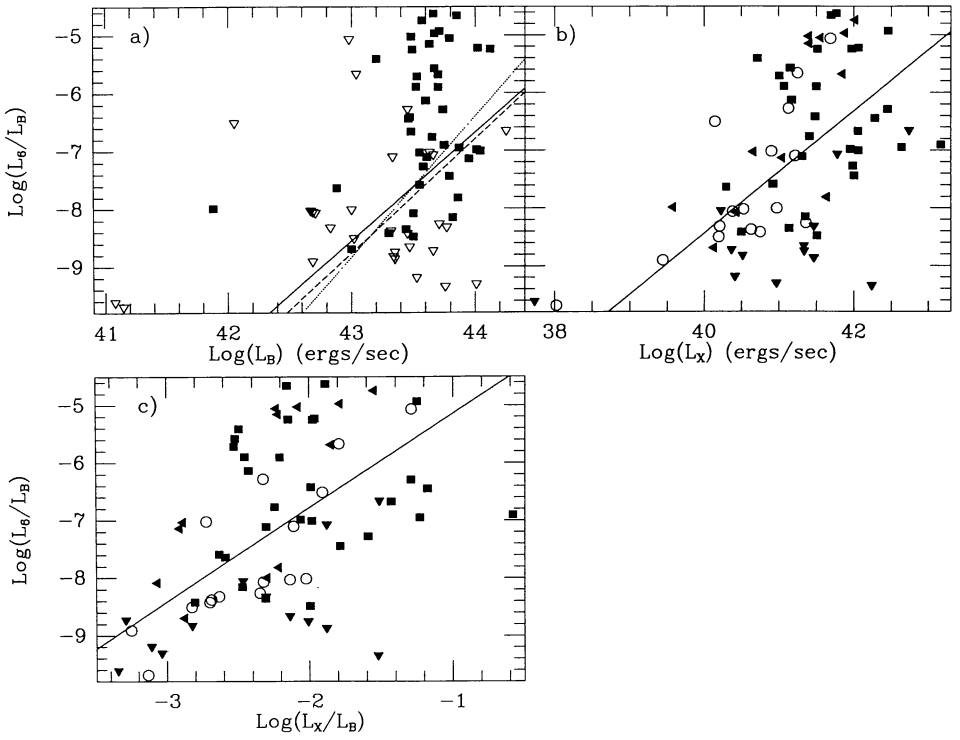

FIG. 23.—L_6/L_B vs. (*a*) L_B, (*b*) L_X, and (*c*) L_X/L_B, for elliptical galaxies only. Symbols and line coding as in Fig. 9.

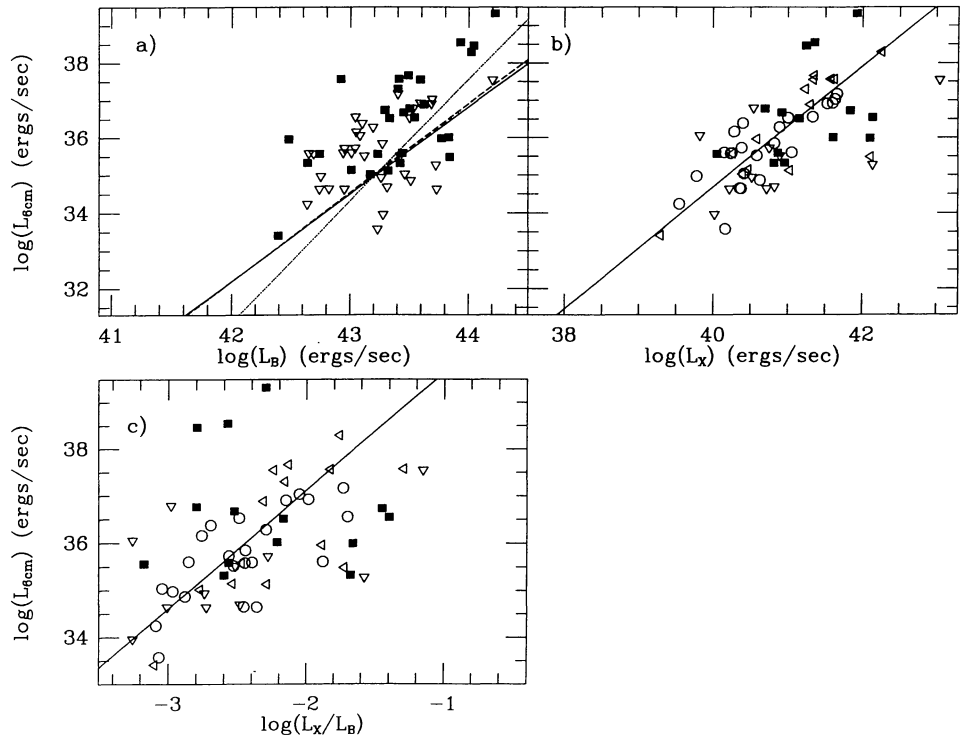

FIG. 24.—L_6 vs. (*a*) L_B, (*b*) L_X, and (*c*) L_X/L_B, for S0 galaxies only. Symbols and line coding as in Fig. 9.

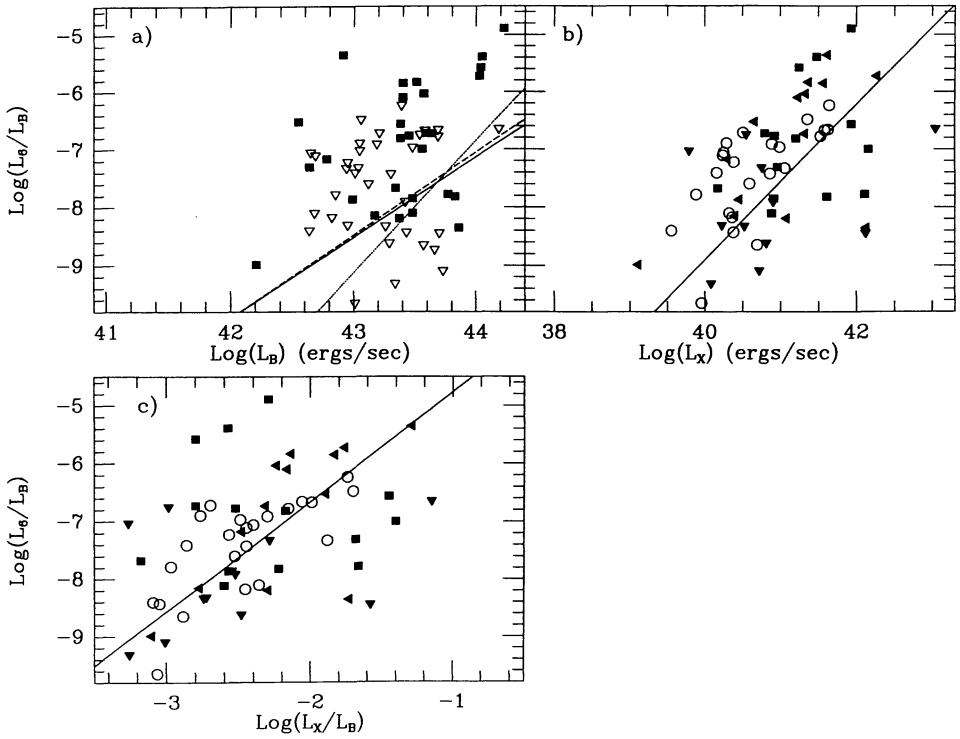

FIG. 25.—L_6/L_B vs. (*a*) L_B, (*b*) L_X, and (*c*) L_X/L_B, for S0 galaxies only. Symbols and line coding as in Fig. 9.

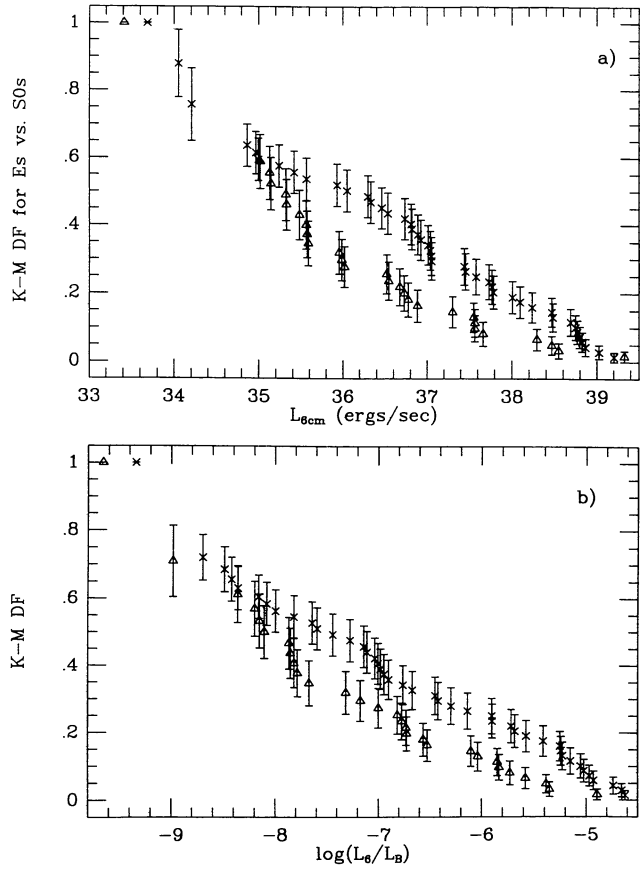

FIG. 26.—Integral K-M DFs of (*a*) L_6 and (*b*) L_6/L_B for our samples of E and S0 galaxies. Symbols as in Fig. 8.

of points in the L_6-L_{100} plane and the range of L_X/L_B for the objects considered (Kim & Fabbiano 1990). Specifically, the systems with the highest L_X/L_B tend to have larger ratio and FIR luminosities than the systems with the lowest L_X/L_B. Furthermore, in the region where the L_{100}'s of the two samples overlap, the high L_X/L_B galaxies are shifted to higher radio luminosities than the low L_X/L_B galaxies. We have repeated this analysis with our current sample. The data are shown for systems with log $(L_X/L_B) > -2.4$ in Figure 27*a* and those with log $(L_X/L_B) < -2.7$ in Figure 27*b*. These ranges correspond to systems with log $(L_X/L_B) > 30.3$ ergs s^{-1} $L_\odot^{-1}$ and log $(L_X/L_B) < 30.0$ ergs s^{-1} $L_\odot^{-1}$ in the units of Kim & Fabbiano (1990). The general pattern discerned by Kim & Fabbiano (1990) remains: systems with high L_X/L_B have generally higher radio and FIR luminosities than those with low L_X/L_B. Furthermore, compared to the rough locus in the L_6-L_{100} plane defined by the low L_X/L_B systems, those with the highest values of L_X/L_B tend to have radio excesses for their FIR luminosities. In agreement with the partial rank analysis presented in § 4.4.1, this result indicates that the presence of a hot ISM in early-type galaxies is a key factor in their ability to generate both radio continuum and FIR emission, and thus argues against the interpretation that radio and FIR emission in early-type galaxies are fueled by external accretion (e.g., Walsh et al. 1989; Forbes 1991). Rather, it is in keeping with the suggestion (FGT) that the hot ISM fuels the central engine responsible for the radio emission.

4.4.3. *Core Radio Emission*

The relationship between X-ray emission and radio-core luminosity was examined by FGT for a sample of 29 objects. Since that study, a large number of arcsecond-scale resolution 6 cm core observations have been published, mainly by Wrobel & Heeschen (1991). Combined with older data on objects not included in the FGT X-ray sample, we now have 6 cm core data for 99 of our sample of 148 galaxies (see Table 1). In Figure 28 we plot L_6 against L_{6co} (the 6 cm radio-core luminosity) for the objects in our sample. The dotted line shows $L_6 \equiv L_{6co}$. The scatter of points below this line can be due either to systematic and statistical errors or to intrinsic source variability.

We have tested for bivariate correlation between the radio core luminosity and the X-ray and optical luminosities as described above. The results of these tests are given in Table 2A. Also shown in Table 2A are the results of correlation analyses performed on the total radio luminosity of the sample for which we have core radio data. In comparing these results, we are thus comparing results drawn from the same sample. The

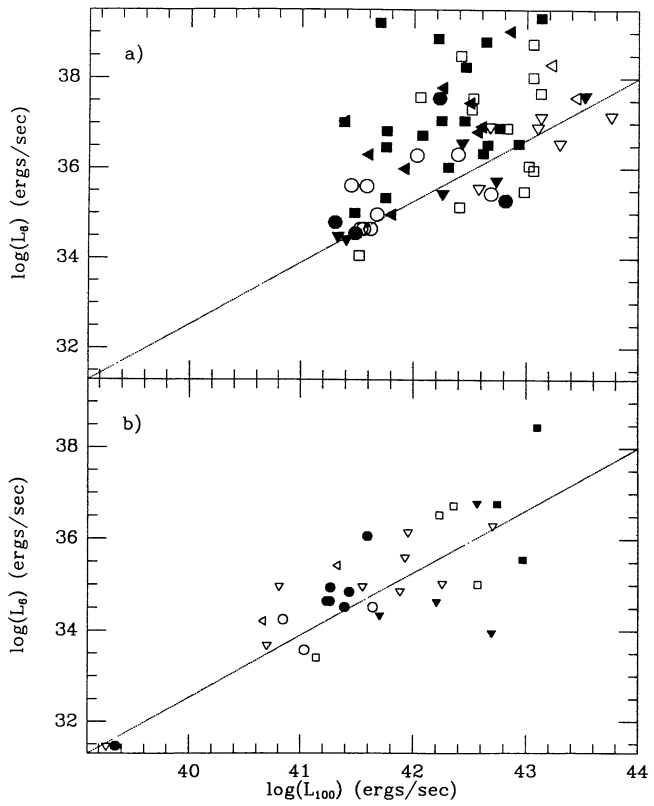

FIG. 27.—L_6 vs. L_{100} for (*a*) galaxies with log $(L_X/L_B) > -2.4$, and (*b*) log $(L_X/L_B) < -2.7$. Symbols are coded as follows: Filled symbols indicate X-ray detections. Open symbols show X-ray upper limits. Squares indicate both 6 cm and 100 μm detections. Circles indicate both 6 cm and 100 μm upper limits. Downward-pointing triangles indicate 100 μm detections and 6 cm upper limits. Left-pointing triangles indicate 6 cm detections and 100 μm upper limits. We also add the same fiducial line (it is *not* a fit line) to both (*a*) and (*b*).

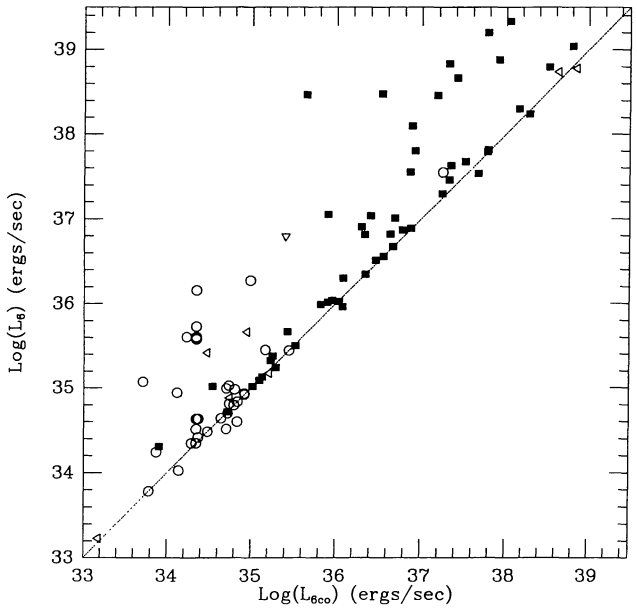

FIG. 28.—L_6 vs. L_{6co}. Symbols as in Fig. 9. The dotted line is $L_6 \equiv L_{6co}$.

tests of L_{6co} with L_X, L_B, and L_X/L_B all show strong statistical correlation, comparable to the results for L_6 for the core sample. We show the results of our regression analysis in Table 3A and Figure 29.

Using the core sample, we find no difference in the slopes of the regressions with X-ray emission for core and total radio power. This may simply be a reflection of our sample being largely core-dominated. We note, also, that there is no significant difference between the fits to the total 6 cm emission for the core sample and those for the full sample (see Table 3A). We find the slope of the relationship between core radio and X-ray luminosities for our sample to be 1.53 ± 0.12—greater than slope 1 at the 4.4 σ level. The relationship between core radio luminosity and the X-ray–to–optical ratio also shows a steep slope (2.92 ± 0.33, inconsistent with slope 1 at the 5.8 σ level). Our slope is consistent with that found by FGT to less than 1 σ (they find a slope of 2.45 ± 0.44). Our results therefore support the notion discussed by FGT that systems with more extensive X-ray halos are able to fuel compact nuclear sources at substantially higher rates than less X-ray–luminous systems.

A partial rank analysis on L_B-L_X-L_X/L_B-L_{6co} shows somewhat stronger trends between L_{6co} and both L_X and L_X/L_B than were found for L_6 in § 4.4.1 above. This is confirmed by a partial rank test including both L_6 and L_{6co}: Both L_X and L_X/L_B are more correlated with *core* radio luminosity than with *total* radio luminosity. However, L_B is clearly more correlated with L_6 than with L_{6co} (see Table 10). This argues that radio cores are fueled by a hot ISM (as suggested by FGT) but that total radio power is more dependent on total luminosity (or mass) and is not intrinsically linked to the presence of a hot ISM. This last finding may have implications for the rate of formation of massive nuclear black holes in early-type galaxies. If the total radio power is a function of the mass of a nuclear black hole, then our result would imply that more massive black holes form in more massive galaxies.

Curiously, when we add L_{12} to the partial rank analysis, and compare the results with those determined for the L_B-L_X-L_X/L_B-L_{12}-L_6 analysis from § 4.4.1 above, we find stronger

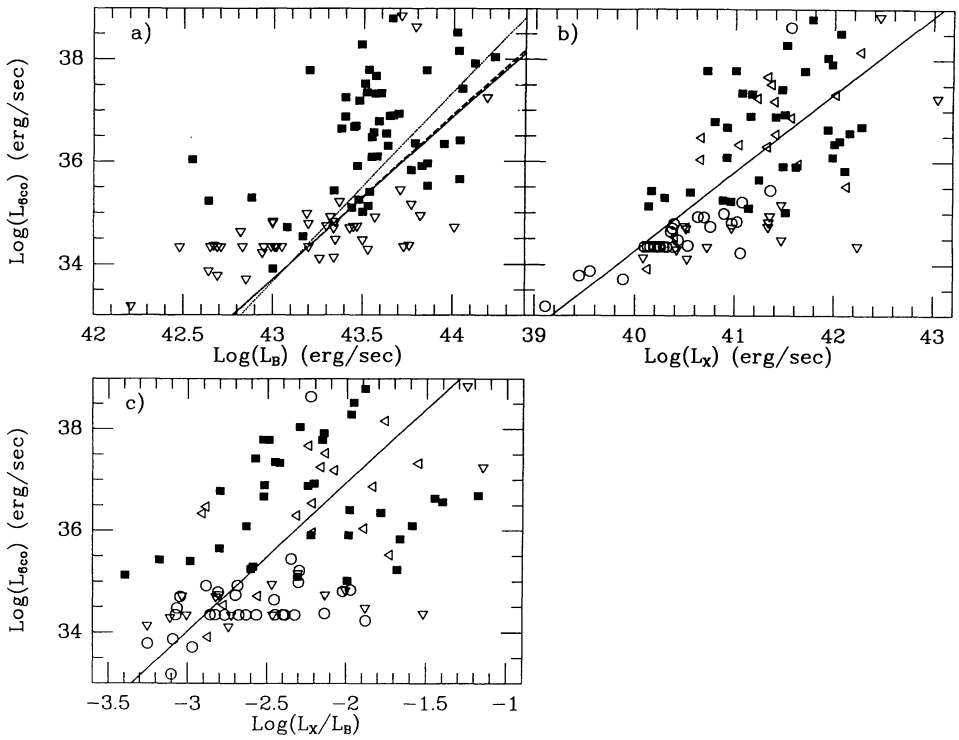

FIG. 29.—L_{6co} vs. (*a*) L_B, (*b*) L_X, and (*c*) L_X/L_B. Symbols and line coding as in Fig. 9.

TABLE 10

PARTIAL SPEARMAN RANK ANALYSIS: 6 CENTIMETER CORE SAMPLE

Test Pair	Held Parameters	Size	Partial Spearman Rank	Probability
L_B-L_X	L_{6co}	99	0.527	<0.005
	L_6	99	0.535	<0.005
	L_X/L_B, L_{6co}	99	0.496	<0.005
	L_X/L_B, L_6	99	0.499	<0.005
	L_{12}, L_{6co}	92	0.459	<0.005
	L_{100}, L_{6co}	93	0.565	<0.005
	L_X/L_B, L_{12}, L_{6co}	92	0.434	<0.005
	L_X/L_B, L_{100}, L_{6co}	93	0.520	<0.005
L_B-L_X/L_B	L_{6co}	99	0.208	0.022
	L_6	99	0.226	0.015
	L_X, L_{6co}	99	−0.034	0.373
	L_X, L_6	99	−0.035	0.369
	L_{12}, L_{6co}	92	0.168	0.060
	L_{100}, L_{6co}	93	0.265	0.007
	L_X, L_{12}, L_{6co}	92	−0.029	0.394
	L_X, L_{100}, L_{6co}	93	0.058	0.296
L_B-L_{12}	L_{6co}	92	0.334	<0.005
	L_X, L_{6co}	92	0.241	0.013
	L_X/L_B, L_{6co}	92	0.331	<0.005
	L_X, L_X/L_B, L_{6co}	92	0.238	0.014
L_B-L_{100}	L_{6co}	93	0.192	0.037
	L_X, L_{6co}	93	0.334	<0.005
	L_X/L_B, L_{6co}	93	0.270	0.006
	L_X, L_X/L_B, L_{6co}	93	0.336	<0.005
L_B-L_{6co}	L_X	99	0.328	<0.005
	L_X/L_B	99	0.478	<0.005
	L_{12}	92	0.476	<0.005
	L_{100}	93	0.416	<0.005
	L_X, L_X/L_B	99	0.327	<0.005
	L_X, L_{12}	92	0.264	0.007
	L_X, L_{100}	93	0.066	0.267
	L_X/L_B, L_{12}	92	0.383	<0.005
	L_X/L_B, L_{100}	93	0.229	0.017
	L_X, L_X/L_B, L_{12}	92	0.262	0.008
	L_X, L_X/L_B, L_{100}	93	0.042	0.348
L_B-L_6	L_X	99	0.394	<0.005
	L_X/L_B	99	0.517	<0.005
	L_X, L_X/L_B	99	0.393	<0.005
L_X-L_X/L_B	L_{6co}	99	0.442	<0.005
	L_6	99	0.470	<0.005
	L_B, L_{6co}	99	0.400	<0.005
	L_B, L_6	99	0.424	<0.005
	L_{12}, L_{6co}	92	0.417	<0.005
	L_{100}, L_{6co}	93	0.391	<0.005
	L_B, L_{12}, L_{6co}	92	0.388	<0.005
	L_B, L_{100}, L_{6co}	93	0.303	<0.005
L_X-L_{12}	L_{6co}	92	0.264	0.007
	L_B, L_{6co}	92	0.117	0.147
	L_X/L_B, L_{6co}	92	0.269	0.006
	L_B, L_X/L_B, L_{6co}	92	0.132	0.115
L_X-L_{100}	L_{6co}	93	−0.177	0.048
	L_B, L_{6co}	93	−0.326	<0.005
	L_X/L_B, L_{6co}	93	−0.047	0.332
	L_B, L_X/L_B, L_{6co}	93	−0.212	0.024
L_X-L_{6co}	L_B	99	0.282	<0.005
	L_X/L_B	99	0.399	<0.005
	L_{12}	92	0.495	<0.005
	L_{100}	93	0.568	<0.005
	L_B, L_X/L_B	99	0.165	0.056
	L_B, L_{12}	92	0.303	<0.005
	L_B, L_{100}	93	0.430	<0.005
	L_X/L_B, L_{12}	92	0.335	<0.005
	L_X/L_B, L_{100}	93	0.353	<0.005
	L_B, L_X/L_B, L_{12}	92	0.177	0.051
	L_B, L_X/L_B, L_{100}	93	0.280	<0.005
L_X-L_6	L_B	99	0.204	0.024
	L_X/L_B	99	0.377	<0.005
	L_B, L_X/L_B	99	0.104	0.167
L_X/L_B-L_{12}	L_{6co}	92	0.047	0.331
	L_B, L_{6co}	92	−0.012	>0.400
	L_X, L_{6co}	92	−0.071	0.254
	L_B, L_X, L_{6co}	92	−0.062	0.283
L_X/L_B-L_{100}	L_{6co}	93	−0.325	<0.005
	L_B, L_{6co}	93	−0.373	<0.005
	L_X, L_{6co}	93	−0.280	<0.005
	L_B, L_X, L_{6co}	93	−0.283	<0.005
L_X/L_B-L_{6co}	L_B	99	0.314	<0.005
	L_X	99	0.219	0.018
	L_{12}	92	0.449	<0.005
	L_{100}	93	0.566	<0.005
	L_B, L_X	99	0.218	0.019
	L_B, L_{12}	92	0.344	<0.005
	L_B, L_{100}	93	0.471	<0.005
	L_X, L_{12}	92	0.245	0.011
	L_X, L_{100}	93	0.350	<0.005
	L_B, L_X, L_{12}	92	0.244	0.012
	L_B, L_X, L_{100}	93	0.346	<0.005
L_X/L_B-L_6	L_B	99	0.251	0.007
	L_X	99	0.183	0.039
	L_B, L_X	99	0.182	0.041
L_{12}-L_{6co}	L_B	92	0.211	0.024
	L_X	92	0.243	0.011
	L_X/L_B	92	0.377	<0.005
	L_B, L_X	92	0.164	0.066
	L_B, L_X/L_B	92	0.202	0.031
	L_X, L_X/L_B	92	0.252	0.009
	L_B, L_X, L_X/L_B	92	0.174	0.054
L_{100}-L_{6co}	L_B	93	0.477	<0.005
	L_X	93	0.606	<0.005
	L_X/L_B	93	0.670	<0.005
	L_B, L_X	93	0.548	<0.005
	L_B, L_X/L_B	93	0.566	<0.005
	L_X, L_X/L_B	93	0.643	<0.005
	L_B, L_X, L_X/L_B	93	0.591	<0.005

evidence for an L_{12}-L_{6co} correlation than for an L_{12}-L_6 correlation (see Table 10). Our analysis on the variables L_B-L_X-L_X/L_B-L_{100}-L_{6co} demonstrates a significantly stronger relationship between L_{100} and L_{6co} than was found for L_{100} and L_6 in § 4.4.1. This indicates that the presence of FIR emission in early-type galaxies is strongly coupled to the ability of these galaxies to generate core radio power, rather than to some global property.

4.5. L_X *versus* H I 21 cm *Emission*

We have compiled the available data on H I 21 cm line emission for the galaxies in our sample. These data are largely obtained from the compilations of Roberts et al. (1991) and Huchtmeier & Richter (1989), supplemented with a few newer references (see notes to Table 1). The H I fluxes (Σ_{H_I}) expressed in Jy km s^{-1} have been converted to M_{H_I} in solar masses, using our distances (D in Mpc) and the standard formula (see Roberts 1975):

$$M_{H_I}(M_\odot) = 2.36 \times 10^5 D^2 \Sigma_{H_I} . \quad (3)$$

For those objects with only upper limits (σ_{H_I}), expressed in janskys (or millijanskys) per channel, we derived H I mass limits from the following relation:

$$M_{H_I}(M_\odot) \leq 2.36 \times 10^5 D^2 3\sigma_{H_I}\Delta v . \quad (4a)$$

The velocity width, Δv, was estimated following Knapp et al. (1985) and Wardle & Knapp (1986):

$$\Delta v = 0.25(L_B/L_\odot)^{1/3} . \quad (4b)$$

Figure 30 shows the H I mass data plotted against L_B, L_X, and L_X/L_B. The plots show no compelling evidence for any correlation, and this is borne out by the results of our bivariate analysis (see Table 2A). Note that we have also tested for correlations with M_{H_I}/L_B, and found nothing. This is in keeping with the results of Knapp et al. (1985). A partial rank analysis on L_B-L_X-L_X/L_B-M_{H_I} shows no evidence for any trends of M_{H_I} with either the optical or the X-ray properties of our sample (see Table 11).

5. SUMMARY AND SUGGESTIONS FOR FUTURE RESEARCH

We have analyzed the relationships between optical luminosity and ISM parameters for the *Einstein* sample of early-type galaxies (P0). This sample is the largest currently available sample of early-type galaxies with X-ray observations. The principal results of this study are as follows:

1. We confirm earlier results (e.g., Forman et al. 1985; Trinchieri et al. 1986; Donnelly et al. 1990) showing a strong, steep correlation between L_B and L_X in early-type galaxies. This correlation holds for all statistical tests applied to the data. It is maintained whether or not we include the Local Group dwarf galaxies NGC 205 and M32 in the analysis. When we fit the data with a power law, we find a slope of 1.8 ± 0.1 for the full sample. Considering only the brighter galaxies, the slope becomes 2.0 ± 0.2. The use of 7S distances does not significantly alter these results. Not surprisingly, we also find strong correlations between L_X and L_X/L_B that are much steeper than slope 1, in the sense that the most X-ray–luminous galaxies have the highest L_X/L_B. Partial rank analysis confirms these trends.

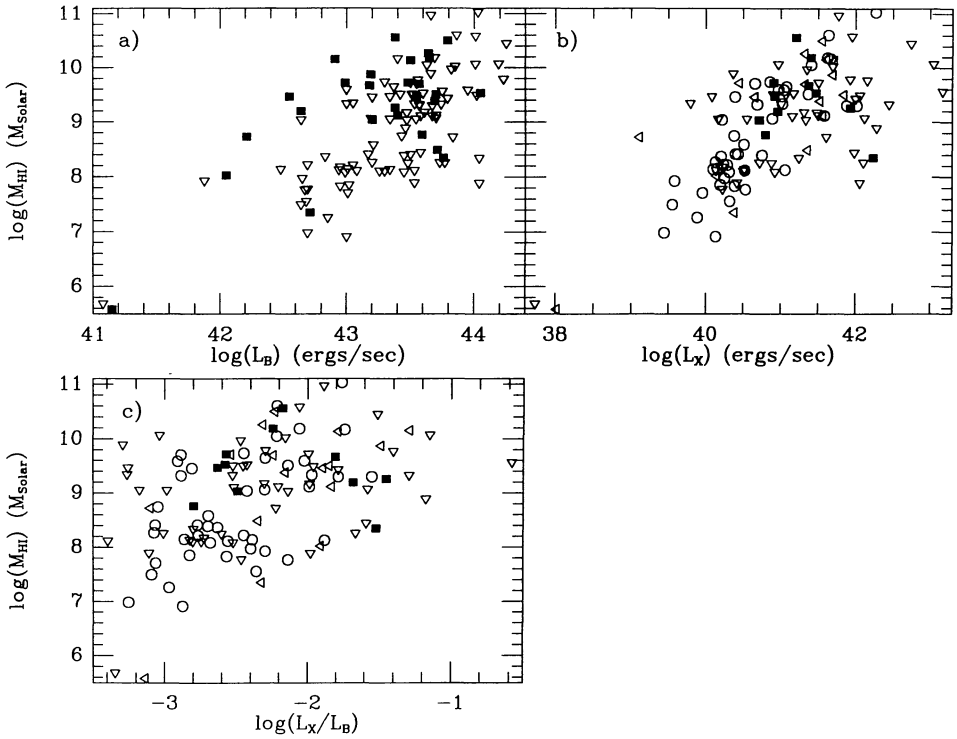

FIG. 30.—M_{H_I} vs. (*a*) L_B, (*b*) L_X, and (*c*) L_X/L_B. Symbols as in Fig. 9.

TABLE 11

PARTIAL SPEARMAN RANK ANALYSIS: H I SAMPLE

Test Pair	Held Parameters	Size	Partial Spearman Rank	Probability
L_B-L_X	M_{H_I}	115	0.693	<0.005
	L_X/L_B, M_{H_I}	115	0.600	<0.005
L_B-L_X/L_B	M_{H_I}	115	0.435	<0.005
	L_X, M_{H_I}	115	0.031	0.371
L_B-M_{H_I}	L_X	115	0.048	0.308
	L_X/L_B	115	0.094	0.171
	L_X, L_X/L_B	115	0.044	0.322
L_X-L_X/L_B	M_{H_I}	115	0.602	<0.005
	L_B, M_{H_I}	115	0.463	<0.005
L_X-M_{H_I}	L_B	115	0.114	0.120
	L_X/L_B	115	0.098	0.161
	L_B, L_X/L_B	115	0.052	0.295
L_X/L_B-M_{H_I}	L_B	115	0.145	0.064
	L_X	115	0.106	0.139
	L_B, L_X	115	0.105	0.144

2. We find a significant difference in the slope of the L_X-L_B correlation between low-L_X galaxies ($\log L_X \leq 40.5$) and high-L_X galaxies. In the former, $L_X \propto L_B^{\sim 1}$, confirming the analysis of FGT, who suggested that there is a significant difference between the emission mechanisms of low- and high-L_X early-type galaxies based on their loci in the L_X-L_B diagram. This result is also in agreement with the differences in the average X-ray spectra of low- and high-L_X/L_B found by Kim et al. (1992b).

3. We find a significant correlation between L_X and C_{21} in the sense that galaxies with higher L_X have more pronounced low-energy cutoffs. Partial rank analysis indicates that the bivariate L_X/L_B-C_{21} correlation is actually driven by the dependence of both these variables on L_X. These results are in keeping with recent *ROSAT* observations showing intrinsically softer X-ray spectra for lower L_X and L_X/L_B galaxies.

4. Analyses of separate samples of E and S0 galaxies each yield strong correlations between L_B-L_X and L_X-L_X/L_B. The regression slopes for these morphological subsamples are consistent with each other, and with the above results for the full sample. Comparison of the Kaplan-Meier distribution functions for the two morphological subsamples indicates that the S0 galaxies have lower mean L_X (at the 2.8 σ level) and L_X/L_B (at the 3.5 σ level) than do the E galaxies, but that their L_B DFs are not significantly different (the mean L_B of the E galaxies is brighter than that of the S0 galaxies, but only at the 1.8 σ level). Thus S0 galaxies of a given optical luminosity are less able to maintain a significant halo of coronal gas than are E galaxies. We speculate that this is due to the increased fraction of rotational energy and shallower total potential of S0 compared to E galaxies due to the presence of disks.

5. We find a strong correlation between L_B and L_{12} for our full sample. The power-law slope of this correlation is 1.0 ± 0.1, in keeping with the expectation (e.g., Knapp et al. 1989; Knapp et al. 1992) that 12 μm emission from early-type galaxies should come mainly from circumstellar dust and cool stellar photospheres. If this is the case, then we would expect the slope of the L_X-L_{12} to be the same as that of the L_X-L_B correlation. Instead, we find them to differ by $\sim$2.5 σ. Partial rank analysis indicates that the dominant underlying L_X-L_B and L_B-L_{12} relationships are what drive the bivariate L_X-L_{12} correlation. Considering the E and S0 galaxies separately, we find that the discrepancy between the observed and expected L_X-L_{12} behavior for our sample is due to the S0 galaxies having excess 12 μm emission for their optical luminosity, compared to the E galaxies. We speculate that this may be due to a contribution to the 12 μm flux from dust heated in star-forming regions in S0 disks.

6. We find no compelling evidence for a trend of L_{100} with L_X for the full sample from our either our bivariate or partial rank analysis. This may indicate that the dusty ISM in early-type galaxies is accreted. Alternatively, grains created in early-type galaxies may be destroyed relatively quickly by the hot ISM and ISFR in these galaxies. There is evidence for significant L_B-L_{100} and L_{12}-L_{100} correlations. These suggest that the second interpretation is more likely correct.

7. The lack of correlation between L_X and L_{100} is more pronounced for the E galaxies than for the full sample. There is evidence for such a trend for the S0 galaxies from the bivariate analysis, but it is not confirmed by the partial rank analysis. The L_{12}-L_{100} trend found for the full sample appears to be entirely driven by the S0 galaxies, as no evidence for such a trend exists among the E galaxies. This L_{12}-L_{100} correlation for the S0 galaxies is much stronger than any L_B-L_{12} relationship, arguing that much of the 12 μm emission from the S0 galaxies is interstellar, rather than photospheric in origin.

8. Differences between *IRAS* colors of our sample and the IBGS are consistent with lower dust temperatures and with higher average contribution of stellar (or circumstellar) emission to the MIR for the early-type sample than for the IBGS. The distribution of our sample in the Γ-Θ plane defined by Helou et al. (1991) is consistent with this interpretation. The distributions of the E and S0 galaxies in this plane further argues for a significant spiral-like interstellar dust contribution to the ISM of S0 galaxies. Optical-*IRAS* color-color plots provide further evidence that extinction is significant for some of the galaxies in our sample, and essentially all of these galaxies are S0s (see also points 5 and 7 above).

9. We find strong bivariate correlations between L_6 (and L_6/L_B) and L_B, L_X, and L_X/L_B. Partial rank analysis shows the L_B-L_6 trend to be the strongest of these, but all three are statistically significant. In particular, we cannot account for the L_X/L_B-L_6 relationship as being driven by underlying trends of these variables with L_B. Thus we find evidence for an underlying physical relationship between total radio power and X-ray–to–optical ratio. Regression analysis yields slopes much steeper than unity for the trends of L_6 with both L_X and L_X/L_B, arguing that this is *not* an example of a "bright-things-are-bright" correlation.

10. The strongest trend we find with L_6 from our partial rank analysis is that with L_{100}: the presence of an FIR-emitting ISM appears strongly coupled to the ability of early-type galaxies to generate nonthermal radio emission. We have confirmed the suggestion of Kim & Fabbiano (1990) that there is a relationship between L_X/L_B and the distribution of points in the L_6-L_{100} plane. Specifically, the systems with high L_X/L_B tend

to have higher L_6 and L_{100} than those with low L_X/L_B. Further, for a given L_{100}, the X-ray–bright galaxies are shifted to higher L_6 compared to the X-ray–faint galaxies. It appears from this that a hot ISM is a key factor for the generation of radio continuum emission in early-type galaxies. This mutual dependence between X-ray, radio, and FIR properties is in keeping with the idea that cooling flows may be responsible for fueling the active nucleus (FGT), and that the FIR from early-type galaxies with nonthermal radio sources is due to emission from dust heated by the nuclear engine rather than from externally accreted material (e.g., Walsh et al. 1989; Knapp et al. 1992).

11. There is no evidence for any difference between the E and the S0 galaxies in their radio to X-ray properties. We do find an L_{12}-L_6 trend for the S0 galaxies that is not present for the E galaxies. This further argues that there is a substantial nonphotospheric component to the 12 μm emission of S0 galaxies. In keeping with earlier studies (e.g., Wrobel & Heeschen 1991), we find that the E galaxies tend to have higher radio luminosities than the S0 galaxies at the $\sim$2.5 σ level.

12. When we analyze radio core data for our sample, we find bivariate correlations with L_X and L_X/L_B comparable to those found for total radio emission. The regression slopes are consistent with those computed for total radio emission also. These results are in agreement with those from the smaller sample of FGT. Partial rank analysis shows stronger correlations between L_{6co} and X-ray properties than those found for L_6. Thus the hot ISM in early-type galaxies does appear to be linked to core rather than total nonthermal radio activity. L_B, however, is more strongly coupled to L_6 than to L_{6co}. It thus appears that radio cores are fueled by a hot ISM (as suggested by FGT) but that total radio power is related to total mass (assuming the mass of an early-type galaxy to scale with its optical luminosity) rather than to the presence of a hot ISM. This last point suggests that if massive black holes are the nuclear engines, the mass of the black hole is larger in more massive galaxies.

13. We find stronger correlations of L_{12} and L_{100} with L_{6co} than with L_6. This reinforces the conclusion that substantial FIR emission is related to nuclear processes in early-type galaxies. It also supports the idea that there is a significant (nuclear) interstellar contribution to the MIR emission.

14. We find no evidence for a correlation of $M_{H\,I}$ with X-ray properties. This is in keeping with the results of Knapp et al. (1985), and is consistent with the hypothesis that the H I in E galaxies is accreted material.

There are a number of avenues that suggest themselves for further research based on the results of this study. One is the extension of the current work to consideration of observables related to the structure and stellar populations of the galaxies in our sample. We are undertaking this project and will report on our results in subsequent papers of this series. A second possibility that we are considering is to expand the current sample by constructing a similar X-ray database from the *ROSAT* observations of normal early-type galaxies. A subsequent analysis of such a combined *Einstein*-*ROSAT* X-ray database could also make use of the growing and now substantial collection of Hα data on early-type galaxies (Pogge & Eskridge 1987, 1993; Kim 1989; Shields 1991; Trinchieri and di Serego Alighieri 1991; Buson et al. 1993; Goudfrooij et al. 1994). Finally, we have conducted an ensemble study of the global properties of galaxies. While such a study is useful in identifying overall correlations between various global properties, only detailed, high-resolution studies of a substantial sample of early-type galaxies, in wavelengths ranging from X-rays through radio emission, will reveal the details of the physics underlying the feedback between the overall structure and the ISM in early-type galaxies.

We would like to thank Jay Gallagher, Glen Mackie, and Ginevra Trinchieri for their comments on this study as it has progressed. We would also like to thank Eric Feigelson and Michael LaValley for providing us with the latest versions of the ASURV software package. G. F. would like to thank the Aspen Summer School for the opportunity to focus on this project. P. B. E. would like to thank the organizers and participants of the Third Teton Summer School, where early results of this project were discussed. This research has made use of the NASA/IPAC Extragalactic Database (NED), which is operated by the Jet Propulsion Laboratory, Caltech, under contract with the National Aeronautics and Space Administration. D. W. K. acknowledges support by KOSEF grant 923-0200-007-2. We are grateful to the National Aeronautics and Space Administration for support of this research under LTSA grant NAGW2681 and contract NAS8-39073 (AXAF Science Center).

REFERENCES

Arp, H. 1966, ApJS, 14, 1
Bender, R., Paquet, A., & Nieto, J.-L. 1991, A&A, 246, 349
Bernlohr, K. 1993, A&A, 268, 25
Bertin, G., Pignatelli, E., & Saglia, R. P. 1993, A&A, 271, 381
Bertola, F., Galletta, G., Kotanyi, C., & Zeilinger, W. W. 1988, MNRAS, 234, 733
Binggeli, B., Sandage, A., & Tammann, G. A. 1988, ARA&A, 26, 509
Binney, J., & Tremaine, S. 1987, Galactic Dynamics (Princeton: Princeton Univ. Press)
Birkinshaw, M., & Davies, R. L. 1985, ApJ, 291, 32
Bothun, G. D., Lonsdale, C. J., & Rice, W. 1989, ApJ, 341, 129
Bottinelli, L., & Gouguenheim, L., 1977, A&A, 54, 641
Bottinelli, L., Gouguenheim, L., Fouqué, & Paturel, G. 1990, A&AS, 82, 391
Boulanger, F., Beichman, C., Désert, F. X., Helou, G., Pérault, M., & Ryter, C. 1988, ApJ, 332, 328
Bregman, J. N., Hogg, D. E., & Roberts, M. S. 1992, ApJ, 387, 484
Bridle, A. H., & Fomalont, E. B. 1978, AJ, 83, 704
Bridle, A. H., & Perley, R. A. 1984, ARA&A, 22, 319
Burns, J. O., Feigelson, E. D., & Schreier, E. J. 1983, ApJ, 273, 128
Buson, L. M., et al. 1993, A&A, 280, 409
Calvani, M., Fasano, G., & Franceschini, A. 1989, AJ, 97, 1319
Canizares, C. R., Fabbiano, G., & Trinchieri, G. 1987, ApJ, 312, 503
Ciotti, L., D'Ercole, A., Pellegrini, S., & Renzini, A. 1991, ApJ, 376, 380
Condon, J. J., Frayer, D. T., & Broderick, J. J. 1991, AJ, 101, 362
Corwin, H. G., Jr., de Vaucouleurs, A., & de Vaucouleurs, G. 1985, Southern Galaxy Catalogue (Austin: Univ. Texas Press)
David, L. P., Forman, W., & Jones, C. 1991, ApJ, 380, 39
Davidge, T. J. 1992, ApJ, 397, 457
de Vaucouleurs, G., de Vaucouleurs, A., Corwin, H. G., Jr., Buta, R. J., Paturel, G., & Fouqué, P. 1991, Third Reference Catalogue of Bright Galaxies (New York: Springer-Verlag) (RC3)

Disney, M. J., & Wall, J. V. 1977, MNRAS, 179, 235
Donnelly, R. H., Faber, S. M., & O'Connell, R. M. 1990, ApJ, 354, 52
Eder, J. A., Giovanelli, R., & Haynes, M. P. 1991, AJ, 102, 572
Ekers, R. D., & Ekers, J. A. 1973, A&A, 24, 247
Ekers, R. D., et al. 1989, MNRAS, 236, 737
Eskridge, P. B., & Pogge, R. W. 1991, AJ, 101, 2056
Fabbiano, G. 1989, ARA&A, 27, 87
Fabbiano, G., Gioia, I. M., & Trinchieri, G. 1988, ApJ, 324, 749
———. 1989, ApJ, 347, 127 (FGT)
Fabbiano, G., Kim, D.-W., & Trinchieri, G. 1992, ApJS, 80, 531 (P0)
———. 1994, ApJ, 429, 94
Fabbiano, G., Klein, U., Trinchieri, G., & Wielebinski, R. 1987, ApJ, 312, 111
Fabbiano, G., Miller, L., Trinchieri, G., Longair, M., & Elvis, M. 1984, ApJ, 277, 115
Fabbiano, G., & Schweizer, F. 1994, ApJ, submitted
Faber, S. M., & Gallagher, J. S. 1976, ApJ, 204, 365
Faber, S. M., Wegner, G., Burstein, D., Davies, R. L., Dressler, A., Lynden-Bell, D., & Terlevich, R. J. 1989, ApJS, 69, 763 (7S)
Feigelson, E. D., & Babu, G. J. 1992a, ApJ, 397, 55
———. 1992b, Statistical Challenges in Modern Astronomy (New York: Springer-Verlag)
Feigelson, E. D., & Nelson, P. I. 1985, ApJ, 293, 192
Feretti, L., Giovannini, G., Gregorini, L., Parma, P., & Zamorani, G. 1984, A&A, 139, 55
Fich, M., & Hodge, P. W. 1991, ApJ, 374, L17
Forbes, D. A. 1991, MNRAS, 249, 779
Forman, W., Jones, C., & Tucker, W. 1985, ApJ, 293, 102
Forman, W., Schwarz, J., Jones, C., Liller, W., & Fabian, A. C. 1979, ApJ, 234, L27
Fosbury, R. A. E., Mebold, U., Goss, H. M., & Dopita, M. A. 1978, MNRAS, 183, 549
Frank, J., & Gisler, G. 1976, MNRAS, 176, 533
Fullmer, L., & Lonsdale, C. 1989, Catalogued Galaxies and Quasars Observed in the *IRAS* Survey, Version 2 (Pasadena: JPL)
Gallagher, J. S., Knapp, G. R., Faber, S. M., & Balick, B. 1977, ApJ, 215, 463
Geldzahler, B. J., & Fomalont, E. B. 1978, AJ, 83, 1047
Giacconi, R., et al. 1979, ApJ, 230, 540
Gisler, G. 1976, A&A, 51, 137
Goudfrooij, P. 1991, Messenger, 63, 42
Goudfrooij, P., Hansen, L., Jørgensen, H. E., & Nørgaard-Nielsen, H.-U. 1994, A&AS, 105, 341
Gunn, J. E., & Gott, J. R. 1972, ApJ, 176, 1
Haynes, R. F., Herter, T., Barton, A. S., & Benensohn, J. S. 1990, AJ, 99, 1740
Haynes, R. F., Huchtmeier, W. K. H., Siegman, B. C., & Wright, A. E. 1975, A Compendium of Radio Measurements of Bright Galaxies (Melbourne: CSIRO)
Helou, G. 1986, ApJ, 311, L33
Helou, G., Ryter, C., & Soifer, B. T. 1991, ApJ, 376, 505
Hickson, P. 1982, ApJ, 255, 382
Hoyle, F. 1960, MNRAS, 120, 338
Huchtmeier, W. K., & Richter, O.-G. 1989, A General Catalog of H I Observations of Galaxies (New York: Springer-Verlag)
Humason, M. L., Mayall, N. U., & Sandage, A. R. 1956, AJ, 61, 97
Hummel, E., Beck, R., & Dettmar, R.-J. 1991, A&AS, 87, 309
Hummel, E., van der Hulst, J. M., & Dickey, J. M. 1984, A&A, 134, 207
Impey, C., & Gregorini, L. 1993, AJ, 105, 853
Isobe, T., Feigelson, E. D., Akritas, M. G., & Babu, G. J. 1990, ApJ, 364, 104
Isobe, T., Feigelson, E. D., & Nelson, P. I. 1986, ApJ, 306, 490
Johnson, D. W., & Gottesman, S. T. 1983, ApJ, 275, 549
Johnson, H. E., & Axford, W. I. 1971, ApJ, 165, 381
Jura, M. 1986, ApJ, 306, 483
Jura, M., Kim, D.-W., Knapp, G. R., & Guhathakurta, P. 1987, ApJ, 312, L11
Kendall, M., & Stuart, A. 1976, The Advanced Theory of Statistics, Vol. 2 (New York: Macmillan)
Killeen, N. E. B., Bicknell, G. V., & Ekers, R. D. 1986, ApJ, 302, 306
———. 1988, ApJ, 325, 180
Kim, D.-W. 1989, ApJ, 346, 653
Kim, D.-W., & Fabbiano, G. 1990, in Ap&SS Conf. Proc. 160, Windows on Galaxies, ed. G. Fabbiano, J. S. Gallagher, & A. Renzini (Dordrecht: Kluwer), 293
———. 1994, ApJ, in press
Kim, D.-W., Fabbiano, G., & Trinchieri, G. 1992a, ApJS, 80, 645
———. 1992b, ApJ, 393, 134
Knapp, G. R., Gallagher, J. S., & Faber, S. M. 1978, AJ, 83, 139
Knapp, G. R., Guhathakurta, P., Kim, D.-W., & Jura, M. 1989, ApJS, 70, 329
Knapp, G. R., Gunn, J. E., & Wynn-Williams, C. G. 1992, ApJ, 399, 76
Knapp, G. R., Turner, E. L., & Cunniffe, P. E. 1985, AJ, 90, 454
Kormendy, J. 1985, ApJ, 295, 73
Kritsuk, A. G. 1992, A&A, 261, 78
LaValley, M. P., Isobe, T., & Feigelson, E. D. 1992, BAAS, 24, 839
Lonsdale, C. J., Helou, G., Good, J. C., & Rice, W. 1985, Catalogued Galaxies and Quasars in the *IRAS* Survey (Pasadena: JPL)
Maltby, P., & Moffet, A. T. 1962, ApJS, 7, 141
Marston, A. P. 1988, MNRAS, 231, 333
Mathews, W. G., & Baker, J. C. 1971, ApJ, 170, 241
Mayall, N. U. 1939, PASP, 51, 282
Neff, S. G., & Hutchings, J. B. 1992, AJ, 103, 1746
Pellegrini, S., & Fabbiano, G. 1994, ApJ, 429, 105
Phillips, M. M., Charles, P. A., & Baldwin, J. A. 1983, ApJ, 266, 485
Pogge, R. W., & Eskridge, P. B. 1987, AJ, 93, 291
———. 1993, AJ, 106, 1405
Rice, W., Lonsdale, C. J., Soifer, B. T., Neugebauer, G., Kopan, E. L., Lloyd, L. A., deJong, T., & Habing, H. J. 1988, ApJS, 68, 91
Roberts, M. S. 1975, in Stars and Stellar Systems, Vol. 9, Galaxies and the Universe, ed. A. Sandage, M. Sandage, & J. Kristian (Chicago: Univ. Chicago Press), 309
Roberts, M. S., Hogg, D. E., Bregman, J. N., Forman, W. R., & Jones, C. 1991, ApJS, 75, 751
Rowan-Robinson, M., & Crawford, J. 1989, MNRAS, 238, 523
Sadler, E. M., Jenkins, C. R., & Kotanyi, C. G. 1989, MNRAS, 240, 591
Sage, L. J., & Wrobel, J. M. 1989, ApJ, 344, 204
Sandage, A. 1961, A Hubble Atlas of Galaxies (Washington, DC: Carnegie Institution of Washington)
Schmitt, J. H. M. M. 1985, ApJ, 293, 178
Shields, J. C. 1991, AJ, 102, 1314
Soifer, B. T., Boehmer, L., Neugebauer, G., & Sanders, D. B. 1989, AJ, 98, 766
Soifer, B. T., Sanders, D. B., Madore, B. F., Neugebauer, G., Danielson, G. E., Elias, J. H., Lonsdale, C. J., & Rice, W. L. 1987, ApJ, 320, 238
Stanger, V. J., & Warwick, R. S. 1986, MNRAS, 220, 363
Sulentic, J. W. 1976, ApJS, 32, 171
Thronson, H. A., Jr., & Bally, J. 1987, ApJ, 319, L63
Thronson, H. A., Jr., Tacconi, L., Kenney, J., Greenhouse, M. A., Margulis, M., Tacconi-Garman, L., & Young, J. S. 1989, ApJ, 344, 747
Trinchieri, G., & di Serego Alighieri, S. 1991, AJ, 101, 1647
Trinchieri, G., & Fabbiano, G. 1985, ApJ, 296, 447
Trinchieri, G., Fabbiano, G., & Canizares, C. R. 1986, ApJ, 310, 637
Trinchieri, G., Kim, D.-W., Fabbiano, G., & Canizares, C. 1994, ApJ, 428, 555
van Gorkom, J. H., Knapp, G. R., Ekers, R. D., Ekers, D. D., Laing, R. A., & Polk, K. S. 1989, AJ, 97, 708
Vereshchagin, S. V., Smirnov, M. A., & Tutukov, A. V. 1989, Soviet Astron.—AJ, 33, 269
Véron-Cetty, M.-P., & Véron, P. 1988, A&A, 204, 28
Walsh, D. E. P., Knapp, G. R., Wrobel, J. M., & Kim, D.-W. 1989, ApJ, 337, 209
Wardle, M., & Knapp, G. R. 1986, AJ, 91, 23
Whiteoak, J. B., & Gardner, F. F. 1977, Australian J. Phys., 30, 187
Wilcots, E. M., Hodge, P. W., Eskridge, P. B., Bertola, F., & Buson, L. 1990, ApJ, 364, 87
Wilkinson, A., Browne, I. W. A., Kotanyi, C., Christiansen, W. A., Williams, R., & Sparks, W. B. 1987, MNRAS, 224, 895
Wright, A. E. 1974, MNRAS, 167, 273
Wrobel, J. M. 1991, AJ, 101, 127
Wrobel, J. M., & Heeschen, D. S. 1984, ApJ, 287, 41
———. 1988, ApJ, 335, 677
———. 1991, AJ, 101, 148